Universiteit
Leiden
The Netherlands

Functional and structural neuroimaging in Huntington's disease

Odish, O.F.F.

Citation
Odish, O. F. F. (2019, December 5). *Functional and structural neuroimaging in Huntington's disease*. Retrieved from https://hdl.handle.net/1887/81189

Version:	Publisher's Version
License:	Licence agreement concerning inclusion of doctoral thesis in the Institutional Repository of the University of Leiden
Downloaded from:	https://hdl.handle.net/1887/81189

Note: To cite this publication please use the final published version (if applicable).

Cover Page

Universiteit Leiden

The handle http://hdl.handle.net/1887/81189 holds various files of this Leiden University dissertation.

Author: Odish, O.F.F.
Title: Functional and structural neuroimaging in Huntington's disease
Issue Date: 2019-12-05

Functional and structural neuroimaging in Huntington's disease

Omar F.F. Odish

Financial support for the publication of this thesis was kindly provided by: Leiden University Medical Center, Vereniging van Huntington, Stichting Alkemade-Keuls, UCB Pharma B.V., Teva Nederland B.V., Guerbet Nederland B.V., Sectra Benelux B.V., ChipSoft B.V.

Cover design & layout	Bianca Pijl, www.pijlldesign.nl Groningen, the Netherlands
Printed by	Ipskamp Printing Enschede, the Netherlands
ISBN	978-94-028-1680-8 *(print)* 978-94-028-1682-2 *(digital)*

© 2019 Omar F.F. Odish, Groningen, the Netherlands
All rights reserved. No part of this thesis may be reproduced, stored in a retrieval system, or transmitted in any form or by any means, without prior written permission of the author, or when appropriate, of the publishers of the publications included in this thesis.

Functional and structural neuroimaging in Huntington's disease

Proefschrift

ter verkrijging van
de graad van Doctor aan de Universiteit Leiden,
op gezag van Rector Magnificus prof. mr. C.J.J.M. Stolker,
volgens besluit van het College voor Promoties
te verdedigen op donderdag 5 december 2019
klokke 13.45 uur

door

Omar Ferkad Faraj Odish
geboren te Bagdad, Irak
in 1984

Promotor
Prof. dr. R.A.C. Roos

Copromotores
Dr. dr.h.c.mult. A.L.G. Leemans (Universitair Medisch Centrum Utrecht)
Dr. S.J.A. van den Bogaard

Leden van de promotiecommissie
Prof. dr. J.G. van Dijk
Prof. dr. H.P.H. Kremer (Universitair Medisch Centrum Groningen)
Prof. dr. C.J. Stam (Amsterdam Universitair Medische Centra)
Dr. H.E. Kan

to my parents

Table of contents

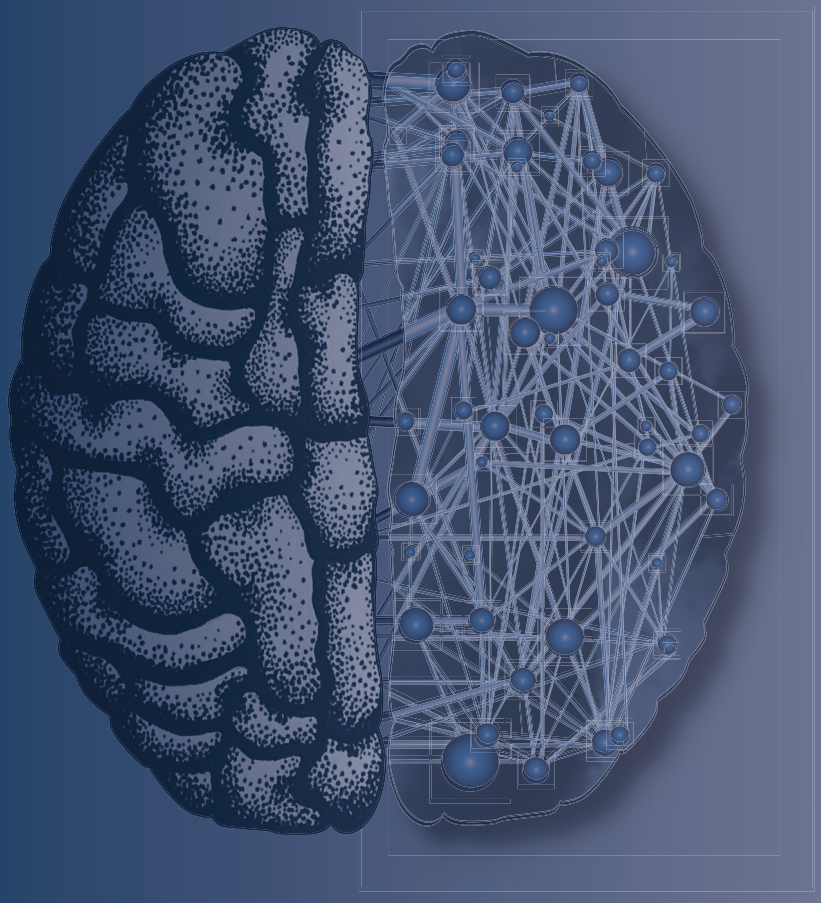

General introduction

CHAPTER 1

General introduction

Huntington's disease (HD) is a relentlessly progressive autosomal dominant neurodegenerative disorder with a broad spectrum of clinical features, characterized by a triad of motor, cognitive and psychiatric signs and symptoms. The disease is caused by a mutation in the Huntingtin gene (*HTT*) on the short arm of chromosome 4.[1] The mutation consists of an expanded cytosine-adenine-guanine (CAG) trinucleotide repeat, with variable penetrance in the range of 36-39 and full penetrance in repeats of 40 and higher.

We have gained a great deal of knowledge on the basis and natural course of HD since the publication of one of the earliest medical descriptions of the "hereditary chorea" by George Huntington in 1872.[2] Unfortunately, there still is no known cure or neuroprotective therapy for the disease and only symptomatic medication is available at present. Huntington's statement about the disorder still holds true: "Once it begins it clings to the bitter end".

The mean age at which the adult form of the disease becomes manifest is between 30 and 50 years.[3] Its course runs for 15-20 years following clinical onset, after which death occurs.[4] The term "manifest" in HD is currently reserved for individuals exhibiting characteristic motor symptoms of the disease. Before this manifest phase, there is a "premanifest" phase, where people do not exhibit evident motor signs of the disease and are seemingly healthy, but can have subtle psychiatric and or cognitive signs and symptoms. The disease is unique among neurodegenerative disorders, as individuals destined to develop the disease can be identified through genetic testing before symptom onset. This provides a window of opportunity for an intervention that could potentially delay or even prevent disease manifestation.

There is an inverse correlation between CAG repeat length and the age of onset of manifest disease, explaining up to 60% of age of motor onset variability.[5] As such, age of onset is not solely explained by the mutation, but also by other yet unknown factors. The disorder exhibits genetic anticipation in the paternal line of inheritance. Anticipation means that the onset of symptoms can occur earlier and often more severely in consecutive generations.[6] After the discovery of the causative mutation for HD in 1993, presymptomatic testing became available for the first time in an autosomal dominant disorder.[7] This major milestone in the history of HD understandably led to hopeful expectation for rapidly finding therapy for the disease and considerable effort has indeed been devoted to understanding the pathophysiology of HD and to find disease-modifying therapies.

More than 25 years after the mutant gene discovery, the first safety studies with potentially promising disease-modifying effects at the gene transcription level have been performed. In September 2015, the first-in-human study looking into the safety of IONIS-HTT_{Rx} (RG6042), an intrathecally administered antisense oligonucleotide (ASO) therapy to reduce mutant HTT (mHTT) protein, was launched in 46 early manifest HD patients (ClinicalTrials.gov Identifier:

NCT02519036). In 34 patients assigned to receive the ASO, the drug proved to be safe and the intended mHTT lowering was demonstrated in a dose-dependent manner, passing the phase II trials.[8] After this initial step, larger studies are now commencing in different stages of the disease to examine whether there indeed is a desirable disease-modifying effect.

In order to measure the effects of these potential therapies, we need to have sensitive markers that correlate with disease state and progression. If the therapeutics have a positive effect on the course of the disease, one would expect these markers to be influenced in a way that reflects slower disease-associated change. Currently used clinical measures, such as the Unified Huntington's Disease Rating Scale total motor score (UHDRS-TMS) and total functional capacity (UHDRS-TFC), are useful in measuring disease-related clinical and functional decline. These are, however, fairly crude semi-quantitative measures with substantial intra- and inter-rater variability, and are not sensitive in detecting subtle changes over short periods of time and certainly not before disease onset.[9-11] Although previous neuroimaging studies have shown potential markers, findings remain inconsistent or lacking association with disease state. For instance, findings from previous longitudinal diffusion magnetic resonance imaging reports are contradictory.[12-14] As such, further exploration of neuroimaging techniques is of great relevance.

In the present work, we aim to find robust parameters/markers corresponding with disease state and measuring progression in different stages of HD in a well-defined population, which can be used as suitable objective surrogate clinical trial endpoints. We put special emphasis on longitudinal study designs, as these provide the most useful clinical progression and parameter change associations. Rapid advances in diagnostic methods in the medical field coupled with advances in analysis methods and ever-increasing computational power provides us with the opportunity to explore different and more complex biological markers (biomarkers). A computational approach to tackle the increasing amount of data generated from functional and structural brain scans increases the likelihood of finding biomarkers specific for the disease. For that reason, we will employ different state-of-the-art approaches to evaluate the potential usefulness of specific markers. Such biomarkers are crucial in order to objectively assess expected disease-modifying properties of a potential therapeutic intervention.

With well-designed large longitudinal international studies aimed at finding biomarkers in HD, such as TRACK-HD and PREDICT-HD, our understanding of the premanifest stage has grown considerably, to the point that we now understand that subtle signs and symptoms in all three above-mentioned clinical domains of the disease are measurably present, sometimes decades before the classic disease signs become manifest.[11,15] Although chorea is the characteristic clinical motor presentation of HD and the striatum is considered to be primarily affected within the histopathological profile, the disease affects a myriad of other neurological functions and should be viewed as a multisystem neurodegenerative disorder of the brain.[16] Even though changes in behaviour, cognition, as well as motor skills often precede the onset of the manifest motor symptoms by decades, sensitive and robust longitudinal markers are still largely lacking in this

phase. The methods we employ in this study are expected to yield useful information about the premanifest stage and the progression towards manifest disease. Finding such markers in these subjects is of particular interest, as they have yet to present clinically with the hallmark motor symptoms of HD. Evidence from HD mice models point to the existence of neuronal dysfunction that is reversible through reduction of mHTT load, which leads to phenotypic and histopathological improvements.[17-20] As such, a strategy focusing on both brain function as well as structure to identify biomarkers in HD seems promising.

Aims and outline of the thesis

The general aim of this thesis is to quantify functional and structural disease-related brain aberrations in Huntington's disease, with the goal of exploring biomarker potential of these different parameters for use in clinical trials. It is important to do so for both the premanifest as well as the manifest stage in order to better understand the "functional and structural natural history" of the disorder and to potentially help guide a therapy aimed at slowing or halting disease progression.

As HD symptoms are most likely a consequence of dysfunctioning brain networks, rather than simply being "striato-centric", we aim to explore which regions or circuits in the network are affected in different stages of the disease and how these may change over time. In Chapter 2, we use this network approach on "resting state" functional magnetic resonance imaging (RS-fMRI) activity patterns of the brain, a method generating spatial covariance patterns of blood oxygenation level dependent (BOLD) signal fluctuations by using independent component analysis. The patterns acquired with this technique are usually referred to as "functional connectivity". We hypothesize that greater changes in functional connectivity occur longitudinally in premanifest gene carriers compared to healthy controls over a follow-up period of three years. As this method is data-driven and lacks a priori assumptions regarding potential disturbances to brain connectivity, it is well suited to explore the earliest signs of functional disturbances before manifest disease occurring in the brain as a whole. This approach may potentially reveal changes in brain function ahead of the occurrence of structural changes. Given the importance of the striatum in the histopathological profile of HD, we additionally include a hypothesis-driven part to the analysis by using a region of interest approach examining a potential striatal functional connectivity change relative to the network.

In Chapter 3, we examine microstructural brain abnormalities occurring in different stages of HD in a two-year follow-up period using diffusion tensor imaging (DTI). As microstructural abnormalities naturally occur before macrostructural abnormalities become evident, we expect this technique to provide more sensitive biomarkers compared to volumetric MRI methods. This diffusion MRI technique quantifies water diffusion in tissue and provides indirect information about the microstructural organization of brain tissue. We use an automated histogram analysis method to assess cross-sectional as well as longitudinal changes occurring within two years of

diffusivity measures in whole-brain white matter, grey matter and the striatum. The choice for an automated method is made consciously, as a straightforward, standardized, fully automated and objective approach for interrogating imaging data will be needed in large clinical trials.
As the network of structural brain connectivity is expected to degrade with disease progression, we use a graph theoretical approach to analyse longitudinal diffusion MRI data (**Chapter 4**). A graph theoretical analysis (GTA) is a powerful mathematical framework for quantifying topological properties of networks, which is able to characterize regional and global structure of networks. We expect this integrated approach to provide new insights into the organization of whole-brain structural connectivity in relation to clinical and cognitive functions in HD over a two-year period, potentially providing usable markers of disease progression. This will be the first-of-its-kind study in HD.

In **Chapter 5** we focus on the evolution of *in vivo* microstructural properties of the occipital cortex in different stages of HD, something which has not been a primary focus in HD research to date. We expect to find measurable abnormalities occurring in a two-year time frame in HD and provide a new region of interest for biomarker research and a measure of disease progression in HD clinical trials. Although the striatum is known to be progressively affected during the disease, it is less well established if other specific regions of the brain are also preferentially impacted in a longitudinal manner. Mounting evidence from whole-brain MRI analysis suggest that the occipital regions are altered early on in the disease.[21-27] Furthermore, post-mortem studies have shown atrophy of the occipital lobe to be most pronounced compared to other cortical areas and histologically the absolute nerve cell numbers of the occipital lobe were found to be reduced.[28,29] Given this evidence of early and preferential involvement of the occipital regions in HD, we set out to study this region using diffusion MRI with a fully automated procedure.

Shifting our focus from MRI investigations to electrophysiological markers, in **Chapter 6** we assess the potential of electroencephalography (EEG) as a biomarker in HD using machine learning automatic classification. EEG abnormalities are known to occur in HD.[30] Through registration of physiologic activity of neurons, quantitative electroencephalography (qEEG) provides objective parameters assessing possible (sub)cortical dysfunction occurring prior to or concomitant with motor or cognitive disturbances observed in the disease. Given the progressive functional deficits seen with disease advancement, it is expected that EEGs of HD patients are different from healthy subjects. To test this hypothesis, automatic analysis methods for such complex data are desirable in order to provide objective and reproducible results. In this cross-sectional study, we use a machine learning method with the aim of automatically classifying EEGs as belonging to HD gene carriers versus healthy controls. Furthermore, we aim to derive qEEG features that correlate with commonly used clinical and cognitive markers in HD research to evaluate biomarker potential.

It is likely that a multimodal approach is needed to have a comprehensive understanding of neuropathology in HD, as any one modality is always limited by its intrinsic properties. In **Chapter 7** we use a multimodal approach to characterize the visual network in HD using different MRI

modalities and visual evoked potentials as an electrophysiological modality. This is done in the light of considerable evidence showing that the visual cortex is one of the first cortical regions in HD to be affected by neuronal loss, as was described above.

In **Chapter 8** we provide summarizing remarks together with potential directions for future research.

References

1 The Huntington's Disease Collaborative Research Group. A novel gene containing a trinucleotide repeat that is expanded and unstable on Huntington's disease chromosomes. Cell 1993;72:971-83.
2 Huntington G. On Chorea. Med Surg Reporter 1872;26:317-21.
3 Roos RA. Huntington's disease: a clinical review. Orphanet J Rare Dis. 2010;5:40.
4 Bates GP, Dorsey R, Gusella JF et al. Huntington disease. Nat Rev Dis Primers 2015;1:15005.
5 Gusella JF, MacDonald ME, Lee JM. Genetic modifiers of Huntington's disease. Mov Disord. 2014;29:1359-1365.
6 Trottier Y, Biancalana V, Mandel JL. Instability of CAG repeats in Huntington's disease: relation to parental transmission and age of onset. J Med Genet. 1994;31:377-82.
7 Harper PS, Lim C, Craufurd D. Ten years of presymptomatic testing for Huntington's disease: the experience of the UK Huntington's Disease Prediction Consortium. Journal of Medical Genetics 2000;37:567-571.
8 Tabrizi SJ, Leavitt BR, Landwehrmeyer GB, et al. Targeting Huntingtin Expression in Patients with Huntington's Disease. N Engl J Med. 2019;380:2307-16.
9 Huntington Study Group. Unified Huntington's Disease Rating Scale: reliability and consistency Mov Disord. 1996;11:136-142.
10 Hogarth P, Kayson E, Kieburtz K, et al. Interrater agreement in the assessment of motor manifestations of Huntington's disease. Mov Disord. 2005;20:293-297.
11 Tabrizi SJ, Scahill RI, Owen G, et al. Predictors of phenotypic progression and disease onset in premanifest and early-stage Huntington's disease in the TRACK-HD study: analysis of 36-month observational data. Lancet Neurol. 2013;12:637-649.
12 Vandenberghe W, Demaerel P, Dom R, et al. Diffusion weighted versus volumetric imaging of the striatum in early symptomatic Huntington disease. J Neurol. 2009;256:109-114.
13 Weaver KE, Richards TL, Liang O, et al. Longitudinal diffusion tensor imaging in Huntington's Disease. Exp Neurol. 2009;216:525-529.
14 Sritharan A, Egan GF, Johnston L, et al. A longitudinal diffusion tensor imaging study in symptomatic Huntington's disease. J Neurol Neurosurg Psychiatry 2010;81:257-262.
15 Paulsen JS, Langbehn DR, Stout JC, et al. Detection of Huntington's disease decades before diagnosis: the Predict-HD study. J Neurol Neurosurg Psychiatry 2008;79:874-880.
16 Rub U, Seidel K, Heinsen H, et al. Huntington's disease (HD): the neuropathology of a multisystem neurodegenerative disorder of the human brain. Brain Pathology 2016;26:726-740.
17 Cummings DM, Milnerwood AJ, Dallérac GM, et al. Aberrant cortical synaptic plasticity and dopaminergic dysfunction in a mouse model of Huntington's disease. Hum Mol Genet. 2006;15:2856-2868.
18 Yamamoto A, Lucas JJ, Hen R. Reversal of neuropathology and motor dysfunction in a conditional model of Huntington's disease. Cell 2000;101:57-66.
19 Datson NA, González-Barriga A, Kourkouta E, et al. The expanded CAG repeat in the huntingtin gene as target for therapeutic RNA modulation throughout the HD mouse brain. PLOS One 2017;12:e0171127.
20 Wang N, Gray M, Lu XH, et al. Neuronal targets for reducing mutant huntingtin expression to ameliorate disease in a mouse model of Huntington's disease. Nat Med. 2014;20:536-541.
21 Tabrizi SJ, Langbehn DR, Leavitt BR, et al. Biological and clinical manifestations of Huntington's disease in the longitudinal TRACK-HD study: cross-sectional analysis of baseline data. Lancet Neurol. 2009;8:791-801.
22 Henley SM, Wild EJ, Hobbs NZ, et al. Relationship between CAG repeat length and brain volume in premanifest and early Huntington's disease. J Neurol. 2009;256:203-212.
23 Rosas HD, Salat DH, Lee SY, et al. Cerebral cortex and the clinical expression of Huntington's disease: complexity and heterogeneity. Brain 2008;131:1057-1068.

24 Muhlau M, Weindl A, Wohlschlager AM, et al. Voxel-based morphometry indicates relative preservation of the limbic prefrontal cortex in early Huntington disease. J Neural Transm 2007;114:367-372.
25 Coppen EM, van der Grond J, Hafkemeijer A, et al. Early grey matter changes in structural covariance networks in Huntington's disease. Neuroimage Clin. 2016;12:806-814.
26 Ciarochi JA, Calhoun VD, Lourens S, et al. Patterns of Co-Occurring Gray Matter Concentration Loss across the Huntington Disease Prodrome. Front Neurol. 2016;7:147.
27 Wu D, Faria AV, Younes L, et al. Mapping the order and pattern of brain structural MRI changes using change-point analysis in premanifest Huntington's disease. Hum Brain Mapp. 2017;38:5035-5050.
28 Lange HW. Quantitative changes of telencephalon, diencephalon, and mesencephalon in Huntington's chorea, postencephalitic and idiopathic parkinsonism. Verhandlungen der Anatomischen Gesellschaft 1981;75:923-925.
29 Rub U, Seidel K, Vonsattel JP, et al. Huntington's Disease (HD): Neurodegeneration of Brodmann's Primary Visual Area 17 (BA17). Brain Pathol. 2015;25:701-711.
30 Nguyen L, Bradshaw JL, Stout JC, et al. Electrophysiological measures as potential biomarkers in Huntington's disease: review and future directions. Brain Res Rev. 2010;64:177-194.

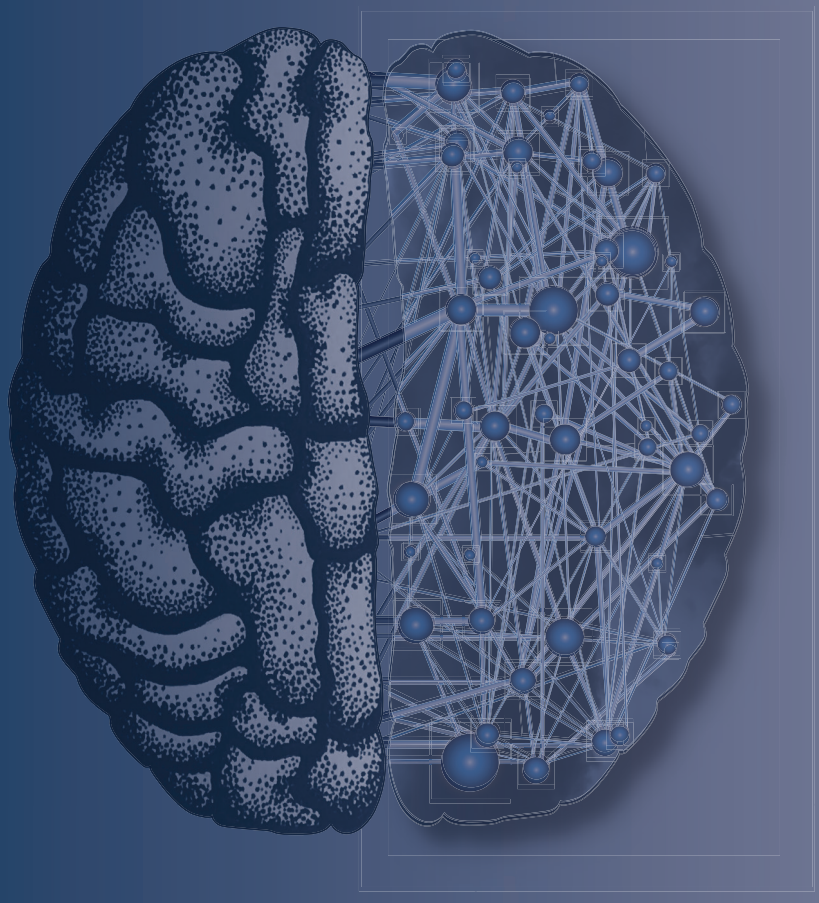

2

Longitudinal resting state fMRI analysis in healthy controls and premanifest Huntington's disease gene carriers: a three-year follow-up study

CHAPTER 2

Omar F.F. Odish[1], Annette A. van den Berg-Huysmans[2], Simon J.A. van den Bogaard[1], Eve M. Dumas[1], Ellen P. Hart[1], Serge A.R.B. Rombouts[2,3,4], Jeroen van der Grond[2], Raymund A.C. Roos[1], on behalf of the TRACK-HD investigator group

[1] Department of Neurology, Leiden University Medical Center, Leiden, The Netherlands
[2] Department of Radiology, Leiden University Medical Center, Leiden, The Netherlands
[3] Institute of Psychology, Leiden University, The Netherlands
[4] Leiden Institute for Brain and Cognition (LIBC), The Netherlands

Human Brain Mapping 2015;36:110-119

Abstract

Background

We previously demonstrated that in the premanifest stage of Huntington's disease (preHD), a reduced functional connectivity exists compared to healthy controls. In the current study we look at possible changes in functional connectivity occurring longitudinally over a period of 3 years, with the aim of assessing the potential usefulness of this technique as a biomarker for disease progression in preHD.

Methods

Twenty-two preHD and 18 healthy control subjects completed resting state fMRI scans in two visits with 3 years in between. Differences in resting state connectivity were examined for eight networks of interest using FSL with 3 different analysis types: a dual regression method, region of interest approach and an independent component analysis. To evaluate a possible combined effect of grey matter volume change and the change in BOLD signal, the analysis was performed with and without voxel-wise correction for grey matter volume. To evaluate possible correlations between functional connectivity change and the predicted time to disease onset, the preHD group was classed as preHD-A if ≥10.9 years and preHD-B if <10.9 years from predicted disease onset. Possible correlations between burden of pathology score and functional connectivity change in preHD were also assessed. Finally, longitudinal change in whole brain and striatal volumetric measures was assessed in the studied cohort.

Results

Longitudinal analysis of the RS-fMRI data revealed no differences in the degree of connectivity change between the groups over a period of 3 years, though a significantly higher rate of striatal atrophy was found in the preHD group compared to controls in the same period.

Conclusions

Based on the results found in this study, the provisional conclusion is that RS- fMRI lacks sensitivity in detecting changes in functional connectivity in HD gene carriers prior to disease manifestation over a 3-year follow-up period.

Introduction

Huntington's disease (HD) is an autosomal dominantly inherited neurodegenerative disorder characterized by motor, cognitive and psychiatric symptoms with a mean age at onset between 30-50 years.[1] It is caused by an expanded CAG trinucleotide repeat in the huntingtin (*HTT*) gene on the short arm of chromosome 4.[2] Magnetic Resonance Imaging (MRI) studies in HD have revealed extensive brain atrophy, most notably in the striatum.[3-9]

A current challenge in HD research is establishing reliable biomarkers for measuring disease progression in HD, both before and after disease manifestation. This is crucial for assessing the efficacy of future proposed therapies. Several large longitudinal studies are currently being conducted for the purpose of establishing such biomarkers.[10-13] Using MRI, these studies have shown that atrophy of different structures in the brains of premanifest gene carriers (preHD), and of the caudate nucleus in particular, is correlated with the estimated years to disease onset (YTO) as calculated by the formula of Langbehn et al.[10-14] This is of particular interest, as these subjects have yet to present clinically with the hallmark motor symptoms of HD.

As the correlations found up to this point only partially predict the rate of clinical deterioration, combining imaging modalities might increase the predictive validity of a potential biomarker. With Resting State functional MRI (RS-fMRI) interregional correlations of blood oxygenation level dependent (BOLD) signal fluctuations between brain regions that are spatially distinct, are measured in the wakeful brain, without challenging it with a particular task. The patterns acquired with this technique are usually referred to as "functional connectivity". RS-fMRI has the theoretical potential of revealing changes occurring in the brain before changes on the structural imaging level are evident, which could be important in targeting the disease in its earliest stages. It may in addition help to unravel compensatory mechanisms responsible for apparently normal brain function despite ongoing neurodegeneration. The technique has already been shown to be a valuable marker for tracking disease progression in Alzheimer's disease, and in mild cognitive impairment.[15,16]

In a previous report, our group has reported functional connectivity differences between controls, preHD and manifest HD subjects, cross-sectionally. The results showed preHD subjects already exhibiting altered functional connectivity with different structures in the brain compared to the matched control group. Importantly, this was still valid after correction for atrophy.[17] The first report detailing reduced cortico-striatal functional connectivity findings in preHD when compared to controls was by Unschuld et al.[18] A recent report by Poudel et al. further confirms findings of functional connectivity reductions in both preHD and manifest HD subjects.[19]

In the current longitudinal study we aim to assess the potential usefulness of this technique as a biomarker for disease progression in the premanifest stage of the disease. We investigate possible changes in functional connectivity occurring longitudinally over a follow-up period of 3 years. With the aim of having a comprehensive interpretation of the acquired data, three separate data analysis methods were applied.

Methods

Subjects

Of the 28 premanifest HD carriers (preHD) and 28 healthy age-matched control subjects who completed RS-fMRI scans during their first visit at the Leiden University Medical Center (LUMC) study site of the TRACK-HD study,[7] 23 preHD and 20 control subjects completed the resting state scans at the second visit, with a 3 year interval between visits. Excluded from analysis were 1 preHD subject due to missing scan volumes and 2 control subjects due to excessive motion artifacts (maximum motion during scan < 4 mm).[20] This resulted in 22 preHD and 18 healthy control subjects that were included in this study (Table I).

Inclusion criteria for study participation for preHD subjects comprised of a positive genetic test with ≥ 40 CAG repeats, the absence of motor disturbances on the total motor score (TMS) of the Unified Huntington's Disease Rating Scale (UHDRS) of more than 5 points and a burden of pathology score greater than 250 ((CAG repeat length - 35.5) x age).[7,21] Age- and gender-matched gene-negative relatives of HD gene carriers and spouses were included as healthy controls. Exclusion criteria for all participants included significant previous head trauma, any neurological or major psychiatric disorder or unwillingness to undergo MRI scanning.[7] Medical history taking, an interview-based assessment and questionnaires were used to ascertain that no major psychiatric disorder could be classified at the time of inclusion and scanning. Consequently, the use of neuroleptic medications or antidepressants was sparse and considered to be of no influence.

For preHD subjects the estimated number of years until disease onset was calculated based on their current age and the CAG repeat length, by means of the formula developed by Langbehn et al.[14]

As previously applied by Tabrizi et al.,[7] for a second analysis, the preHD group was divided at baseline according to the median (10.9 years) for the predicted years to onset into preHD-A (≥10.9 years from predicted onset) and preHD-B (<10.9 years). This resulted in two groups each consisting of 11 subjects (Table II). In a further analysis performed within the preHD group, possible associations between functional connectivity change and burden of pathology score were assessed.

The study was approved by the ethics committee of the LUMC and written informed consent was obtained from all participants following a complete description of the study and procedures. For full details of study parameters, see Tabrizi et al.[7]

Table I. *Group characteristics and clinical scores*

	Healthy controls	preHD (A and B)
N	18	22‡
Gender M/F	7/11	10/12
Age in years (V1), mean (SD)	46.7 (6.9)	43.3 (8.5)
Handedness R/L	18/0	18/4
Level of education (ISCED), median (range)	4 (3)	4 (3)
DART-IQ, mean(SD)	105.3 (9.3)	100.3 (11.6)
BMI in kg/m^2 (V1) , mean (SD)	26.9 (6.6)	24.9 (4.1)
CAG repeat length, mean (SD)	n/a	42.6 (2.6)
Estimated years to onset (YTO), mean (SD)	n/a	11.6 (4.4)
Total functional capacity, mean (SD)		
V1	13.0 (0.0)	12.7 (0.8)
V2	13.0 (0.0)	12.6 (0.9)*
UHDRS-TMS, mean (SD)		
V1	2.4 (2.5)	2.4 (1.5)
V2	2.2 (3.0)	5.4 (5.7)*
SDMT, mean (SD)		
V1	53.7 (8.9)	48.7 (9.7)
V2	58.4 (8.0)	49.4 (10.5)*
BDI-II, mean (SD)		
V1	4.4 (6.3)	5.1 (5.7)
V2	4.8 (5.1)	5.3 (6.0)
Between-scan interval in months, mean (SD)	35.6 (1.20)	35.3 (0.94)

N = number of participants, SD = Standard deviation, n/a = not applicable, ISCED = International Standard Classification of Education, DART-IQ = Dutch Adult Reading Test Intelligence Quotient, CAG = Cytosine-Adenine-Guanine, UHDRS-TMS = Unified Huntington's Disease Rating Scale Total motor score, SDMT = Symbol Digit Modalities Test, BDI-II = Beck Depression Inventory-II, BMI = Body Mass Index, V1 = visit 1, V2 = visit 2.

** Indicates a significant difference at $p < 0.05$.*

‡ Including four subjects progressing to the manifest stage during the three year follow-up period.

Clinical measures

To monitor disease state, the following clinical measures were collected longitudinally for all groups: Unified Huntington's Disease Rating Scale Total Motor Score (UHDRS-TMS), Total Functional Capacity (TFC), Symbol Digit Modalities Test (SDMT) and Beck Depression Inventory-II (BDI-II) scores. The UHDRS-TMS is the traditional measure which defines disease state in HD. The SDMT in particular has been shown to be a sensitive longitudinal cognitive measure in HD, independent of disease related motor effects.[22]

MRI acquisition

MRI acquisition was performed on a 3-Tesla whole body scanner (Philips Achieva, Healthcare, Best, The Netherlands) with an eight channel receive array head coil. An anatomical T1-weighted scan was acquired using an ultrafast gradient echo 3D acquisition sequence with the following imaging parameters: repetition time (TR) = 7.7 ms, echo time (TE) = 3.5 ms, field-of-view = 24 x 24 x 16.4 cm^3, matrix size 224 x 224, with a duration of 9 minutes. For post-processing registration purposes, a high resolution T2*-weighted scan, with the following parameters was collected: repetition time (TR) = 2200 ms, echo time (TE) = 30 ms, field-of-view = 220 x 220 x 168 mm^3, flip angle = 80°, matrix size = 112 x 109 mm^2, with a duration of 46 s. A RS-fMRI scan with the following parameters was obtained: 200 EPI volumes, repetition time (TR) = 2200 ms, echo time (TE) = 30 ms, field-of-view = 220 x 220 x 10.4, resolution = 2.75 x 2.75 x 2.75, no slice gap, flip angle = 80°, matrix size 80 x 79, with a duration of 7.5 minutes. No background music was played during the RS-fMRI scan and to ensure a wakeful disposition participants were asked to keep their eyes open with normal background light.

Pre-processing of resting state data

RS-fMRI images were analysed using FSL 5.0 (fMRIB Software Library; available at *www.fmrib.ox.ac.uk/fsl)*. Pre-processing consisted of motion correction,[23] removal of non-brain tissue,[24] spatial smoothing using a Gaussian kernel of 6 mm full width at half maximum (FWHM) and high-pass temporal filtering equivalent to 100 s (0.01 Hz). After pre-processing, the functional images were registered to the high-resolution T2*-weighted images. These high-resolution images were subsequently registered to the anatomical T1-weighted images. Finally, the anatomical scan was registered to the 2 mm isotropic MNI152 standard space image.[23] These three registration matrices were combined to obtain a matrix for transforming fMRI data from native space to standard space and its inverse (from MNI space to native space). Visual quality control was performed by two qualified raters to ensure correct registration.

Table II. *preHD-A vs. preHD-B, visit 1*

	preHD-A	preHD-B
N	11	11
Gender M/F	3/8	7/4
Age in years, mean (SD)	43.8 (5.8)	43.0 (10.9)
Handedness R/L	9/2	9/2
Level of education (ISCED), median (range)	4 (3)	4 (3)
DART-IQ, mean (SD)	102.3 (9.9)	98.3 (13.2)
BMI in kg/m^2, mean (SD)	25.6 (3.0)	23.1 (2.3)
CAG repeat length, mean (SD)	41.5 (1.4)	43.8 (3.1)*
Estimated years to onset (YTO), mean (SD)	14.4 (4.5)	8.8 (1.6)*
Total functional capacity, mean (SD)	12.7 (0.7)	12.6 (0.9)
UHDRS-TMS, mean (SD)	1.9 (1.5)	2.9 (1.3)
SDMT, mean (SD)	51.6 (9.9)	45.9 (9.1)
BDI-II, mean (SD)	4.5 (6.0)	5.6 (5.7)
Between-scan interval in months, mean (SD)	35.6 (1.0)	34.9 (0.7)

N = number of participants, SD = Standard deviation, ISCED = International Standard Classification of Education, DART-IQ = Dutch Adult Reading Test Intelligence Quotient, CAG = Cytosine-Adenine-Guanine, UHDRS-TMS = Unified Huntington's Disease Rating Scale Total motor score, SDMT = Symbol Digit Modalities Test, BDI-II = Beck Depression Inventory-II, BMI = Body Mass Index.

** Indicates a significant difference at $p < 0.05$.*

Statistical analysis

Statistical analysis of group demographics and clinical measures was performed using IBM SPSS Statistics (version 20.0, IBM Corp., USA). Where appropriate either an independent samples t-test or chi-squared tests were applied. Potential longitudinal change in clinical measures between the groups was also investigated. Difference values were computed and independent samples t-tests on these delta-scores evaluated whether preHD subjects experienced a greater change from visit 1 to visit 2 than control subjects.

Striatal and whole brain volumes were obtained from the TRACK-HD study database.[7,13] These measures were calculated using the Iowa BRAINS method as previously described.[7,13,25,26] Assessment of possible longitudinal volumetric change was performed using a general linear model with age, gender and total brain volume (the latter only for assessing striatal volumes) as covariates in the model.

The functional connectivity analysis was performed in three ways using the dual regression method of FSL, a technique that allows a voxel-wise comparison of resting state functional connectivity.[27] To assess possible associations between the burden of pathology score and functional connectivity change, a regression analysis was preformed within the preHD group only.

Network of interest analysis

First, resting state functional connectivity was determined in terms of similarity of the BOLD fluctuations in the brain in relation to characteristic fluctuations in predefined resting state networks or networks of interest (NOIs). Our choice of resting state networks was based on high reproducibility of these networks from independent component analysis of different data sets.[28,29] These standardized resting state networks parcellate the brain into eight templates that represent over 80% of the total brain volume:[30] 1) medial visual network, 2) lateral visual network, 3) auditory network, 4) sensorimotor system, 5) default mode network, 6) executive control network, 7 and 8) dorsal visual stream networks (Figure 1).[28] To account for noise, a white matter (WM) and a cerebrospinal fluid (CSF) template were included in the analysis.[31-33]

Dual regression analysis (part of FSL 5.0) was performed to identify subject-specific time course and spatial maps. To create the average time course within each network for every subject, the eight resting state networks[28] and the two additional WM and CSF maps[31-33] were used in a linear model fit against each individual subject's fMRI dataset (spatial regression). Hence, WM and CSF activities were included in the regression model as proxy measures for non-neuronal noise. The personalized time courses were subsequently regressed back onto that subject's fMRI dataset to create personal spatial maps (temporal regression). This gives ten 3D images per individual per visit, with voxel-wise the z-scores of functional connectivity to each of the templates. The higher the absolute value of the z-score, the stronger the connectivity to a network.

Independent component analysis

In a second approach, large-scale patterns of functional connectivity were identified by independent component analysis (ICA) using probabilistic ICA as implemented in the MELODIC tool of FSL.[28,34] The original concatenated 4D RS-fMRI dataset was decomposed into sets of time courses and associated spatial maps, to identify different activation components without any model being specified.[34,35] The number of components was fixed to 25 to limit independent component splitting into subcomponents.[15,27]

Subsequently the dual regression analysis as described above was repeated for the group ICA results. This time the 25 independent components were used as spatial regressors, ultimately resulting in 25 z-score maps per individual per visit, reflecting the connectivity strength of each voxel in the brain to each of the 25 independent components.

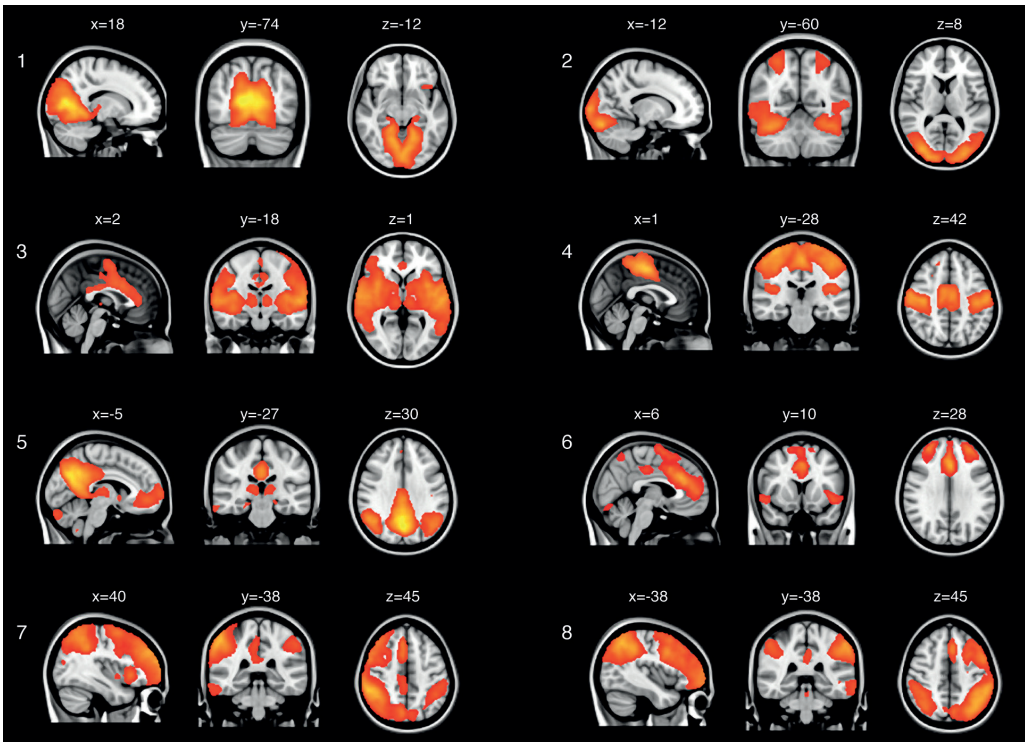

Figure 1. *Saggital, coronal and axial views of the dominant BOLD fluctuations within the eight predefined networks of interest [Beckmann et al., 2005]. All images have been coregistered into the MNI152 standard space template. Numbers at the top of the images denote the MNI coordinates (xyz) and images are shown in radiological orientation.*

Region of interest analysis

Given the overwhelming volume of evidence indicating the striatum as the prime and earliest region affected within the brain in HD, we chose the striatum as a region of interest (ROI) in our analysis. A mask was created to analyse the change in connectivity with the eight NOIs and the 25 independent components of the voxels within this ROI. The mask was based on the probabilistic atlas incorporated in FSL provided by the Harvard Center for Morphometric Analysis and contained the striatum from both hemispheres (Figure 2).[36-39]

Longitudinal change in connectivity per subject and per predefined network/independent component was the main parameter of interest. To assess this change, the individual functional connectivity maps (z-score) from the second visit were subtracted from the corresponding functional connectivity maps from the first visit.

Figure 2. *Axial view of the region of interest (ROI) mask of the striatum shown superimposed on a MNI152 standard image.*

For the between-group analysis, the z-score maps created by dual regression and the maps containing the differences in z-score were collected across subjects into single 4D maps (one per NOI or original independent component, with the fourth dimension being subject identification) and submitted to voxel-based statistical testing. To obtain group averages of maps containing the differences in z-score, a one-sample non-parametric t-test was used and a two-sample t-test was applied to obtain group differences for each of the 8 NOIs and each independent component, using a general linear modelling (GLM) approach as implemented in FSL. Age and gender were included as covariates in the model. To statistically account for potential effects of local structural differences within and between the two groups, grey matter volume of each voxel was included as subject wise and voxel-wise covariates in the GLM design.[40] To evaluate a possible combined effect of grey matter volume change and the change in BOLD signal, the analysis was also performed without voxel-wise correction for grey matter volume.

Voxel-wise non-parametric permutation testing was performed using FSL-randomise (5000 permutations).[41] All statistical maps were family-wise error (FWE) corrected using $p < 0.05$, based on the TFCE statistic image.[42]

Because multiple comparison correction method only corrects the results at the predefined network/independent component level, but does not adjust for the risk of Type 1 error (false positives) induced by increasing the number of components tested simultaneously at high model orders, additional correction for multiple comparisons was done using Bonferroni correction. The multiple comparisons consisted of two comparisons (either connectivity increase or decrease as compared to healthy controls) for 8 NOIs and 25 independent components.

Results

Group characteristics are shown in Table I. Age, gender, handedness and level of education did not differ significantly between controls and preHD subjects. At baseline, no differences were found in UHDRS-TMS, TFC, SDMT, BDI-II, and Dutch Adult Reading Test Intelligence Quotient (DART-IQ) scores. There also was no difference in Body Mass Index (BMI) at baseline. Repeated assessment at 3-year follow-up revealed significantly higher UHDRS-TMS and lower TFC and SDMT scores in the preHD group (Table I). Four of the twenty-two preHD subjects began to exhibit typical HD motor symptoms during the 3-year follow-up period, therefore reaching the definition of early manifest disease stage. The cross-sectional difference in UHDRS-TMS and TFC score between the groups at the second visit was negated after exclusion of these four converter subjects, yet the difference in SDMT score remained significant ($p = 0.07$, $p = 0.36$ and $p = 0.01$, respectively). The difference in SDMT comprised of higher mean scores within the control group when compared to their first visit, while the scores of the preHD group remained stagnant.

The longitudinal change in the UHDRS-TMS was significant when all participants were included ($p = 0.03$), yet this result was only reached as a result of outlier scores: when the four converters were excluded from analysis, this difference vanished ($p = 0.25$).

The longitudinal change in the SDMT score was significant when all participants were included ($p = 0.04$). While the mean SDMT difference in the preHD group remained essentially the same when the four converters were excluded (+0.64 vs. +0.67 difference points, respectively), statistical significance could no longer be reached ($p = 0.06$). See Table III for a view of the mean longitudinal change of the different measures.

No differences in any of the scores outlined above were found while comparing the preHD-A and preHD-B groups, neither at the first or second visit nor longitudinally. The CAG trinucleotide repeat count was significantly higher in the preHD-B relative to the preHD-A group ($p = 0.03$) (Table II; longitudinal change data not shown).

All scans were analysed with and without inclusion of the four converters. All scan analyses were also repeated with exclusion of the four left-handed subjects to avoid any possible lateralization effects. The reported results are with and without voxel-wise correction for grey matter volume, as described in the Methods section. No difference was found in the amount of motion between the groups.

RS-fMRI network analyses

In the eight designated NOIs, longitudinal analysis of the RS-fMRI data revealed no statistically significant differences in the degree of connectivity change between controls and the preHD group. There also were no statistically significant differences between controls and preHD-A and controls and preHD-B subjects. No association could be demonstrated between the degree of connectivity change in the different networks and the groups designated as *far* and *near* from expected onset of motor symptoms, nor with the burden of pathology score.

Table III. *Longitudinal change in clinical scores †, mean difference*

	Healthy controls	preHD (A and B)
N	18	22‡
Total functional capacity, MD (SD)	0.0 (0.0)	-0.1 (0.6)
UHDRS-TMS, MD (SD)	-0.2 (2.9)	3.0 (5.4)*
SDMT, MD (SD)	4.7 (5.7)	0.6 (6.1)*
BDI-II, MD (SD)	0.4 (3.6)	0.2 (5.1)
BMI in kg/m^2, MD (SD)	0.5 (2.3)	-0.4 (1.6)

N = number of participants, MD = mean difference, SD = Standard deviation, UHDRS-TMS = Unified Huntington's Disease Rating Scale Total motor score, SDMT = Symbol Digit Modalities Test, BDI-II = Beck Depression Inventory-II, BMI = Body Mass Index.

** Indicates a significant difference at $p < 0.05$.*

† Longitudinal change denotes scores from visit 1 subtracted from scores from visit 2.

‡ Including four subjects progressing to the manifest stage during the three year follow-up period.

RS-fMRI ICA

Using the ICA method, 25 components were extracted from the data per person per visit and the differences between the two visits compared across the above outlined groups. There were no statistically significant differences in the degree of connectivity change between any of the groups. Dividing the preHD group according to the expected time of motor symptom onset again revealed no significant differences in the degree of connectivity change. Regression analysis using the burden of pathology score revealed no associations with the degree of functional connectivity change within the preHD group.

RS-fMRI ROI analysis

Using the described mask to assess the change of connectivity strength in the voxels within the striatum, no statistically significant differences could be demonstrated between any of the groups described above.

When comparing results from the outlined analysis methods, the ROI analysis provided the closest proximity to achieving a significant longitudinal reduction in functional connectivity in preHD when compared to controls. This was the case with the lateral visual network (NOI 2; $p = 0.08$) and default mode network (NOI 5; $p = 0.11$) (Figure 3). Power analysis using these results show that a minimum of 23 subjects per group would be needed to detect a significant longitudinal reduction in functional connectivity in 3 years within the striatum with the lateral visual network for preHD compared to controls (at 5% FWE rate with a power of 80%).

Table IV provides an overview of significance levels for longitudinal reduction of functional connectivity within the striatum over 3 years in preHD subjects compared to controls with the 8 NOIs.

Longitudinal volumetric analysis

In the 3-year follow-up period, no statistically significant difference in whole brain volume decline was found between controls (0.33%) and preHD (0.58%) ($p = 0.35$).

The striatal volume showed a significantly higher rate of decline over the 3-year period in preHD as compared to controls: 1.45% in the control group versus 7.29% in the preHD groep ($p < 0.001$). Striatal volume decline over the 3 years was significantly higher in both preHD-A (6.62%) and preHD-B (8.15%) when compared to controls ($p < 0.001$). The difference in striatal volume decline rate between preHD-A and preHD-B was not statistically significant over this time period ($p = 0.31$).

Discussion

This study showed no longitudinal difference in functional connectivity change between preHD and healthy control subjects over a period of 3 years. This was also the case when preHD subjects were divided in a preHD-A and preHD-B group based on the expected time to disease onset and when using burden of pathology score as a regressor for functional connectivity change. These conclusions are based on results obtained from three different analysis methods. Results remained the same with and without voxel-wise correction for grey matter volume and while running the analysis with the inclusion and/or exclusion of converters and left-handed subjects.

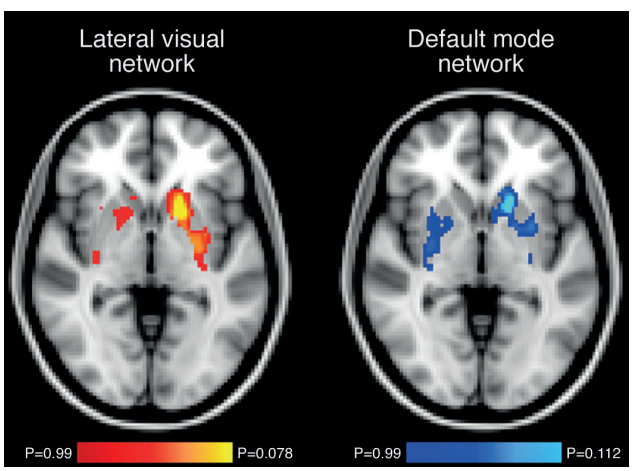

Figure 3. P-value maps of the nonsignificant longitudinal reductions in functional connectivity in preHD compared to controls in the striatum with the lateral visual and default mode networks in the 3-year study period.

Table IV. *Statistical parameters for longitudinal reduction of functional connectivity within the striatum over 3 years in preHD subjects compared to controls with the 8 networks of interest*

	Network of interest (NOI)	Minimal *P*-value	*x*	*y*	*z*	*t*-stat
1	Medial visual	0.356	39	68	42	3.527
2	Lateral visual	0.078	53	69	35	4.175
3	Auditory	0.686	36	56	49	3.280
4	Sensorimotor	0.804	54	62	45	2.491
5	Default mode	0.112	53	70	36	3.845
6	Executive control	0.734	31	69	32	2.327
7	Dorsal visual stream	0.502	59	66	39	3.355
8	Dorsal visual stream	0.262	36	68	29	3.754

x, y, and z denote MNI152 standard space coordinates.

This result, taken together with clinical parameters like the UHDRS-TMS and SDMT showing longitudinal change between the included subjects, and significantly higher longitudinal striatal atrophy rate in preHD compared to controls, alludes to a lack of sensitivity of RS-fMRI in detecting concomitant changes in functional connectivity occurring longitudinally in preHD. This statement should be considered as tentative, as future studies with greater numbers of participants, improved signal-to-noise ratio, different analysis methods and/or a longer follow-up period might be able to demonstrate longitudinal differences in functional connectivity change. That being said, results from this study suggest that even if there is functional connectivity change occurring in the 3-year follow-up period, this is too small to detect with this technique using the highlighted methods with this cohort size, which is a relevant finding in light of longitudinal biomarker research in preHD.

Our study confirms the results found by Seibert et al.[43] Their study reported no change in functional connectivity over a 1 year period. The differences between the study of Seibert et al. and our own were the methodology used, where seeds instead of a priori spatial NOIs were used and subject-native space registration instead of the MNI152 standard space template was applied. The number of subjects examined in that report was higher than in our study: 22 controls and 34 preHD subjects.

Our earlier cross-sectional results suggested that functional connectivity, at the group level, was a fairly sensitive measure to differentiate preHD subjects from controls.[17] As such, we were quite hopeful to demonstrate a divergent longitudinal functional connectivity evolution between the groups, which in turn could serve as a measure for disease progression. We were however

unable to reproduce these results within our baseline cohort, most likely due to the smaller number of subjects that were included, as only those with scans at both time points could be assessed longitudinally. This study can therefore not account for the functional connectivity of the dropouts, as no data are available. Furthermore, the discrepancy in baseline findings might involve deteriorating health prompting more severely affected subjects to drop out prematurely of the study, thus leaving a relatively fitter group for this study. A such, selection bias disproportionately affecting subjects with the fastest rate of clinical deterioration is a possible reason for not finding different functional connectivities between the groups. This spurred using a more comprehensive approach and to base the hypothesis-driven part of the analysis solely by singling out the striatum as the primary region where possible changes in resting state activity are expected, given the fact that it is the region first affected in HD, as was again demonstrated by the volumetric study of the striatum within this cohort. Despite using three different analysis methods, no longitudinal change could be demonstrated in our cohort in a time frame of 3 years with two measurement points. The combination of a highly significant difference in striatal atrophy rate between preHD and controls with a total lack of significant difference in the rate of functional connectivity change between these groups strongly points to a lower sensitivity of RS-fMRI in demonstrating longitudinal change in the preHD population.

A similar sequence of results was found by the study of Wolf et al., where task-based fMRI showed significantly lower activity cross-sectionally in the left prefrontal cortex in preHD, yet failed to demonstrate a significant decline of that activity over a 2-year follow-up period.[44] In that study, the baseline and longitudinally examined cohort consisted of the same subjects. Despite the obvious differences in methodology and spatial parameters used in measuring the BOLD signals, the longitudinal study by Wolf et al. may further consolidate the notion of a lack of sensitivity in detecting BOLD signal changes occurring during a time frame that can be considered feasible for assessing the efficacy of an intervention in preHD.

The strength of our study lies in the application of three different analysis methods which allows for a more comprehensive interpretation of the data. This strength is complemented by the acquisition methodology used: the duration of the RS-scans (>6 min) and acquisition while the patients have their eyes open provide the most robust estimates of functional connectivity as demonstrated by different studies.[45,46]

A limitation of this study is the loss of power due to the expansive testing of various networks and independent components. This expansive testing is however justified given the goal of finding robust and specific functional connectivity changes in preHD for usage as biomarker candidate in a clinical trial setting. Other possible limitations include transforming the data to an atlas volume instead of subject-native space, the relatively small number of tested subjects and possible confounding effects of dropouts, the conceivably short follow-up period in the preHD stage setting and not accounting for possibly confounding covariables such as depression scores in the analysis model.

Based on the results found in this study, the provisional conclusion is that RS-fMRI seems to lack sensitivity in detecting changes in functional connectivity in HD gene carriers prior to disease manifestation over a 3-year follow-up period. This conclusion applies to this selective group of participants and the particular analysis methods used in this study. Results from future longitudinal studies, such as the ongoing Track-On HD study which has larger groups and more time points measured, should be awaited before articulating a definite recommendation on the possible utility of RS-fMRI as a biomarker tracking disease progression in preHD.

Acknowledgments

TRACK-HD is supported by the CHDI Foundation, Inc., a not for profit organization dedicated to finding treatments for Huntington's disease. The authors wish to thank Sarah Tabrizi, University College London, who is the global PI for TRACK-HD and clinical site PI for London, Hans Johnson, University of Iowa, responsible for producing morphometric regional measures of the brain and analysis protocols for medical imaging, and Doug Langbehn, University of Iowa, who is a biostatistician and played a key role in statistical design and data analysis of the TRACK-HD data. The authors also wish to extend their gratitude to the TRACK-HD investigators responsible for collecting the data and to the study participants and their families.

References

1 Roos RA. Huntington's disease: a clinical review. Orphanet J Rare Dis. 2010;5:40.
2 The Huntington's Disease Collaborative Research Group. A novel gene containing a trinucleotide repeat that is expanded and unstable on Huntington's disease chromosomes. Cell 1993;72:971-83.
3 Aylward EH, Liu D, Nopoulos PC, et al. Striatal volume contributes to the prediction of onset of Huntington disease in incident cases. Biol Psychiatry 2012;71:822-8.
4 Dumas EM, van den Bogaard SJ, Ruber ME, et al. Early changes in white matter pathways of the sensorimotor cortex in premanifest Huntington's disease. Hum Brain Mapp. 2012;33:203-12.
5 Hadzi TC, Hendricks AE, Latourelle JC, et al. Assessment of cortical and striatal involvement in 523 Huntington disease brains. Neurology 2012;79:1708-15.
6 Stoffers D, Sheldon S, Kuperman JM, et al. Contrasting gray and white matter changes in preclinical Huntington disease: an MRI study. Neurology 2010;74:1208-16.
7 Tabrizi SJ, Langbehn DR, Leavitt BR, et al. Biological and clinical manifestations of Huntington's disease in the longitudinal TRACK-HD study: cross-sectional analysis of baseline data. Lancet Neurol. 2009;8:791-801.
8 Van den Bogaard SJ, Dumas EM, Ferrarini L, et al. Shape analysis of subcortical nuclei in Huntington's disease, global versus local atrophy--results from the TRACK-HD study. J Neurol Sci. 2011;307:60-8.
9 Vonsattel JP, Keller C, Cortes Ramirez EP. Huntington's disease - neuropathology. Handb Clin Neurol. 2011;100:83-100.
10 Aylward EH, Nopoulos PC, Ross CA, et al. Longitudinal change in regional brain volumes in prodromal Huntington disease. J Neurol Neurosurg Psychiatry 2011;82:405-10.
11 Paulsen JS, Nopoulos PC, Aylward E, et al. Striatal and white matter predictors of estimated diagnosis for Huntington disease. Brain Res Bull. 2010;82:201-7.
12 Tabrizi SJ, Reilmann R, Roos RA, et al. Potential endpoints for clinical trials in premanifest and early Huntington's disease in the TRACK-HD study: analysis of 24 month observational data. Lancet Neurol. 2012;11:42-53.
13 Tabrizi SJ, Scahill RI, Owen G, et al. Predictors of phenotypic progression and disease onset in premanifest and early-stage Huntington's disease in the TRACK-HD study: analysis of 36-month observational data. Lancet Neurol. 2013;12:637-649.
14 Langbehn DR, Brinkman RR, Falush D, et al. A new model for prediction of the age of onset and penetrance for Huntington's disease based on CAG length. Clin Genet. 2004; 65:267-77.
15 Damoiseaux JS, Prater KE, Miller BL, et al. Functional connectivity tracks clinical deterioration in Alzheimer's disease. Neurobiol Aging 2012;33:828-30.
16 Bai F, Watson DR, Shi Y, et al. Specifically progressive deficits of brain functional marker in amnestic type mild cognitive impairment. PLoS One 2011;6:e24271.
17 Dumas EM, van den Bogaard SJ, Hart EP, et al. Reduced functional brain connectivity prior to and after disease onset in Huntington's disease. Neuroimage Clin. 2013;2:377-384.
18 Unschuld PG, Joel SE, Liu X, et al. Impaired cortico-striatal functional connectivity in prodromal Huntington's Disease. Neurosci Lett. 2012;514:204-209.
19 Poudel GR, Egan GF, Churchyard A, et al. Abnormal synchrony of resting state networks in premanifest and symptomatic Huntington disease: the IMAGE-HD study. J Psychiatry Neurosci. 2014;39:87-96.
20 Jenkinson M, Beckmann CF, Behrens TE, et al. FSL. Neuroimage 2012;62:782-790.
21 Penney JB, Jr., Vonsattel JP, MacDonald ME, et al. CAG repeat number governs the development rate of pathology in Huntington's disease. Ann Neurol. 1997;41:689-92.
22 Tabrizi SJ, Scahill RI, Durr A, et al. Biological and clinical changes in premanifest and early stage Huntington's disease in the TRACK-HD study: the 12-month longitudinal analysis. Lancet Neurol. 2011;10:31-42.

23 Jenkinson M, Bannister P, Brady M, et al. Improved optimization for the robust and accurate linear registration and motion correction of brain images. Neuroimage 2002;17:825-41.
24 Smith SM. Fast robust automated brain extraction. Hum Brain Mapp. 2002;17:143-55.
25 Ghayoor, Vaidya JG, Johnson HJ. Development of a novel constellation based landmark detection algorithm. Proc. SPIE 8669, Medical Imaging 2013: Image Processing 86693F.
26 Young KE, Johnson HJ. Robust multi-site MR data processing: iterative optimization of bias correction, tissue classification, and registration. Front Neuroinform. 2013;7:29.
27 Filippini N, MacIntosh BJ, Hough MG, et al. Distinct patterns of brain activity in young carriers of the APOE-epsilon4 allele. Proc Natl Acad Sci U S A 2009;106:7209-14.
28 Beckmann CF, DeLuca M, Devlin JT, et al. Investigations into resting-state connectivity using independent component analysis. Philos Trans R Soc Lond B Biol Sci. 2005;360:1001-13.
29 Damoiseaux JS, Rombouts SA, Barkhof F, et al. Consistent resting-state networks across healthy subjects. Proc Natl Acad Sci U S A 2006;103:13848-53.
30 Khalili-Mahani N, Zoethout RM, Beckmann CF, et al. Effects of morphine and alcohol on functional brain connectivity during "resting state": a placebo-controlled crossover study in healthy young men. Hum Brain Mapp. 2012;33:1003-18.
31 Fox MD, Snyder AZ, Vincent JL, et al. The human brain is intrinsically organized into dynamic, anticorrelated functional networks. Proc Natl Acad Sci U S A 2005;102:9673-8.
32 Cole DM, Smith SM, Beckmann CF. Advances and pitfalls in the analysis and interpretation of resting-state FMRI data. Front Syst Neurosci. 2010;4:8.
33 Birn RM. The role of physiological noise in resting-state functional connectivity. Neuroimage 2012;62:864-70.
34 Beckmann CF, Smith SM. Probabilistic independent component analysis for functional magnetic resonance imaging. IEEE Trans Med Imaging 2004;23:137-52.
35 McKeown MJ, Makeig S, Brown GG, et al. Analysis of fMRI data by blind separation into independent spatial components. Hum Brain Mapp. 1998;6:160-88.
36 Makris N, Goldstein JM, Kennedy D, et al. Decreased volume of left and total anterior insular lobule in schizophrenia. Schizophr Res. 2006;83:155-71.
37 Frazier JA, Chiu S, Breeze JL, et al. Structural brain magnetic resonance imaging of limbic and thalamic volumes in pediatric bipolar disorder. Am J Psychiatry 2005;162:1256-65.
38 Desikan RS, Segonne F, Fischl B, et al. An automated labeling system for subdividing the human cerebral cortex on MRI scans into gyral based regions of interest. Neuroimage 2006;31:968-80.
39 Goldstein JM, Seidman LJ, Makris N, et al. Hypothalamic abnormalities in schizophrenia: sex effects and genetic vulnerability. Biol Psychiatry 2007;61:935-45.
40 Oakes TR, Fox AS, Johnstone T, et al. Integrating VBM into the General Linear Model with voxelwise anatomical covariates. Neuroimage 2007;34:500-8.
41 Nichols TE, Holmes AP. Nonparametric permutation tests for functional neuroimaging: a primer with examples. Hum Brain Mapp. 2002;15:1-25.
42 Smith SM, Nichols TE. Threshold-free cluster enhancement: addressing problems of smoothing, threshold dependence and localisation in cluster inference. Neuroimage 2009;44:83-98.
43 Seibert TM, Majid DS, Aron AR, et al. Stability of resting fMRI interregional correlations analyzed in subject-native space: a one-year longitudinal study in healthy adults and premanifest Huntington's disease. Neuroimage 2012;59:2452-63.
44 Wolf RC, Sambataro F, Vasic N, et al. Longitudinal functional magnetic resonance imaging of cognition in preclinical Huntington's disease. Exp Neurol. 2011;231:214-22.

45 Yan C, Liu D, He Y, et al. Spontaneous brain activity in the default mode network is sensitive to different resting-state conditions with limited cognitive load. PLoS One 2009;4:e5743.
46 Van Dijk KR, Hedden T, Venkataraman A, et al. Intrinsic functional connectivity as a tool for human connectomics: theory, properties, and optimization. J Neurophysiol. 2010;103:297-321.

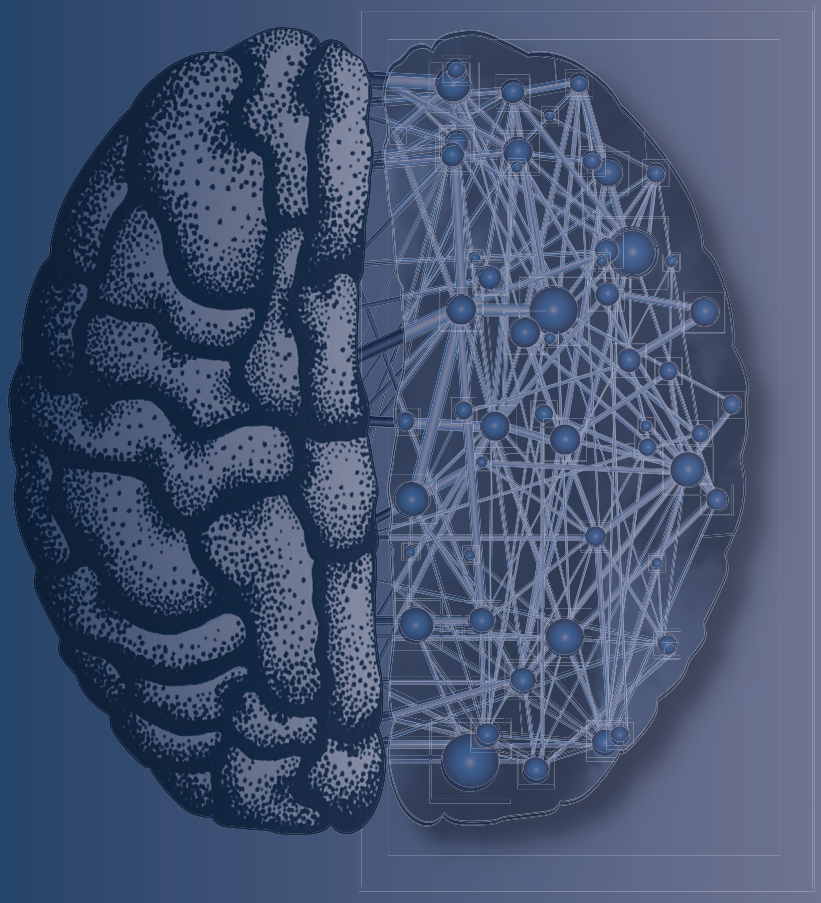

3

Microstructural brain abnormalities in Huntington's disease: a two-year follow-up

CHAPTER 3

Omar F.F. Odish[1], Alexander Leemans[2], Robert H.A.M. Reijntjes[1], Simon J.A. van den Bogaard[1], Eve M. Dumas[1], Ron Wolterbeek[3], Chantal M.W. Tax[2], Hugo J. Kuijf[2], Koen L. Vincken[2], Jeroen van der Grond[4], Raymund A.C. Roos[1]

[1] Department of Neurology, Leiden University Medical Center, Leiden, The Netherlands
[2] Image Sciences Institute, University Medical Center Utrecht, Utrecht, The Netherlands
[3] Department of Biostatistics, Leiden University Medical Center, Leiden, The Netherlands
[4] Department of Radiology, Leiden University Medical Center, Leiden, The Netherlands

Human Brain Mapping 2015;36:2061-2074

Abstract

Background

Diffusion Tensor Imaging (DTI) provides indirect information about the quality of the microstructural organization of tissues. In this 2-year follow-up study, we assess both cross-sectional and time-related changes of striatal and whole-brain microstructural properties in different stages of Huntington's disease (HD) using DTI.

Methods

From the TRACK-HD study, 22 premanifest gene carriers (preHD), 10 early manifest HD and 24 controls were scanned at baseline and 2-year follow-up. Stratification of the preHD group into a far (preHD-A) and near (preHD-B) to predicted disease onset was performed. Age-corrected histograms of whole-brain white matter (WM), grey matter (GM) and striatal diffusion measures were computed and normalised by the number of voxels in each subject's data set.

Results

Higher cross-sectional mean, axial and radial diffusivities were found in both WM ($p \leq 0.001$) and GM ($p \leq 0.001$) of the manifest HD compared to the preHD and control groups. In preHD, only WM axial diffusivity (AD) was higher than in controls ($p \leq 0.01$). This finding remained valid only in preHD-B ($p \leq 0.001$). AD was also higher in the striatum of preHD-B compared to controls and preHD-A ($p \leq 0.01$). Fractional anisotropy (FA) lacked sensitivity in differentiating between the groups. Histogram peak heights were generally lower in manifest HD compared to the preHD and control groups. No longitudinal differences were found in the degree of diffusivity change between the groups in the two year follow-up. There was a significant relationship between diffusivity and neurocognitive measures.

Conclusions

Alterations in cross-sectional diffusion profiles between manifest HD subjects and controls were evident, both in whole-brain and striatum. In the preHD stage, only AD alterations were found, a finding suggesting that this metric is a sensitive marker for early change in HD prior to disease manifestation. The individual diffusivities were superior to FA in revealing pathologic microstructural brain alterations. Diffusion measures were well related to clinical functioning and disease stage.

Introduction

Huntington's disease (HD) is a neurodegenerative autosomal dominant disorder. It is caused by an increased CAG (Cytosine-Adenine-Guanine) repeat within the huntingtin gene on the short arm of chromosome 4.[1] The mutant huntingtin protein triggers a pathogenic cascade responsible for neuropathology in the brain.[2,3] This results in cognitive, motor, and psychiatric symptoms. The brain as a whole is impacted, though preferential striatal volume loss has been extensively documented by post-mortem histopathological as well as *in vivo* magnetic resonance imaging (MRI) studies.[4-9]

Even though no medication is currently available to cure or slow-down the disease, it remains crucial to have a clear understanding of the typical evolution of brain changes in the disease to determine when microstructural changes start and how fast degeneration occurs. This is necessary to define optimal intervention starting points as well as possibly providing an objective tool to determine the impact of candidate therapies, especially in the premanifest (preHD) phase where clinical measures are lacking.

Diffusion tensor imaging (DTI) is an MRI technique that can quantify water diffusion within tissue.[10-13] The diffusion tensor in every voxel can be described by its three eigenvectors and eigenvalues ($\lambda1, \lambda2, \lambda3$). These eigenvalues quantify the diffusion in three orthogonal orientations and are typically synthesized to axial ($= \lambda1$) and radial ($= (\lambda2 + \lambda3)/2$) diffusivities.

Another popular diffusion measure is fractional anisotropy (FA), which is a function of the eigenvalues, and ranges from 0 (completely isotropic diffusion) to 1 (completely anisotropic diffusion), with higher values generally corresponding to a higher directional coherence of tissue organization. High FA occurs for example in healthy white matter (WM) which typically has a parallel-oriented micro-architecture. Another commonly reported diffusivity measure is the mean diffusivity (MD), which is the average of the three eigenvalues. In this study we evaluate and report these measures as well as the separate underlying eigenvalues, as these may provide complementary information about the nature of microstructural change.[14,15] It is possible that certain metrics are more selectively affected and, therefore, might be more sensitive to longitudinal change. For example, when changes in axial diffusivity (AD) are proportional to radial diffusivity (RD), the FA value may not be very informative.[16]

In a previous study, we evaluated cross-sectional group differences in FA and MD between controls, preHD and manifest HD subjects using a region-of-interest and fiber tractography analysis approach.[17] In that study, MD proved to be more sensitive in differentiating between the groups compared to FA. Findings from previous longitudinal reports remain inconsistent.[18-20] With inherent limitations such as inter-user variability to nonautomated methods such as hand drawn regions-of-interest, we chose an automated histogram analysis method in this work to assess cross-sectional as well as time-related changes of diffusivity measures occurring within 2 years. We hypothesized that lower FA and higher MD, AD and RD values would be found in

subjects with manifest HD when compared to preHD subjects and controls, reflective of higher microstructural disorganization in the manifest group. In addition, we hypothesized that MD would be elevated in preHD subjects when compared to controls based on results from our previous work.[17] Grey matter (GM) diffusivity was assessed separately to assess potential higher sensitivity towards alteration compared to WM, fully bearing in mind the limitations of the tensor model in GM. Associations between neurocognitive measures and diffusivity findings were assessed for potential usage as surrogate markers or predictors for these findings. Also, associations between diffusivity and the expected time to disease onset were assessed to test the hypothesis that sensitivity of diffusivity measures in detecting disturbances in preHD subjects increases with shorter proximity to expected disease onset.

As a subanalysis, diffusion in the left and right hemispheres was assessed individually. This was done to explore the hypothesis of preferential degeneration of the dominant versus the non-dominant hemisphere. Plausibly increased lifetime excitotoxic exposure due to higher activation could lead to such a finding in HD. We hypothesized that diffusion parameters indicative of greater neuronal damage were represented more readily in the dominant hemisphere, as findings from previous studies have suggested.[21-24] To the best of our knowledge, this is the first study exploring this hypothesis and the first to apply histogram analysis to (longitudinal) DTI data in HD as well as to separately assess microstructural properties of both whole-brain GM and WM.

Materials and methods

Participants

As part of the TRACK-HD study, 90 participants were included at baseline at the Leiden University Medical Center (LUMC) study site (for details see Tabrizi et al.).[7] DTI was added to the standard MRI protocol. At baseline, DTI was not performed in ten participants because of claustrophobia, and another nine were excluded from analysis due to excessive movement artefacts. Of the remaining 71 subjects, 62 subjects completed DTI scans at both visits. Of these 62, a further six subjects were excluded from analysis due to excessive movement artefacts at the second visit. The longitudinal cohort included in this work was thus comprised of 56 subjects: 24 healthy controls, 22 preHD and ten early manifest HD (Table I).

Inclusion criteria for the preHD group were a CAG repeat ≥ 40 with a total motor score on the Unified Huntington's Disease Rating Scale (UHDRS-TMS) ≤ five. Inclusion criteria for the early manifest HD group were a CAG repeat ≥ 40, with a UHDRS-TMS ≥ five and a Total Functional Capacity score (TFC) ≥ seven. A further inclusion criterion for both the preHD and early manifest HD group consisted of a burden of pathology score greater than 250 ((CAG repeat length - 35.5) x age).[7,25] Healthy gene negative family members or partners were recruited as control subjects. None of the participants suffered from a concomitant neurological disorder, a major psychiatric diagnosis or had a history of severe head injury.

Table I. *Group characteristics and clinical scores*

		Healthy controls	preHD (A and B)	preHD-A	preHD-B	Manifest HD
N		24	22‡	11	11	10
Gender M/F		11/13	9/13	4/7	5/6	4/6
Age in years (at V1), mean (SD)		49.0 (8.2)	43.6 (8.7)	44.2 (5.7)	43.0 (11.2)	50.2 (9.3)
Handedness R/L		20/4	18/4	9/2	9/2	9/1
Level of education (ISCED), median (range)		4 (3)	4 (3)	4 (3)	4 (3)	4 (3)
DART-IQ, mean (SD)		105.0 (9.4)	100.5 (11.2)	101.3 (9.7)	99.6 (13.0)	101.8 (13.5)
CAG repeat length, mean (SD)		n/a	42.6 (2.7)	41.3 (1.4)	43.9 (3.1)^	42.5 (1.2)
Estimated years to onset, mean (SD)		n/a	11.8 (4.7)	14.9 (4.7)	8.6 (1.8)^	n/a
Total functional capacity, mean (SD)						
	V1	13.0 (0.2)	12.8 (0.5)	12.7 (0.7)	12.8 (0.4)	11.0 (1.5)Φ
	V2	12.9 (0.5)	12.6 (0.9)	12.7 (0.6)	12.5 (1.0)	10.3 (2.2)Φ
UHDRS-TMS, mean (SD)						
	V1	2.6 (2.5)	2.6 (1.5)	2.0 (1.5)	3.1 (1.2)	14.6 (7.7)Φ
	V2	2.1 (1.6)	5.7 (5.1) ¥	3.5 (2.2)	8.3 (6.1)*^	23.0 (12.1)Φ
SDMT, mean (SD)						
	V1	49.4 (8.9)	50.1 (11.0)	53.5 (9.3)	46.7 (11.9)	41.2 (9.2)Φ
	V2	50.9 (9.3)	50.6 (10.0)	54.7 (10.0)	46.6 (8.5)^	39.2 (10.6)Φ
SWR, mean (SD)						
	V1	100.1 (13.2)	91.9 (14.2)*	95.6 (9.6)	88.3 (17.3)*	87.7 (14.7)*
	V2	102.0 (15.6)	87.9 (15.7)*	91.4 (9.4)	84.4 (20.0)*	86.4 (18.6)*
BDI-II, mean (SD)						
	V1	4.1 (4.4)	6.4 (6.4)	4.9 (6.0)	7.9 (6.8)	10.2 (8.2)*
	V2	3.9 (4.1)	5.1 (5.6)	3.2 (4.9)	6.9 (5.9)	8.2 (8.4)
Between-scan interval in months, mean (SD)		23.0 (0.8)	23.0 (0.7)	23.2 (0.6)	22.7 (0.7)	23.5 (0.7)

*N = number of participants, SD = Standard deviation, n/a = not applicable, ISCED = International Standard Classification of Education, DART-IQ = Dutch Adult Reading Test Intelligence Quotient, CAG = Cytosine-Adenine-Guanine, UHDRS-TMS = Unified Huntington's Disease Rating Scale-Total Motor Score, SDMT = Symbol Digit Modalities Test, SWR = Stroop Word Reading task, BDI-II = Beck Depression Inventory-II, V1 = visit 1, V2 = visit 2. Significance at p ≤ 0.05 level: * significantly different from controls, Φ significantly different from controls and preHD, ¥ significantly different from controls and HD, ^ significantly different from preHD-A.*
‡ Including five subjects progressing to the early manifest stage during the two year follow-up period.

Hemispheric dominance was defined using a standardised neuropsychological questionnaire.[26] For preHD subjects, the predicted years to disease onset was calculated using the CAG repeat length and age-based survival analysis of Langbehn et al.[27]

As previously applied by Tabrizi et al.,[7] to assess the effect of expected proximity to disease onset on diffusion parameters, the preHD group was divided at baseline according to the median (10.9 years) for the predicted years to disease onset into preHD-A (≥ 10.9 years) and preHD-B (< 10.9). This resulted in two groups each consisting of eleven subjects (Table I).

The study was approved by the Medical Ethics Committee of the LUMC and written informed consent was obtained from all participants. For full details of study parameters, see Tabrizi et al.[7]

Clinical measures

To monitor disease state, the following clinical measures were evaluated longitudinally for all groups: UHDRS-TMS, TFC, Symbol Digit Modalities Test (SDMT), Stroop Word Reading (SWR) and Beck Depression Inventory-II (BDI-II) scores.

The UHDRS-TMS is the traditional measure which defines manifest disease state in HD. The SDMT and SWR in particular have been shown to be sensitive longitudinal neurocognitive measures in HD, independent of disease related motor effects.[28]

Magnetic resonance imaging acquisition

MRI acquisition was performed with a 3-Tesla whole-body scanner (Philips Achieva, Healthcare, Best, The Netherlands) with an eight channel SENSE head coil. T1-weighted image volumes were acquired using a 3D MPRAGE acquisition sequence with the following imaging parameters: TR = 7.7 ms, TE = 3.5 ms, FOV = 24 x 24 cm^2, matrix size 224 x 224, number of slices = 164, slice thickness = 1.00 mm, and no slice gap. A single-shot echo-planar diffusion tensor imaging sequence was applied with 32 measurement directions and the following scan parameters:[11] TR = 10,004 ms, TE = 56 ms, FOV = 220 x 220 mm^2 with an acquisition matrix of 112 x 110, 2.00 mm slice thickness, transversal slice orientation, no slice gap, flip angle = 90°, reconstruction voxel dimensions of 1.96 x 1.96 x 2.00 mm^3, number of slices = 64, *b*-value = 1,000 s/mm^2, halfscan factor = 0.61. Parallel imaging (SENSE) was used with a reduction factor of two, NSA = one, and fat suppression was applied. DTI acquisition time was 6.55 min.

Image processing

The DTI data was processed as described in Deprez et al.[29] In summary, this consisted of the following steps: (1) Correction for subject motion and eddy current induced distortions;[30] (2) Correction for echo planar images based deformations due to magnetic field inhomogeneities by registration to the T1-weighted images;[31] (3) Tensor estimation using the iteratively reweighted linear least squares approach after outlier detection and removal by REKINDLE ($\kappa = 6$).[32,33]

The brain regions were segmented into WM and GM regions (Figure 1) using SPM 8 with default settings (revision 4667, 27-Feb-2012).[34] Brain regions were left/right divided with the method described by Kuijf et al.[35]

Histogram analysis

A spherical erosion filter (radius 2 mm) was applied to the brain masks (WM/GM; left/right) to minimize the inclusion of partial-volume affected voxels.[36,37] The histograms of the diffusion measures were computed from these segmented brain regions. Subsequently, histograms were normalised by the number of voxels in each subject's data set to create the group mean histograms.[38]

With histogram analysis, frequency distributions of selected DTI measures of designated voxels can be obtained. While not providing any region-specific information, this type of analysis is highly sensitive in detecting differences as the entire brain is included. Moreover, it provides a straightforward, fully automated and objective approach for interrogating imaging data. The resulting summarizing whole-brain measures are suitable for comparing diffusion between groups[29] and its value has been previously demonstrated in multiple sclerosis and CADASIL.[39-41] This type of analysis can also be applied to any given selection of voxels of interest. Given the importance of the striatum in the histopathological profile of HD, diffusion values for this structure were additionally evaluated in this study. The following diffusion features for whole-brain WM were investigated: FA, MD, AD and RD. In addition, for the whole-brain GM (including striatum) the MD, AD and RD were studied. The outcome measures were the mean and distribution peak heights of the histograms. Because two outcome measures were tested against two tissue types, p-values for omnibus F-tests were Bonferroni corrected to adjust for the increased risk of type one error and considered to be statistically significant at $p \leq 0.05/4 = 0.0125$.

Obtaining striatal masks

Striatal masks were obtained as described previously.[42] In summary, T1-weighted images were segmented with the FAST and FIRST tools from the fMRI of the Brain Software Library (http://www.fmrib.ox.ac.uk/fsl/).[43-45] This provided individual brain masks for the following structures: the caudate nucleus and the putamen, both of these forming the striatum. Figure 1 shows such a segmentation result superimposed on a T1-weighted image. To correct for potential partial volume effects, an eroded mask of these segmentations was created by removing one voxel in-plane for all the aforementioned voxels of interest.

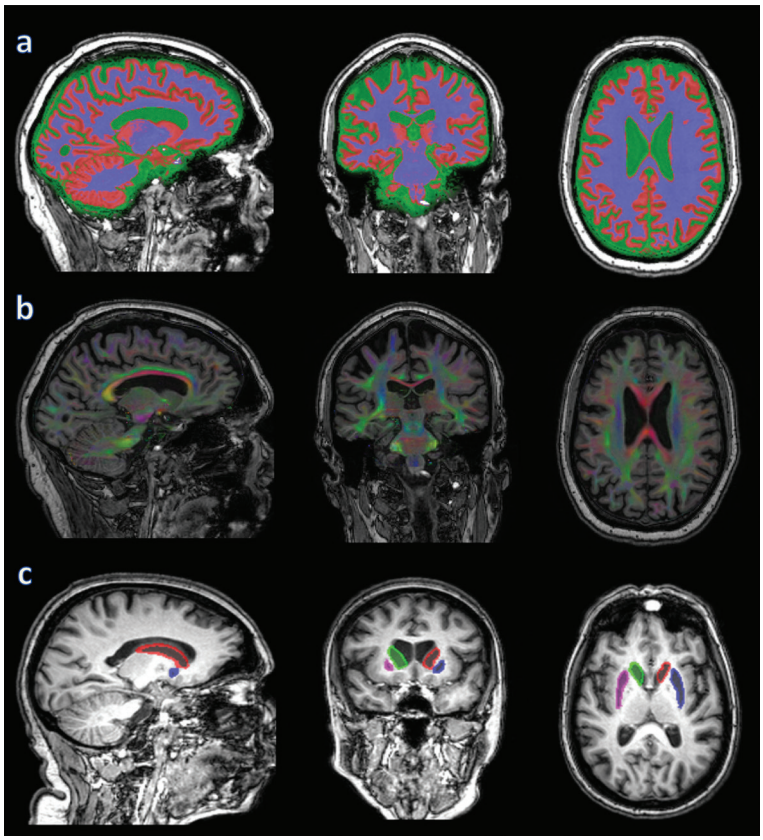

Figure 1. *From left to right: sagittal, coronal and axial images: a. brain segmentation into WM (blue), GM (red) and CSF (green); b. directionally colour encoded fractional anisotropy map; c. striatal mask: red = left caudate nucleus and blue = left putamen; green = right caudate nucleus and pink = right putamen.*

Statistical analysis

We used linear mixed models (in R version 3.0.0, R Foundation for Statistical Computing, Vienna, Austria) to model the various outcome variables with patient as a random factor to accommodate the within-person repeated nature of the data and to assess the effect of group, corrected for age at time of scanning as a co-variable. Correlations between neurocognitive measures and DTI findings were tested in the model.

Statistical analyses of group demographics were performed with SPSS (version 20, IBM, USA). Distributions and assumptions were checked. Either Analysis of Variance (ANOVA) or chi-squared tests were applied where this was appropriate. Potential longitudinal change in clinical measures between the groups was also investigated. Difference values were computed and an ANOVA was performed on these delta-scores to evaluate potential group differences. In case of a significant

omnibus F-test, exploratory post hoc analysis using Fisher's least significant difference was performed to assess which means were significantly different from each other. Differences in group demographics between preHD-A and preHD-B were compared using either independent samples t-tests or chi-squared tests, where appropriate.

Paired samples t-tests were performed to assess cross-sectional interhemispheric differences in DTI measures within the groups after excluding lefthanders. Lefthanders consisted of four control, four preHD and one manifest HD subjects. The longitudinal evolution of the interhemispheric diffusion measures was assessed with the aforementioned linear mixed model.

Table II. *Mean whole-brain DTI parameters. MD, AD and RD are shown x10³ for readability*

	Healthy controls	preHD (A and B)	preHD-A	preHD-B	Manifest HD
N	24	22	11	11	10
FA-WM	0.434 (0.008)	0.435 (0.012)	0.435 (0.014)	0.435 (0.014)	0.421 (0.014)Φ*
MD-WM	0.754 (0.010)	0.764 (0.016)	0.758 (0.017)	0.767 (0.017)	**0.783 (0.018)Φ*** **
MD-GM	0.767 (0.004)	0.777 (0.010)	0.768 (0.024)	0.778 (0.024)	**0.805 (0.012)Φ*** **
AD-WM	1.123 (0.005)	**1.140 (0.011)¥****	1.131 (0.012)	**1.149 (0.012)ə*** **	**1.172 (0.013)Φ*** **
AD-GM	0.924 (0.013)	0.934 (0.019)	0.923 (0.025)	0.938 (0.025)¤	**0.965 (0.021)Φ*** **
RD-WM	0.560 (0.011)	0.566 (0.017)	0.562 (0.019)	0.568 (0.019)	**0.589 (0.019)Φ*** **
RD-GM	0.702 (0.004)	0.711 (0.010)	0.706 (0.012)	0.716 (0.012)ˆ	**0.736 (0.012)Φ*** **

Data is shown as mixed model-based estimates of the group means corrected for age (S.E.)
*Φ significantly different from controls and preHD, ¥ significantly different from controls and HD, ə significantly different from controls, preHD-A and HD, *p ≤ 0.05 **p ≤ 0.01 ***p ≤ 0.001, bold values indicate sustained significant difference following Bonferroni correction (p ≤ 0.0125), ¤ p = 0.08, ˆ p = 0.07.*
FA = fractional anisotropy; MD = mean diffusivity; AD = axial diffusivity; RD = radial diffusivity; WM = white matter; GM = grey matter.

Results

Group characteristics and clinical scores

The groups did not differ significantly in terms of gender, handedness, level of education, intelligence quotient or body mass index. A trend toward a difference in age between the groups was found (p = 0.06), with premanifest subjects being generally younger compared to both controls and subjects with manifest HD. No statistical difference was found in CAG repeat count between preHD and manifest HD subjects. The between-scan interval was not significantly different between the groups.

At baseline, significantly lower scores for subjects with manifest HD were found in TFC, SDMT and SWR when compared to both controls and preHD subjects. Higher scores for subjects with manifest HD were found for UHDRS-TMS and BDI-II when compared to both controls and preHD

subjects. For the preHD group, a significantly lower baseline score compared to controls was found for SWR (Table I).

Repeated assessment after 2-year follow-up revealed similar score differences between the groups. Progression of five of the 22 preHD subjects to the early manifest stage during the follow-up period gave rise to a significantly higher UHDRS-TMS when compared to controls. The only significant difference in longitudinal change of clinical scores was found in higher UHDRS-TMS, both when considering the preHD group (including those progressing to the early manifest stage) and the manifest HD group. Other scores showed no significant longitudinal differences in this cohort (Supplementary Table I).

Comparing the preHD-A and preHD-B groups, no significant cross-sectional score differences were found during the first visit. At the second visit, the preHD-B group showed a significantly higher UHDRS-TMS and lower SDMT score compared to preHD-A.
Significant longitudinal change was found only in the UHDRS-TMS, where the difference was higher in preHD-B relative to preHD-A (Table I; longitudinal change data not shown).

Diffusion tensor imaging histogram measures

Diffusivity values of whole-brain white matter
At baseline, all whole-brain WM diffusivity measures in the manifest HD group differed significantly from both controls and preHD subjects (Table II): FA values were reduced and MD, AD and RD were increased. Upon applying Bonferroni correction for multiple testing, all these differences remained statistically significant except for the difference in FA (see Supplementary Figures 1 and 2 for group and visit histogram plots of WM FA, including separate plots for the left and right hemisphere). Elevations in MD, AD and RD were all highly significant ($p \leq 0.001$) (see Figure 2 for histogram plots of WM MD).

Only AD in the preHD group differed significantly from both controls and subjects with manifest HD and was lower for the controls and higher for subjects with manifest HD, even after applying Bonferroni correction ($p \leq 0.01$). No statistically significant differences in FA ($p = 0.83$), MD ($p = 0.10$) or RD ($p = 0.33$) were found between controls and preHD subjects.

Dividing the preHD group in preHD-A and preHD-B revealed higher AD values only in the preHD-B group compared to both preHD-A and controls, even after Bonferroni correction ($p \leq 0.001$). No significant differences were observed in any of the diffusivity measures between controls and preHD-A (Table II). No significant longitudinal differences were found in the degree of whole-brain WM diffusivity change in any of the measures between the groups (without correction for multiple testing).

Results of histogram peak height comparison of whole-brain WM are provided in Supplementary material.

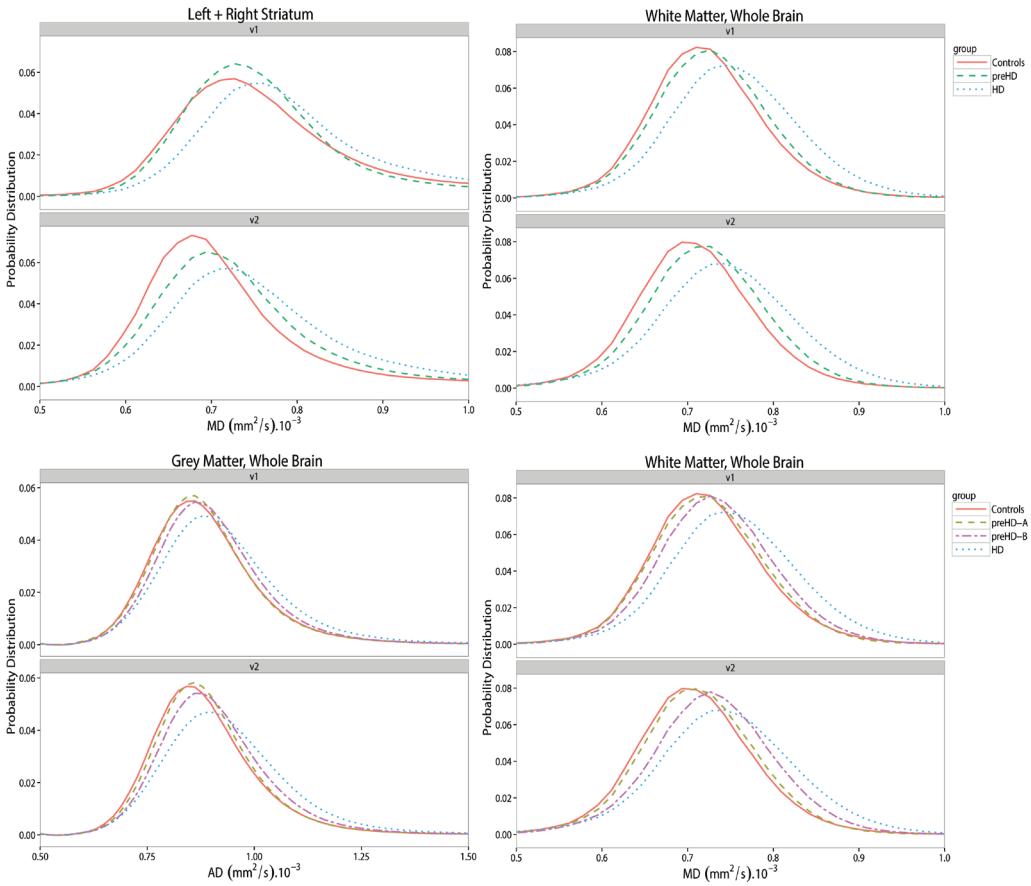

Figure 2. Histogram plots of MD (= mean diffusivity) and AD (= axial diffusivity) in whole brain white, grey matter and the striatum. Group diffusivities are plotted against the visits. v1 = visit 1, v2 = visit 2.

Diffusivity values of whole-brain grey matter and striatum

At baseline, MD, AD and RD values of whole-brain GM were significantly higher for the manifest HD group compared to both controls and preHD subjects ($p \leq 0.001$; Table II). This remained the case after Bonferroni correction for multiple testing. Figure 2 shows histogram plots for whole-brain GM AD.

No significant differences in whole-brain GM diffusivity measures were found between preHD subjects and controls. Upon dividing the preHD group in preHD-A and preHD-B, a trend was found in the preHD-B group toward higher values of AD and RD compared to controls ($p = 0.08$ and $p = 0.07$, respectively; Table II).

Baseline MD, AD and RD values in the striatum of subjects with manifest HD were significantly higher compared to both controls and preHD subjects (Table III). Upon applying Bonferroni correction for multiple testing, these differences remained statistically significant except for RD. See Figure 2 for group histogram plots of striatal MD. Separate plots for MD of the left and right striatum are shown in Supplementary Figure 3.

Table III. *Mean striatal DTI parameters. Values are of left and right striatum together. MD, AD and RD are shown x10³ for readability*

	Healthy controls	preHD (A and B)	preHD-A	preHD-B	Manifest HD
N	24	22	11	11	10
MD	0.686 (0.075)	0.695 (0.037)	0.648 (0.044)	0.758 (0.043)	**0.816 (0.045)Φ****
AD	1.130 (0.093)	1.177 (0.027)¤	1.127 (0.032)	**1.227 (0.031)Ǝ****	**1.235 (0.034)Φ****
RD	0.658 (0.108)	0.641 (0.039)	0.595 (0.048)	0.684 (0.047)	0.764 (0.049)Φ*

Data is shown as mixed model-based estimates of the group means corrected for age (S.E.)
*Φ significantly different from controls and preHD, Ǝ significantly different from controls and preHD-A, ¤ p = 0.08 (compared to controls), *p ≤ 0.05 **p ≤ 0.01, bold values indicate sustained significant difference following Bonferroni correction (p ≤ 0.0125). MD = mean diffusivity; AD = axial diffusivity; RD = radial diffusivity.*

No significant baseline differences in striatal diffusivity measures were found between preHD subjects and controls, only a trend toward a higher AD in the preHD group (p = 0.08). Upon dividing the preHD group in preHD-A and preHD-B, a significantly higher Bonferroni corrected striatal AD value was found in preHD-B only, compared to both controls and preHD-A ($p \leq 0.01$; Table III). Exploratory analysis to assess whether this effect was more prominent when assessing striatal substructures separately, revealed a trend towards AD elevation in the caudate and a significantly higher AD in the putamen in preHD-B (caudate: p = 0.06; putamen: p = 0.02) compared to both controls and preHD-A. This result was therefore less sensitive than the combined assessment of both substructures ($p \leq 0.01$), and would not have survived Bonferroni correction. No significant longitudinal differences were found in the degree of whole-brain GM or in striatal diffusivity change in any of the measures between the groups (without correction for multiple testing). Results of histogram peak height comparison of whole-brain GM and striatum are provided in Supplementary material.

Neurocognitive and diffusivity measures

In Table IV, significant correlations between neurocognitive measures and baseline whole- brain diffusivity measures are shown (correlations with peak heights are not shown). As no specific group effects were found on correlations between diffusion parameters and neurocognitive measures, the following applied to all participants included in the study with a CAG repeat expansion irrespective of their group. The SDMT score was found to predict WM FA ($p \leq 0.01$): the higher the SDMT score, the higher the FA (Supplementary Figure 4). The SDMT score was also found to predict WM MD ($p \leq 0.01$): the higher the SDMT score, the lower the MD (Figure 3).

The SWR score was found to predict GM MD ($p \leq 0.05$): the higher the SWR score, the lower the MD (Supplementary Figure 5). The SDMT score was found to predict peak height in GM MD ($p \leq 0.05$): the higher the SDMT score, the higher the peak height. The SDMT score was also found to predict peak height of WM AD ($p \leq 0.01$): the higher the SDMT score, the lower the peak height. Both SDMT and SWR scores were found to predict GM AD ($p \leq 0.05$): the higher the score, the lower the AD. The SDMT score was found to predict peak height of GM AD ($p \leq 0.05$): the higher the SDMT score, the higher the peak height.

The SDMT score was found to predict WM RD ($p \leq 0.01$): the higher the SDMT score, the lower the RD. In the striatum, the SDMT score alone was found to predict AD ($p \leq 0.05$): the higher the SDMT score, the lower the AD (data not shown).

Interhemispheric differences in diffusivity measures

In Supplementary Table III, baseline differences in diffusivity measures of the left minus right hemisphere are shown, both for WM and GM. Only right handed subjects were included for this analysis. Many small, though significant interhemispheric differences were found. The magnitude and direction of these differences were similar in all groups (controls, preHD and manifest HD) with no statistical significance in these differences between the groups.

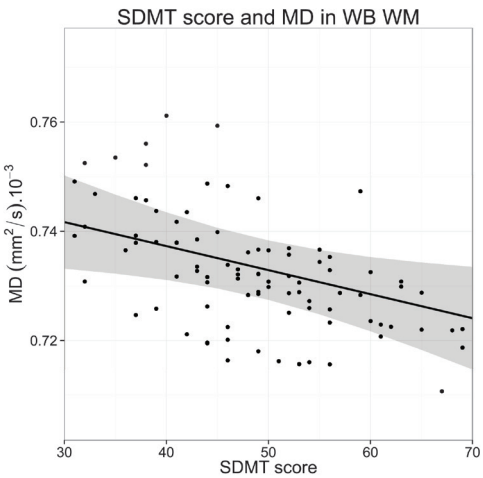

Figure 3. *Relationship plot of Symbol Digit Modalities Test (SDMT) score and whole brain (WB) white matter (WM) mean diffusivity (MD). Data points shown are mixed model-based estimates.*

No significant interhemispheric longitudinal differences between the groups were found in the degree of change of any of the diffusion measures of the WM, GM and the striatum, neither in the means nor histogram peak heights (without correction for multiple testing).

Table IV. *Mean whole-brain DTI parameters and neurocognitive measures correlations (corrected for age)*

	Diffusion parameter	SDMT score	*P*	Diffusion parameter	SWR score	*P*
FA-WM	↑ 1.2%	↑ 10 points	≤ 0.01	/	/	/
MD-WM	↓ 0.7%	↑ 10 points	≤ 0.01	/	/	/
MD-GM	/	/	/	↓ 0.4%	↑ 10 points	≤ 0.05
AD-WM	/	/	/	/	/	/
AD-GM	↓ 0.5%	↑ 10 points	≤ 0.05	↓ 0.4%	↑ 10 points	≤ 0.05
RD-WM	↓ 1.0%	↑ 10 points	≤ 0.01	/	/	/
RD-GM	/	/	/	/	/	/

This table is valid for all participants with a CAG repeat expansion included in the study, as no specific group effects were found on correlations between diffusion parameters and neurocognitive measures.
↑ = increase, ↓ = decrease, / = no significant correlation.
FA = fractional anisotropy; MD = mean diffusivity; AD = axial diffusivity; RD = radial diffusivity; WM = white matter; GM = grey matter.

Discussion

The major findings from this study were significantly higher MD, AD and RD values in both WM and GM in subjects with manifest HD compared to preHD and control subjects. In preHD subjects, only WM AD proved to be a sensitive measure to differentiate between the study groups. This finding remained valid only in preHD-B upon dividing the preHD group according to the median predicted years to onset. Another significantly different finding in preHD subjects was observed again only in preHD-B in a higher AD of the striatum compared to both controls and preHD-A. No significant longitudinal differences were found in any of the diffusivity measures between any of the groups, neither in the means nor peak heights. Finally, significant relationships between neurocognitive and diffusivity measures were demonstrated.

Findings of increased MD, AD and RD values in subjects with manifest HD are in line with results from previous reports.[46-48] Although a reduction in WM FA in manifest HD was found, this finding did not maintain significance after correction for multiple testing, rendering it a far less sensitive marker for disease state in HD. This finding of individual diffusivities providing more sensitive measures for revealing pathologic microstructural brain alterations compared to FA, was in line with findings from a previous study in HD and Alzheimer's disease.[16,48] The results presented here are also in agreement with previous findings by our group, where MD was reported to be a more sensitive measure than FA in distinguishing HD subjects from controls.[17] Just as in the Alzheimer's disease study of Acosta-Cabronero et al.,[16] changes found in this study were more prominent in AD than in RD, yet not enough to substantially influence FA. This provides a possible explanation for the seemingly discrepant findings of FA alterations in HD research, as the proportions of eigenvalues could be more specifically altered in studies of distinct WM regions giving rise to a modified FA.

The presence of an increased AD in whole-brain WM and in the striatum of preHD-B, provides evidence for ongoing neurodegeneration prior to disease manifestation, a finding that is echoed by results from previous MRI volumetric investigations in preHD.[4,6-8,49] Higher AD in preHD has been previously reported by Stoffers et al.,[6] although in that study this finding was highly localized and accompanied by more pronounced and widespread increases in RD, a finding which was not replicated here. Furthermore, in the study of Stoffers et al., RD seemed to correlate with the predicted years to disease onset, while AD lacked such correlation.[6] This stands in contrast to our findings of lack of significant increases in RD irrespective of preHD group stratification and higher AD being found primarily in preHD individuals who are closest to predicted years to disease onset. The discrepancy in these findings could very well be attributed to the differing methodologies applied in analysing the data and possibly due to the difference in scanner field strength used. In GM, no significantly different diffusivities were present between preHD subjects and controls, except for the above-mentioned higher AD in the striatum of preHD-B, which is a deep GM structure. The differences found in peak heights were only present in subjects with manifest HD, not in the preHD group, alluding to a less sensitive measure in detecting differences between manifest HD, preHD, and controls.

Exploration of the longitudinal evolution of diffusivity measures, without correction for multiple comparisons, provided no significant group differences. Results from previous longitudinal DTI studies in HD are heterogeneous. In the study of Weaver et al.,[19] significant longitudinal decreases in WM FA and AD were reported over a one year period. That study consisted of seven controls, four preHD and three manifest HD subjects, where the seven (pre)manifest subjects were compared to the controls. In another study by Sritharan et al.[20] with 17 controls and 18 manifest HD subjects, no longitudinal change in the MD of the caudate, putamen, thalamus and corpus callosum could be demonstrated over a one year period, while baseline MD was significantly higher in the caudate and putamen of subjects with manifest HD compared to controls. A similar finding in MD was reported by Vandenberghe et al.[18] in eight manifest HD subjects over a two year period. Results from the present study are in agreement with findings from the latter two studies, with significant cross-sectional differences found in combination with a lack of significant longitudinal differences in the evolution of these measures within the 2-year study-period. The lack of longitudinal differences in the diffusion profile between the groups in this study could be due to a low sensitivity of this approach in detecting small changes over time or due to a true absence of observable significant alterations of this profile using DTI in the 2-year time frame.

Relationships between neurocognitive and diffusivity measures were demonstrated in our study. The SDMT and SWR scores were associated with some diffusivity measures, where the SDMT seemed to be more readily associated with WM diffusivity measures, while SWR showed associations only with GM AD and MD. The only exception to this pattern in the whole-brain analysis, was the inverse relationship found between SDMT scores and GM AD values. These findings are important in light of selecting the most suitable cognitive measures to assess, depending on the prime target of a treatment intervention. The SDMT, considered to be a measure for information-processing speed and working memory, has also been found to be

more associated with white than grey matter lesions in multiple sclerosis.[50] In the current study, the SDMT provided for the best predictive value for baseline diffusivity measures, as reflected by both the magnitude as well as the statistical significance of these associations. As was the case in the recent study by Poudel et al.,[51] we found a significant inverse relationship between SDMT and WM RD in HD. Our results did not, however, reproduce their finding for the same inverse relationship with SWR. In the striatum, an inverse relationship was found only between the SDMT score and AD. This finding is reinforced by the recent morphometric analysis report in preHD by Harrington et al.,[52] where the SDMT score was found to be positively associated with putaminal volume.

Additional findings from our interhemispheric subanalysis of diffusion parameters revealed very small, though highly significant interhemispheric differences in diffusivity measures within the groups. There were, however, no indications for a preferential degeneration to the dominant hemisphere in (pre)HD subjects, as no significant group differences were found in interhemispherical diffusion parameters. To the best of our knowledge this is the first study exploring this hypothesis using DTI in (pre)HD subjects. Interhemispheric variations in diffusivity measures in the healthy human brain have been previously reported.[53,54]

It should be stressed that inferral of underlying alterations to biological substance through changes in eigenvalues is not trivial, especially in GM.[55,56] As such, it is quite challenging to draw solid conclusions about underlying neuropathology based on diffusion parameters. The progressive histopathological features of HD are numerous. Disturbed membrane systems of neurons, with derangement of all membranes that form the cell were found in a histological study by Tellez-Nagel et al.[57] Loss of small spiny neurons in the caudate and putamen with subsequent astrocytosis,[58] and decreased neuronal densities with increased oligodendroglial densities,[59] the latter found already in preHD,[60] have been described. The primary role of the oligodendrocyte is providing myelin to neuronal axons. In HD mouse models, inhibition of the peroxisome-proliferator-activated receptor gamma coactivator 1 α in oligododrocytes by mutant huntingtin was found to be responsible for abnormal myelination.[61] WM atrophy due to myelin breakdown is supported by histological and imaging examinations in HD subjects.[62] Significantly reduced total brain, GM and WM volumes through atrophy have been demonstrated through a post mortem study in seven HD brains.[63] These various, diverse changes could result in a competing influence on the diffusion tensor model based on the individual contributions and timing of each change. In a DTI-histological study of the quinolinic acid rat model of HD, Van Camp et al.[64] demonstrated that DTI was more sensitive in detecting subtle changes in the affected structures compared to histology. In that study, increases in MD, AD, and RD were detected six weeks after neurotoxin infusion as compared to the sham injected control group, with histological findings of necrotic cells involvement with shrunken cytoplasm and spongiosis.

In this study, the pattern found in the manifest HD group of higher MD, AD, and RD values without substantial changes to FA, likely reflects an increase in tissue permeability, extra- cellular space fluid and interaxonal spacing due to neural tissue loss,[65,66] allowing the three eigenvalues to grow

proportionally due to faster diffusion of water, hereby effecting only the size of the tensor without influencing its shape.[16] This pattern of diffusivity changes, which has been associated with chronic WM degeneration,[67,68] has previously been reported in HD[48] and other neurodegenerative disorders, such as amyotrophic lateral sclerosis[69] and hereditary spastic paraplegia.[70] Findings from the histologically verified DTI study of the quinolinic acid rat model of HD, suggest that this pattern could point to cytoplasmic alterations and spongiosis.[64] In our complete preHD cohort, only WM AD showed a significantly raised value compared to controls. Increased AD may indicate WM axonal atrophy and was suggested to be useful in identifying early changes in persons with a high risk at developing Alzheimer's disease, prior to cognitive decline.[71] Taken together, these findings suggest that both axonal degeneration as well as demyelination play an important role in WM pathophysiology of HD and are present throughout the entire brain. Given that the earliest detected abnormality is represented in the WM AD in preHD subjects, this could indicate that axonal degeneration precedes myelin abnormalities in WM at this stage of the neurodegenerative process, reinforcing findings by Hobbs et al.[48] and further supporting this hypothesis. The GM diffusivity findings presented here suggest that tissue boundaries become less well defined in the cortical ribbon and the striatum in HD.[55]

Strengths of this study include the longitudinal design which has the advantage of evaluating the evolution of diffusivity measures in a well-defined study group with a similar between-scan interval. All scans were acquired on the same scanner using the same protocol, which keeps test-retest variation in DTI to a minimum.[72] Exploration of the full tensor behaviour is a further strength, as demonstrated by the better sensitivity in revealing differences between the groups in this study relative to FA characteristics. For the whole-brain analyses we applied an automated histogram analysis, which reduces user error and provides a more suitable standardized analysis method in multicentre study settings. The limitation presented with whole-brain analysis is the loss of topographic information. Also, proper interpretation of the underlying biological causes to alterations found in the diffusion profile remains restricted, as many different fiber orientations are found in diffusion images of the brain.[73] That does not, however, preclude the ability of assessing the value of this type of analysis for identifying biomarker potential and tracking disease-related modifications to the diffusion profile in time. This limitation was nonetheless addressed by applying this analysis specifically to the striatum. A further limitation was the relatively low number of manifest participants. This was mainly driven by disease progression in the cohort, where longitudinal scans or the ability to comply with study protocol deemed impossible, leaving the outcome measures presented here to more likely be an underestimation of the true extent of diffusion disturbances in the HD brain.

To conclude, alterations in cross-sectional diffusion profiles between manifest HD subjects and controls were evident both in whole-brain and striatum. In preHD, only AD alterations were found, a finding that applied only to preHD-B upon group stratification. This suggests that AD may be a sensitive marker for early change in HD gene carriers prior to disease manifestation. The individual diffusivities proved to be more sensitive in distinguishing pathologic microstructural alterations to the HD brain than FA characteristics. This study showed no longitudinal differences in any

of the diffusivity measures between the groups. Larger study samples could provide additional information on the longitudinal biomarker potential of DTI measures. However, based on the results presented here, this potential is expected to be limited.

Acknowledgments

TRACK-HD is supported by CHDI/High Q Foundation Inc., a not for profit organization dedicated to finding treatments for Huntington's disease. The research of A.L. is supported by VIDI Grant 639.072.411 from the Netherlands Organisation for Scientific Research (NWO). The authors wish to thank Sarah Tabrizi, University College London, who is the global PI for TRACK-HD and clinical site PI for London. The authors also wish to extend their gratitude to the TRACK-HD investigators responsible for collecting the data and to the study participants and their families.

References

1 The Huntington's Disease Collaborative Research Group. A novel gene containing a trinucleotide repeat that is expanded and unstable on Huntington's disease chromosomes. Cell 1993;72:971-983.
2 Tobin AJ, Signer ER. Huntington's disease: the challenge for cell biologists. Trends Cell Biol. 2000;10:531-536.
3 Ross CA, Tabrizi SJ. Huntington's disease: from molecular pathogenesis to clinical treatment. Lancet Neurol. 2011;10:83-98.
4 Aylward EH, Liu D, Nopoulos PC, Ross CA, et al. Striatal volume contributes to the prediction of onset of Huntington disease in incident cases. Biol Psychiatry 2012;71:822-828.
5 Hadzi TC, Hendricks AE, Latourelle JC, et al. Assessment of cortical and striatal involvement in 523 Huntington disease brains. Neurology 2012;79:1708-1715.
6 Stoffers D, Sheldon S, Kuperman JM, et al. Contrasting gray and white matter changes in preclinical Huntington disease: an MRI study. Neurology 2010;74:1208-1216.
7 Tabrizi SJ, Langbehn DR, Leavitt BR, et al. Biological and clinical manifestations of Huntington's disease in the longitudinal TRACK-HD study: cross-sectional analysis of baseline data. Lancet Neurol. 2009;8:791-801.
8 Van den Bogaard SJ, Dumas EM, Ferrarini L, et al. Shape analysis of subcortical nuclei in Huntington's disease, global versus local atrophy--results from the TRACK-HD study. J Neurol Sci. 2011;307:60-68.
9 Vonsattel JP, Keller C, Cortes Ramirez EP. Huntington's disease - neuropathology. Handb Clin Neurol. 2011;100:83-100.
10 Basser PJ, Mattiello J, LeBihan D. MR diffusion tensor spectroscopy and imaging. Biophys J. 1994;66:259-267.
11 Jones DK, Leemans A. Diffusion tensor imaging. Methods Mol Biol. 2011;711:127-144.
12 Pierpaoli C, Jezzard P, Basser PJ, et al. Diffusion tensor MR imaging of the human brain. Radiology 1996;201:637-648.
13 Tournier JD, Mori S, Leemans A. Diffusion tensor imaging and beyond. Magn Reson Med. 2011;65:1532-1556.
14 Alexander AL, Lee JE, Lazar M, et al. Diffusion tensor imaging of the brain. Neurotherapeutics 2007;4:316-329.
15 Concha L. A macroscopic view of microstructure: Using diffusion-weighted images to infer damage, repair, and plasticity of white matter. Neuroscience 2014;276:14-28.
16 Acosta-Cabronero J, Williams GB, Pengas G, et al. Absolute diffusivities define the landscape of white matter degeneration in Alzheimer's disease. Brain 2010;133:529-539.
17 Dumas EM, van den Bogaard SJ, Ruber ME, et al. Early changes in white matter pathways of the sensorimotor cortex in premanifest Huntington's disease. Hum Brain Mapp. 2012;33:203-212.
18 Vandenberghe W, Demaerel P, Dom R, et al. Diffusion-weighted versus volumetric imaging of the striatum in early symptomatic Huntington disease. J Neurol. 2009;256:109-114.
19 Weaver KE, Richards TL, Liang O, et al. Longitudinal diffusion tensor imaging in Huntington's Disease. Exp Neurol. 2009;216:525-529.
20 Sritharan A, Egan GF, Johnston L, et al. A longitudinal diffusion tensor imaging study in symptomatic Huntington's disease. J Neurol Neurosurg Psychiatry 2010;81:257-262.
21 Lambrecq V, Langbour N, Guehl D, et al. Evolution of brain gray matter loss in Huntington's disease: a meta-analysis. Eur J Neurol. 2013;20:315-321.
22 Muhlau M, Gaser C, Wohlschlager AM, et al. Striatal gray matter loss in Huntington's disease is leftward biased. Mov Disord. 2007;22:1169-1173.
23 Rosas HD, Liu AK, Hersch S, et al. Regional and progressive thinning of the cortical ribbon in Huntington's disease. Neurology 2002;58:695-701.

24 Thieben MJ, Duggins AJ, Good CD, et al. The distribution of structural neuropathology in pre-clinical Huntington's disease. Brain 2002;125:1815-1828.
25 Penney JB, Jr., Vonsattel JP, MacDonald ME, et al. CAG repeat number governs the development rate of pathology in Huntington's disease. Ann Neurol. 1997;41:689-692.
26 Oldfield RC. The assessment and analysis of handedness: the Edinburgh inventory. Neuropsychologia 1971;9:97-113.
27 Langbehn DR, Brinkman RR, Falush D, et al. A new model for prediction of the age of onset and penetrance for Huntington's disease based on CAG length. Clin Genet. 2004;65:267-277.
28 Tabrizi SJ, Scahill RI, Durr A, et al. Biological and clinical changes in premanifest and early stage Huntington's disease in the TRACK-HD study: the 12-month longitudinal analysis. Lancet Neurol. 2011;10:31-42.
29 Deprez S, Billiet T, Sunaert S, et al. Diffusion tensor MRI of chemotherapy-induced cognitive impairment in non-CNS cancer patients: a review. Brain Imaging Behav. 2013;7:409-435.
30 Leemans A, Jones DK. The B-matrix must be rotated when correcting for subject motion in DTI data. Magn Reson Med. 2009;61:1336-1349.
31 Irfanoglu MO, Walker L, Sarlls J, et al. Effects of image distortions originating from susceptibility variations and concomitant fields on diffusion MRI tractography results. Neuroimage 2012;61:275-288.
32 Tax CMW, Otte WM, Viergever MA, et al. REKINDLE: Robust Extraction of Kurtosis INDices with Linear Estimation. Magn Reson Med. 2014;73:794-808.
33 Veraart J, Sijbers J, Sunaert S, et al. Weighted linear least squares estimation of diffusion MRI parameters: strengths, limitations, and pitfalls. Neuroimage 2013;81:335-346.
34 Ashburner J, Friston KJ. Unified segmentation. Neuroimage 2005;26:839-851.
35 Kuijf HJ, van Veluw SJ, Geerlings MI, et al. Automatic Extraction of the Midsagittal Surface from Brain MR Images using the Kullback-Leibler Measure. Neuroinformatics 2013;12:395-403.
36 Cercignani. Strategies for Patient-Control Comparison of Diffusion MR Data. In: Jones DK, editor. Diffusion MRI. Oxford University 2010;p 485-499.
37 Van den Boomgaard R, van Balen R. Methods for fast morphological image transforms using bitmapped binary images. Graphical Models and Image Processing 1992;54:252-258.
38 Roine U, Roine T, Salmi J, et al. Increased coherence of white matter fiber tract organization in adults with Asperger syndrome: a diffusion tensor imaging study. Autism Res. 2013;6:642-650.
39 Cercignani M, Inglese M, Pagani E, et al. Mean diffusivity and fractional anisotropy histograms of patients with multiple sclerosis. AJNR Am J Neuroradiol. 2001;22:952-958.
40 Vrenken H, Pouwels PJ, Geurts JJ, et al. Altered diffusion tensor in multiple sclerosis normal-appearing brain tissue: cortical diffusion changes seem related to clinical deterioration. J Magn Reson Imaging 2006;23:628-636.
41 Holtmannspotter M, Peters N, Opherk C, et al. Diffusion magnetic resonance histograms as a surrogate marker and predictor of disease progression in CADASIL: a two-year follow-up study. Stroke 2005;36:2559-2565.
42 Van den Bogaard SJ, Dumas EM, Milles J, et al. Magnetization transfer imaging in premanifest and manifest Huntington disease. AJNR Am J Neuroradiol. 2012;33:884-889.
43 Zhang Y, Brady M, Smith S. Segmentation of brain MR images through a hidden Markov random field model and the expectation-maximization algorithm. IEEE Trans Med Imaging 2001;20:45-57.
44 Patenaude B, Smith SM, Kennedy DN, et al. A Bayesian model of shape and appearance for subcortical brain segmentation. Neuroimage 2011;56:907-922.
45 Smith SM, Jenkinson M, Woolrich MW, et al. Advances in functional and structural MR image analysis and implementation as FSL. Neuroimage 2004;23 Suppl 1:S208-S219.

46 Bohanna I, Georgiou-Karistianis N, Sritharan A, et al. Diffusion tensor imaging in Huntington's disease reveals distinct patterns of white matter degeneration associated with motor and cognitive deficits. Brain Imaging Behav. 2011;5:171-180.
47 Della NR, Ginestroni A, Tessa C, et al. Regional distribution and clinical correlates of white matter structural damage in Huntington disease: a tract-based spatial statistics study. AJNR Am J Neuroradiol. 2010;31:1675-1681.
48 Hobbs NZ, Cole JH, Farmer RE, et al. Evaluation of multi-modal, multi-site neuroimaging measures in Huntington's disease: Baseline results from the PADDINGTON study. Neuroimage Clin. 2012;2:204-211.
49 Paulsen JS, Nopoulos PC, Aylward E, et al. Striatal and white matter predictors of estimated diagnosis for Huntington disease. Brain Res Bull. 2010;82:201-207.
50 Papadopoulou A, Muller-Lenke N, Naegelin Y, et al. Contribution of cortical and white matter lesions to cognitive impairment in multiple sclerosis. Mult Scler. 2013;19:1290-1296.
51 Poudel G, Stout JC, Dominguez DJ, et al. White matter connectivity reflects clinical and cognitive status in Huntington's disease. Neurobiol Dis. 2014;65:180-187.
52 Harrington DL, Liu D, Smith MM, et al. Neuroanatomical correlates of cognitive functioning in prodromal Huntington disease. Brain Behav. 2014;4:29-40.
53 Park HJ, Westin CF, Kubicki M, et al. White matter hemisphere asymmetries in healthy subjects and in schizophrenia: a diffusion tensor MRI study. Neuroimage 2004;23:213-223.
54 Yoshiura T, Noguchi T, Hiwatashi A, et al. Intra- and interhemispheric variations of diffusivity in subcortical white matter in normal human brain. Eur Radiol. 2010;20:227-233.
55 Beaulieu C. The basis of anisotropic water diffusion in the nervous system - a technical review. NMR Biomed 2002;15:435-455.
56 Jones DK, Knosche TR, Turner R. White matter integrity, fiber count, and other fallacies: the do's and don'ts of diffusion MRI. Neuroimage 2013;73:239-254.
57 Tellez-Nagel I, Johnson AB, Terry RD. Studies on brain biopsies of patients with Huntington's chorea. J Neuropathol Exp Neurol. 1974;33:308-332.
58 Vonsattel JP, Myers RH, Stevens TJ, et al. Neuropathological classification of Huntington's disease. J Neuropathol Exp Neurol. 1985;44:559-577.
59 Myers RH, Vonsattel JP, Paskevich PA, et al. Decreased neuronal and increased oligodendroglial densities in Huntington's disease caudate nucleus. J Neuropathol Exp Neurol. 1991;50:729-742.
60 Gomez-Tortosa E, MacDonald ME, Friend JC, et al. Quantitative neuropathological changes in presymptomatic Huntington's disease. Ann Neurol. 2001;49:29-34.
61 Xiang Z, Valenza M, Cui L, et al. Peroxisome-proliferator-activated receptor gamma coactivator 1 alpha contributes to dysmyelination in experimental models of Huntington's disease. J Neurosci. 2011;31:9544-9553.
62 Bartzokis G, Lu PH, Tishler TA, et al. Myelin breakdown and iron changes in Huntington's disease: pathogenesis and treatment implications. Neurochem Res. 2007;32:1655-1664.
63 Halliday GM, McRitchie DA, Macdonald V, et al. Regional specificity of brain atrophy in Huntington's disease. Exp Neurol. 1998;154:663-672.
64 Van Camp N, Blockx I, Camon L, et al. A complementary diffusion tensor imaging (DTI)-histological study in a model of Huntington's disease. Neurobiol Aging 2012;33:945-959.
65 Sen PN, Basser PJ. A model for diffusion in white matter in the brain. Biophys J. 2005;89:2927-2938.
66 Sotak CH. Nuclear magnetic resonance (NMR) measurement of the apparent diffusion coefficient (ADC) of tissue water and its relationship to cell volume changes in pathological states. Neurochem Int. 2004;45:569-582.

67 Burzynska AZ, Preuschhof C, Backman L, et al. Age-related differences in white matter microstructure: region-specific patterns of diffusivity. Neuroimage 2010;49:2104-2112.
68 Concha L, Gross DW, Wheatley BM, et al. Diffusion tensor imaging of time-dependent axonal and myelin degradation after corpus callosotomy in epilepsy patients. Neuroimage 2006;32:1090-1099.
69 Metwalli NS, Benatar M, Nair G, et al. Utility of axial and radial diffusivity from diffusion tensor MRI as markers of neurodegeneration in amyotrophic lateral sclerosis. Brain Res. 2010;1348:156-164.
70 Oguz KK, Sanverdi E, Has A, et al. Tract-based spatial statistics of diffusion tensor imaging in hereditary spastic paraplegia with thin corpus callosum reveals widespread white matter changes. Diagn Interv Radiol. 2013;19:181-186.
71 Gold BT, Johnson NF, Powell DK, et al. White matter integrity and vulnerability to Alzheimer's disease: preliminary findings and future directions. Biochim Biophys Acta 2012;1822:416-422.
72 Takao H, Hayashi N, Kabasawa H, et al. Effect of scanner in longitudinal diffusion tensor imaging studies. Hum Brain Mapp. 2012;33:466-477.
73 Jeurissen B, Leemans A, Tournier JD, et al. Investigating the prevalence of complex fiber configurations in white matter tissue with diffusion magnetic resonance imaging. Hum Brain Mapp. 2013;34:2747-2766.

Supplementary material

Peak heights of whole-brain white matter

At baseline, peak heights of whole-brain WM histograms were generally lower in the manifest HD group compared to controls and preHD subjects (Supplementary Table II). In the manifest HD group, significantly lower peak heights were found for MD and RD. These differences remained significant upon Bonferroni correction (both at $p \leq 0.01$).

In the preHD group, histogram peak heights were similar to controls. Dividing the preHD group in preHD-A and preHD-B revealed a significantly lower value in peak height of the RD of the preHD-B group compared to controls ($p \leq 0.05$). This difference did not survive Bonferroni correction.

No significant longitudinal differences were found in the degree of whole-brain WM peak height change in any of the measures between the groups (without correction for multiple testing).

Peak heights of whole-brain grey matter and striatum

At baseline, histogram peak heights of whole-brain GM MD and AD in the manifest HD group were significantly lower compared to controls and preHD subjects (Supplementary Table II; striatal data not shown). The difference in MD peak height did not survive correction for multiple testing, while AD peak height remained significant ($p \leq 0.001$). There was a trend towards a lower peak height of RD in manifest HD compared to controls and preHD ($p = 0.08$).

No significant baseline peak height differences were observed between preHD subjects and controls in whole-brain GM. Dividing the preHD group in preHD-A and preHD-B revealed a significantly lower value in AD peak height only in preHD-B compared to controls ($p = 0.05$), not surviving correction for multiple testing.

Baseline histogram peak heights of striatal MD and RD in subjects with manifest HD were significantly lower compared to controls and preHD subjects ($p \leq 0.01$ and $p = 0.03$, respectively). No significant peak height differences were observed between preHD subjects and controls in striatal diffusivity measures. Dividing the preHD group in preHD-A and preHD-B did not alter this result. No significant longitudinal differences were found in the degree of whole-brain GM nor in striatal histogram peak height change in any of the measures between the groups (without correction for multiple testing).

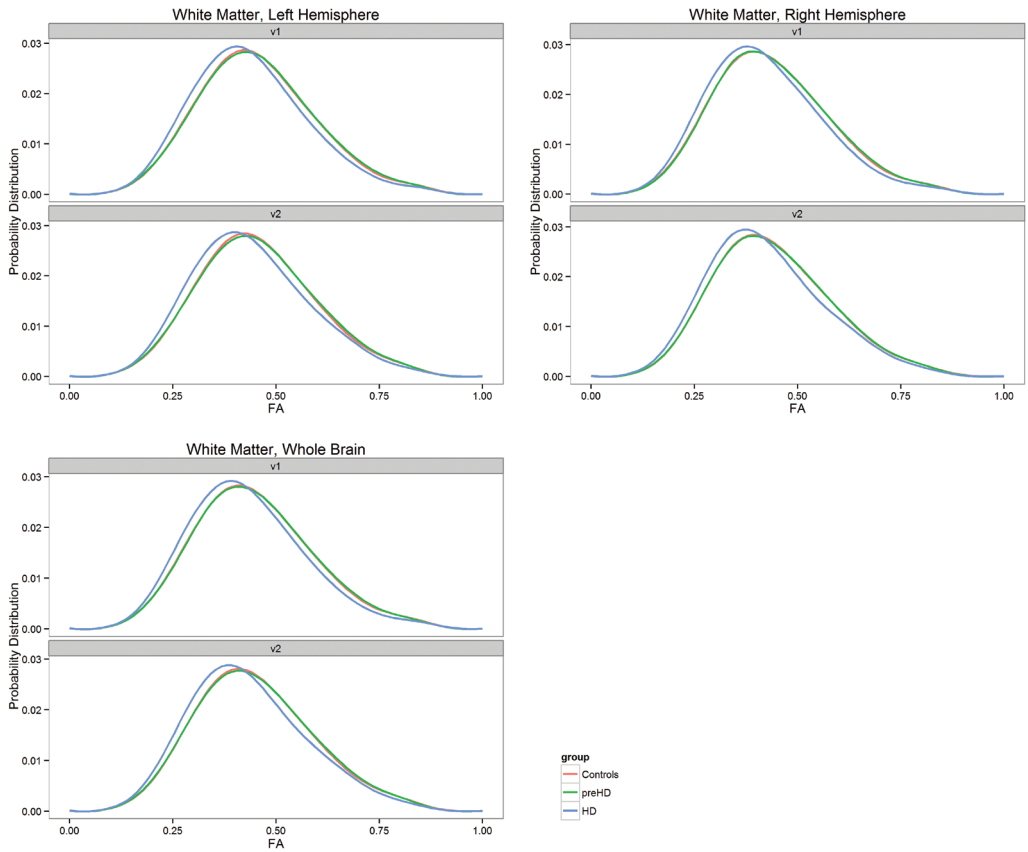

Supplementary Figure 1. *White matter fractional anisotropy (FA) histogram plots of the groups, per hemisphere and of whole brain, plotted against the visits. v1 = visit 1, v2 = visit 2.*

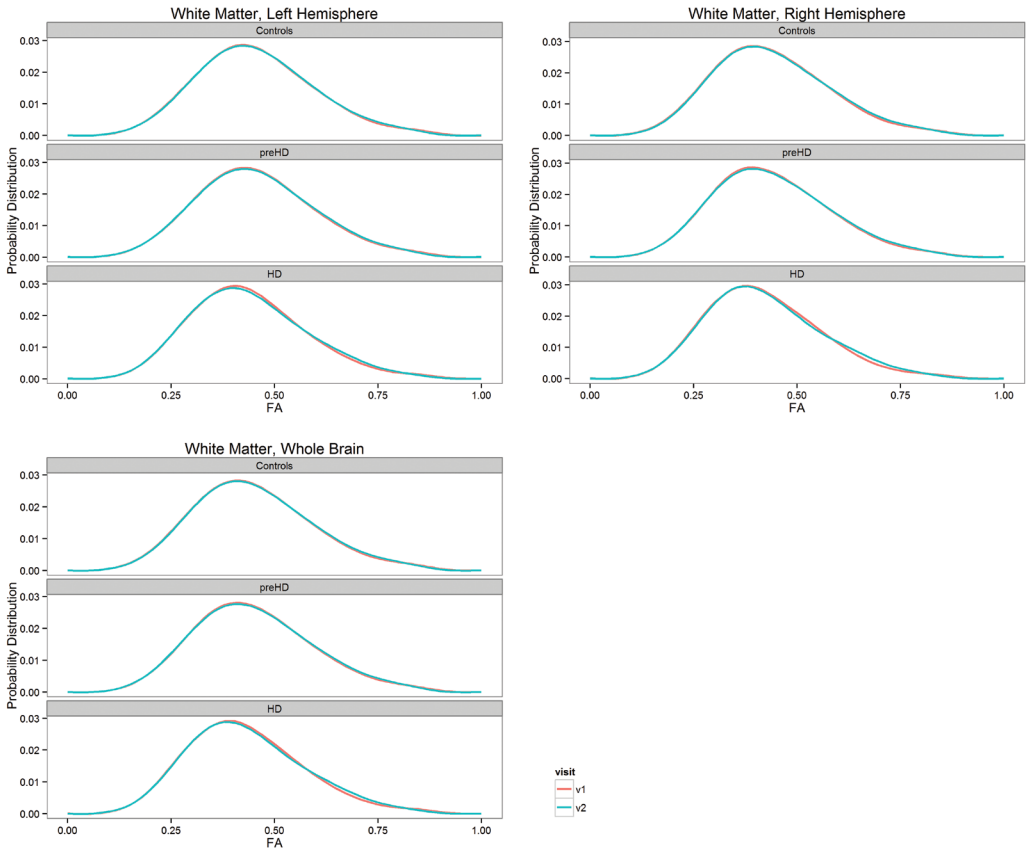

Supplementary Figure 2. *White matter fractional anisotropy (FA) histogram plots of the visits, per hemisphere and of whole brain, plotted per group. v1 = visit1, v2 = visit2.*

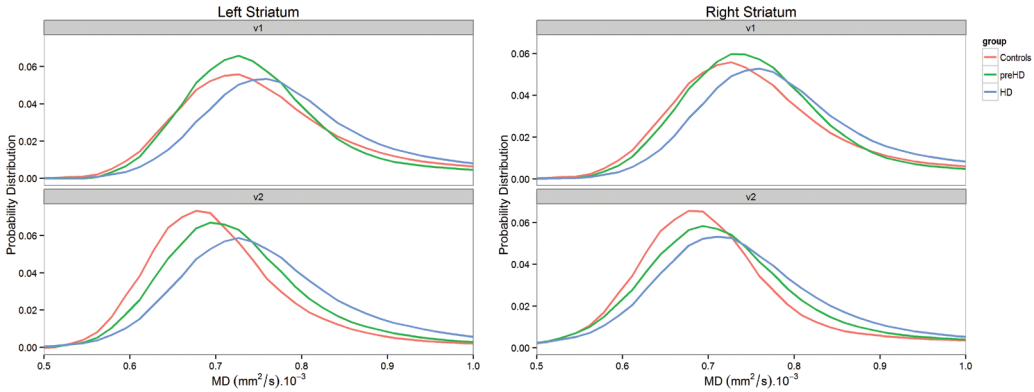

Supplementary Figure 3. *Separate plots for left and right striatal mean diffusivity (MD) histograms of the groups, plotted against the visits. v1 = visit 1, v2 = visit 2.*

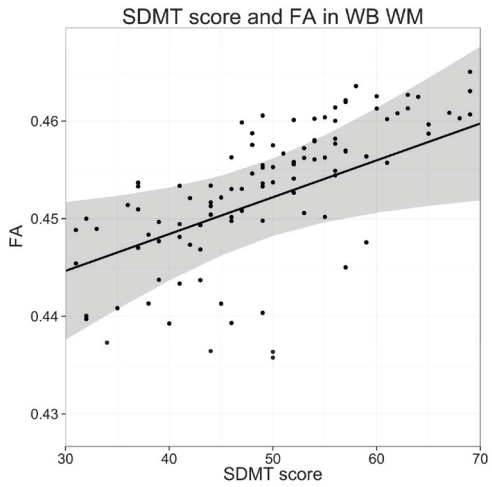

Supplementary Figure 4. *Relationship plot of Symbol Digit Modalities Test (SDMT) score and whole brain (WB) white matter (WM) fractional anisotropy (FA). Data points shown are mixed model-based estimates.*

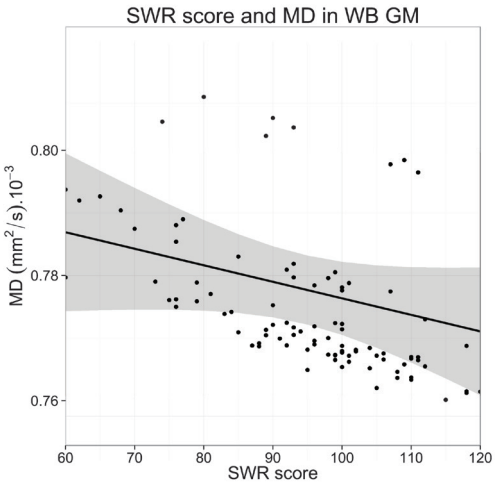

Supplementary Figure 5. *Relationship plot of Stroop Word Reading (SWR) task score and whole brain (WB) grey matter (GM) mean diffusivity (MD). Data points shown are mixed model-based estimates.*

Supplementary Table I. *Longitudinal change in clinical scores†, mean difference*

	Healthy controls	preHD (A and B)	Manifest HD
N	24	22‡	10
Total functional capacity, mean (SD)	-0.1 (0.5)	-0.2 (0.8)	-0.7 (1.7)
UHDRS-TMS, mean (SD)	-0.5 (2.3)	3.3 (4.5)*	8.4 (5.9)Φ
SDMT, mean (SD)	1.5 (5.8)	0.6 (6.3)	-2.0 (5.5)
SWR, mean (SD)	1.9 (8.7)	-4.1 (8.2)	-1.3 (10.9)
BDI-II, mean (SD)	-0.3 (3.7)	-1.4 (2.6)	-2.0 (4.1)

N = number of participants, SD = Standard deviation, UHDRS-TMS = Unified Huntington's Disease Rating Scale-Total Motor Score, SDMT = Symbol Digit Modalities Test, SWR = Stroop Word Reading task, BDI-II = Beck Depression Inventory-II.

*Significance at p ≤ 0.05 level: * significantly different from controls, Φ significantly different from controls and preHD.*

† Longitudinal change denotes scores from visit 1 subtracted from scores from visit 2.

‡ Including five subjects progressing to the early manifest stage during the two year follow-up period.

Supplementary Table II. *Mean DTI whole-brain peak height (shown $x10^3$ for readability). Data is shown as mixed model-based estimates of the group means corrected for age (S.E.)*

	Healthy controls	preHD (A and B)	Manifest HD
N	24	22	10
FA-WM	30.6 (1.2)	30.1 (1.6)	31.4 (1.7)
MD-WM	106.4 (7.3)	103.6 (10.0)	**96.8 (10.7)****
MD-GM	65.1 (5.1)	64.9 (6.7)	60.7 (7.1)*
AD-WM	31.1 (2.2)	34.6 (4.5)	34.3 (4.7)
AD-GM	64.4 (4.6)	62.5 (6.0)	**57.5 (6.4)*****
RD-WM	62.3 (3.0)	60.2 (4.1)	**58.6 (4.4)****
RD-GM	58.0 (4.7)	58.0 (6.1)	54.8 (6.5) (p=0.08)

**p ≤ 0.05 **p ≤ 0.01 ***p ≤ 0.001, bold values indicate sustained significant difference following Bonferroni correction (p ≤ 0.0125).*

FA = fractional anisotropy; MD = mean diffusivity; AD = axial diffusivity; RD = radial diffusivity; WM = white matter; GM = grey matter.

Supplementary Table III. *Interhemispheric differences in DTI measures from visit 1; values shown as left minus right hemisphere. Differences in MD, AD and RD are shown x10³ for readability. Only right handed subjects are included*

	Healthy controls		preHD (A and B)		Manifest HD	
N	20		18		9	
	Mean (SD)	*P*	Mean (SD)	*P*	Mean (SD)	*P*
FA-WM	0.017 (0.006)	≤ 0.001	0.017 (0.006)	≤ 0.001	0.016 (0.006)	≤ 0.001
MD-WM	-0.006 (0.006)	≤ 0.001	-0.005 (0.007)	0.018	-0.010 (0.007)	0.003
MD-GM	-0.006 (0.008)	0.008	-0.003 (0.009)	0.205	-0.004 (0.011)	0.272
AD-WM	0.007 (0.010)	0.003	0.009 (0.012)	0.005	0.002 (0.009)	0.605
AD-GM	0.001 (0.010)	0.681	0.001 (0.010)	0.631	0.004 (0.014)	0.377
RD-WM	-0.013 (0.006)	≤ 0.001	-0.012 (0.006)	≤ 0.001	-0.016 (0.008)	≤ 0.001
RD-GM	-0.009 (0.007)	≤ 0.001	-0.008 (0.010)	0.003	-0.008 (0.016)	0.174

FA = fractional anisotropy; MD = mean diffusivity; AD = axial diffusivity; RD = radial diffusivity; WM = white matter; GM = grey matter.

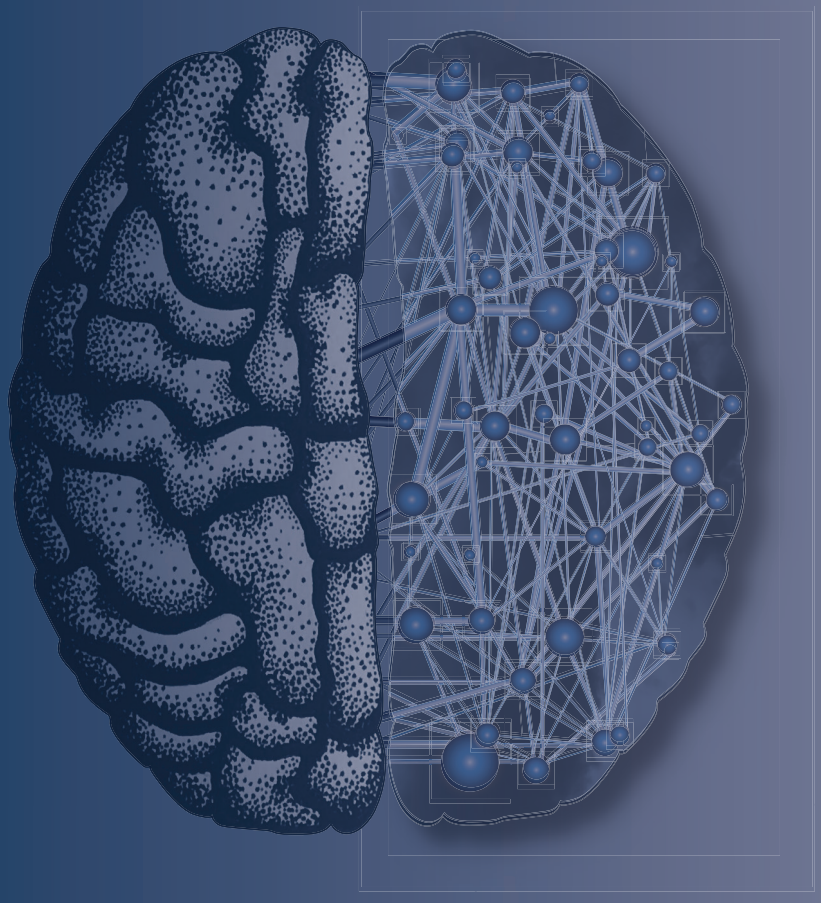

Dynamics of the connectome in Huntington's disease: a longitudinal diffusion MRI study

CHAPTER 4

4

Omar F.F. Odish[1]*, Karen Caeyenberghs[2]*, Hadi Hosseini[3],
Simon J.A. van den Bogaard[1], Raymund A.C. Roos[1], Alexander Leemans[4]

[1] Department of Neurology, Leiden University Medical Center, Leiden, The Netherlands
[2] School of Psychology, Faculty of Health Sciences, Australian Catholic University, Melbourne, Australia
[3] Department of Psychiatry and Behavioral Sciences, School of Medicine, Stanford University, Stanford, CA, USA
[4] Image Sciences Institute, University Medical Center Utrecht, Utrecht, The Netherlands
* Equal contribution

NeuroImage: Clinical 2015;9:32-43

Abstract

Background

Huntington's disease (HD) is associated with abnormal structure and function of different brain regions. Looking for reliable early markers for development of disease which may be too subtle to detect with conventional analysis methods, we applied graph theoretical analysis to diffusion magnetic resonance imaging data to assess both cross-sectional and time-related changes of the connectome in different stages of the disease.

Methods

We constructed weighted structural networks and calculated their topological properties. Twenty-two premanifest HD (preHD), 10 early manifest HD and 24 healthy controls completed baseline and two-year follow-up scans. We stratified the preHD group based on their predicted years to disease onset into a far (preHD-A) and near (preHD-B) to disease onset group. We collected clinical and behavioural measures per assessment time point.

Results

We found a significant reduction over time in nodal betweenness centrality both in the early manifest HD and preHD-B groups as compared to the preHD-A and control groups, suggesting a decrease of importance of specific nodes to overall network organization in these groups (FDR adjusted *ps* < 0.05). Additionally, we found a significant longitudinal decrease of the clustering coefficient in preHD when compared to healthy controls (FDR adjusted $p < 0.05$), which can be interpreted as a reduced capacity for internodal information processing at the local level. Furthermore, we demonstrated dynamic changes to hub-status loss and gain in both preHD and early manifest HD. Finally, we found significant cross-sectional as well as longitudinal relationships between graph metrics and clinical and neurocognitive measures.

Conclusions

This study demonstrates divergent longitudinal changes to the connectome in (pre) HD compared to healthy controls. This provides novel insights into structural correlates associated with clinical and cognitive functions in HD and possible compensatory mechanisms at play in preHD.

Introduction

Recent years have seen an increase in work pertained to finding and developing biomarkers for Huntington's disease (HD) and its premanifest stage (preHD). HD is an autosomal dominant neurodegenerative disorder caused by an elongated cytosine-adenine-guanine (CAG) repeat on the short arm of chromosome 4, which leads to the production of mutated huntingtin protein.[1] Prominent white and grey matter atrophy appear in the course of the disease.[2-5] This results in cognitive deterioration, including slower processing speed, attentional problems, executive control deficits and ultimately dementia, but also motor signs such as chorea, bradykinesia, rigidity and dystonia and psychiatric symptoms such as depression, anxiety and apathy.

Finding biomarkers that assess progression towards disease manifestation and follow disease advancement at the clinical stage, is of importance in the light of understanding the impact of intervention trials. One of the most promising methods currently being deployed to probe for biomarker potential is diffusion MRI, which can characterize tissue microstructure via the diffusion of water molecules.[6-9] Based on this technique, several cross-sectional studies in HD have provided evidence for abnormal structural organization of the brain, typically using region of interest and tract-based spatial statistics analyses.[10-14] However, findings from longitudinal reports using diffusion MRI in HD remain inconsistent.[15-17]

In the study by Weaver et al.,[17] the tract-based spatial statistics approach was used to compare scans from seven controls, four preHD and three manifest HD subjects obtained one year apart. Significant longitudinal decreases in white matter fractional anisotropy and axial diffusivity in the seven (pre)manifest subjects were found compared to the healthy controls. In another study by Sritharan et al. with 17 controls and 18 manifest HD subjects,[15] a region of interest approach did not reveal longitudinal changes in the mean diffusivity of the caudate, putamen, thalamus and corpus callosum over a one year period, while baseline mean diffusivity was found to be significantly higher in the caudate and putamen of subjects with manifest HD compared to controls. A similar finding for mean diffusivity was reported by Vandenberghe et al. in eight manifest HD subjects over a two year period,[16] also using a region of interest approach. These inconsistencies in the literature might very well be attributed to inconsistencies in defining the regions of interest or to other methodological limitations, such as those recently described for tract-based spatial statistics.[18] As longitudinal sensitivity to detecting disease progression is an essential quality of a biomarker, and given the abovementioned apparent lack of uniformity in previous longitudinal reports, we used a graph theoretical approach to analyse our data from a new perspective.

A graph theoretical analysis (GTA) is a powerful mathematical framework for quantifying topological properties of networks. This type of analysis moves away from the traditional neuroimaging approach of examining individual components of the brain, such as regions of interest, towards characterizing regional or global structure of networks. In recent years,

this paradigm shift from segregation to integration has emerged as a useful strategy for characterizing functional and structural brain networks in healthy and clinical groups, including other neurodegenerative diseases such as Alzheimer's disease,[19-23] neuroimmunological disorders such as multiple sclerosis,[24,25] but also in traumatic brain injury[26,27] and schizophrenia[28,29]. Using network based statistics, one recent cross-sectional study by Poudel et al. provided evidence for aberrant white matter cortico-striatal connectivity in HD compared to controls based on diffusion MRI data.[30] However, little research has been done on the dynamics of structural brain networks using a *longitudinal* design.

GTA may provide more insights into structural changes that can develop over the course of the condition, which may be too subtle to be detected at the local level. We therefore investigated network dynamics of the connectome in individuals from a well-defined cohort (TRACK-HD study, Tabrizi et al.)[31] assessed systematically and prospectively across multiple time points. This could provide new insights into the development of topological organization of whole-brain structural connectivity in HD, possibly providing usable markers quantifying disease progression. Such biomarkers can potentially be used, in turn, as targets for modification in therapeutic trial settings, especially in the premanifest phase where the priority lies in preventing or delaying manifestation of this devastating disorder. It is also important to examine potential associations between currently used cognitive and clinical measures in HD and (disrupted) network properties, thereby providing a more tangible 'real-world' sense to the complexity of brain structure and function.

Materials and methods

Participants

As part of the TRACK-HD study, 90 participants were included at baseline at the Leiden University Medical Center (LUMC) study site. Recruitment procedures and inclusion criteria have been published previously (for details see Tabrizi et al.)[5]. Diffusion MRI was added to the standard MRI protocol. At baseline, diffusion MRI was not performed in ten participants because of claustrophobia, and another nine were excluded from analysis due to excessive motion artefacts, which caused significant data corruptions, such as large signal dropouts and intra-volume inter-slice distortions. Such corrupted data sets were deemed unusable for inclusion in the study and were therefore not considered for further processing and analysis. Of the remaining 71 subjects, 62 subjects completed diffusion MRI scans at both visits with an average between-scan interval of 23 months. Of these 62, a further six subjects were excluded from analysis due to excessive motion artefacts at the second visit. The longitudinal cohort included in this work was thus comprised of 56 subjects: 24 healthy controls, 22 preHD and 10 early manifest HD subjects (Table I).

Inclusion criteria for the preHD group were a CAG repeat ≥ 40 with a total motor score on the Unified Huntington's Disease Rating Scale (UHDRS-TMS) ≤ five.[5] Moreover, to assess the effect of expected proximity to disease onset on diffusion parameters, the preHD group was divided at baseline according to the median (10.9 years) for the predicted years to disease onset into

preHD-A (≥ 10.9 years) and preHD-B (< 10.9). The predicted years to disease onset was based on a formula by Langbehn et al.[32] using CAG repeat length and age-based survival analysis. This resulted in two groups (preHD-A and preHD-B) each consisting of 11 subjects (Table I). Inclusion criteria for the early manifest HD group were a CAG repeat ≥ 40, with a UHDRS-TMS ≥ five and a Total Functional Capacity score (TFC) ≥ seven. For both the preHD and early manifest HD groups, a burden of pathology score greater than 250 ((CAG repeat length - 35.5) x age) was applied as a further inclusion criterion.[5,33] Healthy gene negative family members or partners were recruited as control subjects. None of the participants suffered from a concomitant neurological disorder, a major psychiatric diagnosis, or had a history of severe head injury.

Demographics, clinical information, and neurocognitive measures of interest are provided in Table I. From the neurocognitive battery administered, the Stroop Word Reading (SWR) task and the Trail Making Task (TMT) were chosen as measures of interest, as these tasks have shown promising results as cognitive disease-state markers in HD research.[31,34,35] In short, the SWR task consisted of the instruction of reading a set of words of colours (red, green and blue) as fast as possible within 45 seconds. The number of correct responses was computed using the number of items completed, with higher scores reflecting faster processing speed. The SWR has been used as a sensitive outcome measure in studies identifying predictors of longitudinal decline in HD, independent of disease related motor effects.[31] Furthermore, the TMT was administered which requires inhibition, updating, and switching, and consists of two parts, Trails A and Trails B. In Trails A, letters from A to Y are distributed across the page and participants are asked to draw lines connecting the letters from the alphabet in the right order, without lifting the pencil from the page. In Trails B, the page contains the numbers from 1 to 12 and letters from A to L and participants must connect the symbols by alternating the sequence between numbers and letters, that is, A-1-B-2-C-3...L-12. The dependent variable was the switch cost calculated by subtracting time to complete part A from part B. The validated Dutch version of the National Adult Reading Test (DART) was used to assess the intelligence quotient.[36] Finally, the Beck Depression Inventory-II (BDI-II) was administered, which is a 21-question multiple-choice self-report inventory, one of the most widely used instruments for measuring severity of depression. All participants completed both baseline as well as follow-up MRI, cognitive and clinical evaluation. The study was approved by the Medical Ethics Committee of the LUMC and written informed consent was obtained from all participants.

MRI acquisition

MRI acquisition was performed with a 3-Tesla whole-body scanner (Philips Achieva, Healthcare, Best, The Netherlands) using an eight channel SENSE head coil. T1-weighted image volumes were acquired using a 3D MPRAGE acquisition sequence with the following imaging parameters: TR = 7.7 ms, TE = 3.5 ms, FOV = 24 x 24 cm^2, matrix size 224 x 224, number of slices = 164, slice thickness = 1.00 mm, and no slice gap. A single-shot echo-planar diffusion tensor imaging sequence was applied with 32 measurement directions and the following scan parameters:[7] TR = 10,004 ms, TE = 56 ms, FOV = 220 x 220 mm^2 with an acquisition matrix of 112 x 110, 2.00 mm slice thickness, transversal slice orientation, no slice gap, flip angle = 90°, reconstruction voxel

dimensions of 1.96 x 1.96 x 2.00 mm^3, number of slices = 64, b-value = 1,000 s/mm^2, halfscan factor = 0.61. Parallel imaging (SENSE) was used with a reduction factor of two, NSA = one, and fat suppression was applied. Diffusion MRI acquisition time was 6.55 min.

Table I. *Group demographics with clinical and behavioural scores*

		Healthy controls	Premanifest HD (A and B)	preHD-A	preHD-B	Early manifest HD
N		24	22‡	11	11	10
Gender M/F		11/13	9/13	4/7	5/6	4/6
Age in years (at V1), mean (SD)		49.0 (8.2)	43.6 (8.7)	44.2 (5.7)	43.0 (11.2)	50.2 (9.3)
Handedness R/L		20/4	18/4	9/2	9/2	9/1
Level of education (ISCED), median (range)		4 (3)	4 (3)	4 (3)	4 (3)	4 (3)
DART-IQ, mean (SD)		105.0 (9.4)	100.5 (11.2)	101.3 (9.7)	99.6 (13.0)	101.8 (13.5)
CAG repeat length, mean (SD)		n/a	42.6 (2.7)	41.3 (1.4)	43.9 (3.1)^	42.5 (1.2)
Estimated years to onset, mean (SD)		n/a	11.8 (4.7)	14.9 (4.7)	8.6 (1.8)^	n/a
Total functional capacity, mean (SD)	V1	13.0 (0.2)	12.8 (0.5)	12.7 (0.7)	12.8 (0.4)	11.0 (1.5)Φ
	V2	12.9 (0.5)	12.6 (0.9)	12.7 (0.6)	12.5 (1.0)	10.3 (2.2)Φ
UHDRS-TMS, mean (SD)	V1	2.6 (2.5)	2.6 (1.5)	2.0 (1.5)	3.1 (1.2)	14.6 (7.7)Φ
	V2	2.1 (1.6)	5.7 (5.1)¥	3.5 (2.2)	8.3 (6.1)*^	23.0 (12.1)Φ
SWR, mean (SD)	V1	100.1 (13.2)	91.9 (14.2)*	95.6 (9.6)	88.3 (17.3)*	87.7 (14.7)*
	V2	102.0 (15.6)	87.9 (15.7)*	91.4 (9.4)	84.4 (20.0)*	86.4 (18.6)*
Switch cost of TMT in seconds, mean (SD)	V1	37.0 (17.4)	41.8 (24.6)	36.4 (15.9)	47.2 (30.9)	63.5 (41.6)Φ
	V2	38.9 (27.0)	38.0 (28.6)	30.8 (19.2)	45.8 (35.7)	75.0 (63.4)Φ
BDI-II, mean (SD)	V1	4.1 (4.4)	6.4 (6.4)	4.9 (6.0)	7.9 (6.8)	10.2 (8.2)*
	V2	3.9 (4.1)	5.1 (5.6)	3.2 (4.9)	6.9 (5.9)	8.2 (8.4)
Between-scan interval in months, mean (SD)		23.0 (0.8)	23.0 (0.7)	23.2 (0.6)	22.7 (0.7)	23.5 (0.7)

*HD = Huntington's disease, N = number of participants, SD = Standard deviation, n/a = not applicable, ISCED = International Standard Classification of Education, DART-IQ = Dutch Adult Reading Test Intelligence Quotient, CAG = Cytosine-Adenine-Guanine, UHDRS-TMS = Unified Huntington's Disease Rating Scale-Total Motor Score, SWR = Stroop Word Reading task, TMT = Trail Making Task, BDI-II = Beck Depression Inventory-II, V1 = visit 1, V2 = visit 2. Significance at p ≤ 0.05 level: * significantly different from controls, Φ significantly different from controls and pre-manifest HD, ¥ significantly different from controls and early manifest HD, ^ significantly different from preHD-A. ‡ Including five subjects progressing to the early manifest stage during the two year follow-up period.*

Diffusion MRI processing

Diffusion MRI data were analysed using the diffusion MR toolbox 'ExploreDTI'.[37] Data were corrected for subject motion, eddy current distortions, and susceptibility artefacts due to the magnetic field inhomogeneity prior to diffusion tensor estimation with the REKINDLE method.[37-40] Whole-brain fibre tractography was performed using constrained spherical deconvolution[41-43] with a uniform seed point resolution of 2 mm^3, an angle threshold of 30 degrees, a fibre orientation distribution threshold of 0.1, and maximum harmonic order of 4.

Connectivity matrices

One structural network was generated for each subject using the subject's diffusion MRI data. A network was defined as a set of nodes (denoting anatomical regions of the parcellation scheme) and interconnecting edges (denoting fibre trajectories between cortical and subcortical regional nodes that have been reconstructed). Moreover, we assigned a continuous weight (i.e., number of streamlines) to each edge of the graph, which resulted in weighted graphs. Because tractography does not differentiate between efferent and afferent fibres, the reconstructed graphs were all undirected. We describe here some of the major steps that we went through from diffusion MRI processing to computing the topological metrics of the graph. Figure 1 shows a flowchart for the process of obtaining connectivity matrices. The Automated Anatomical Labeling (AAL) atlas (and labels/masks)[44] was registered to the diffusion MRI data using a non-linear transformation[45] with fractional anisotropy as target image contrast[46]. The AAL atlas regions, which are commonly used to derive the nodes in GTA of neuroimaging data, are presented in Figure 2. The AAL template is not a pure cortical grey matter mask but includes tissues from both cortical grey matter and subcortical white matter.[44,47] Defining seed voxels throughout the brain parenchyma ensures that the computed trajectories originated from the white matter tissue underlying the cortical region or adjacent to subcortical structures. The average percentage of network tracts connecting a pair of regions was 2.39×10^{-4}. The numbers of streamlines connecting each pair of AAL regions were aggregated into a 90 x 90 connectivity matrix (the cerebellar regions were not included). We refer the interested reader to the online Supplementary video for a three-dimensional example of a resulting connectome (http://dx.doi.org/10.1016/j.nicl.2015.07.003).

Graph theory metrics

We used the Brain Connectivity Toolbox (BCT) (Rubinov and Sporns, https://sites.google.com/site/bctnet/)[48] and the longitudinal plugin of the Graph Analysis Toolbox,[49-51] to investigate network metrics of segregation, integration, and centrality. Network measures were computed over a range of density thresholds. Thresholding at an absolute value would have resulted in networks with different degrees across groups, introducing a confound when comparing measures between groups.[52] Network measures were examined over a range of network densities for which the networks were not fragmented (each node had at least one connection with another node in the graph) and displayed small- world properties (non-random graphs).[51] The network densities ranging from 0.10 to 0.40 fulfilled these criteria. We compared the networks in this density range in steps of 0.05. The graph metrics were quantified at both the network and regional levels from the weighted networks. The equations to calculate each of these measures can be found in Rubinov and Sporns (https://sites.google.com/site/bctnet/measures/list).[48] We only provide brief explanations for each of the network properties used in this study:

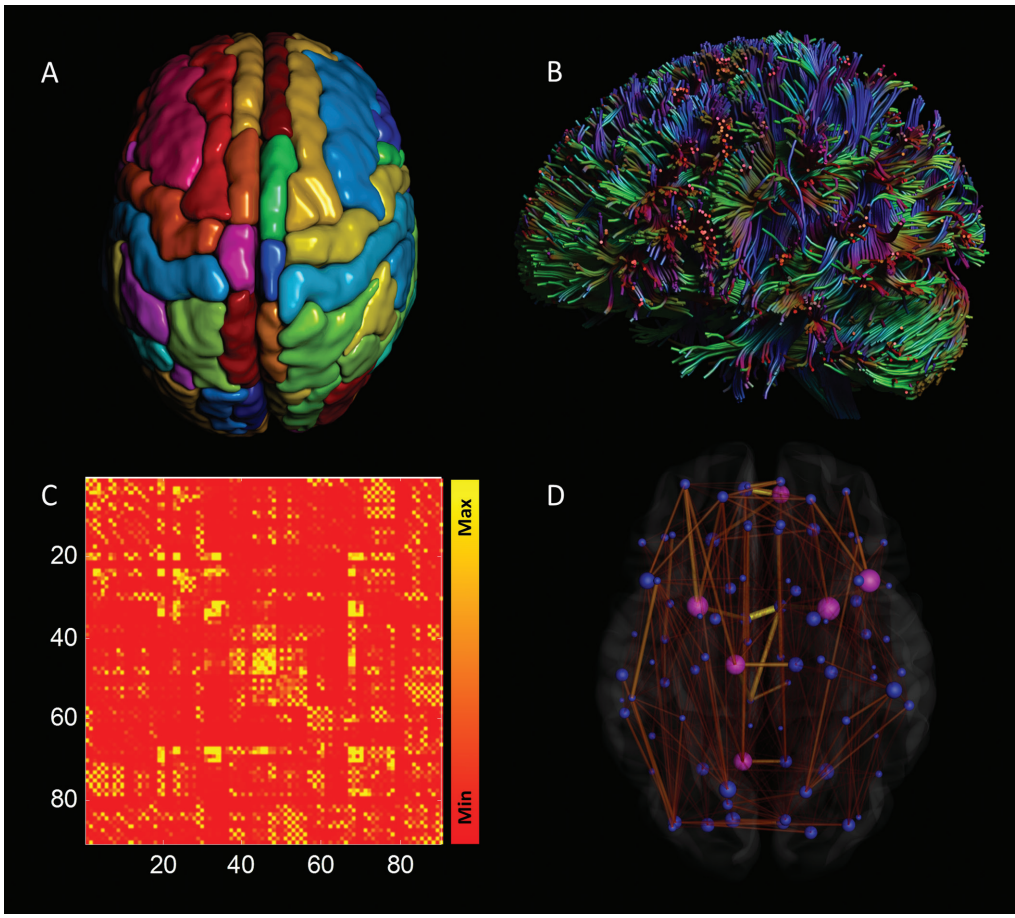

Figure 1. *Flow chart for constructing a diffusion MRI based network. (A) An Automated Anatomical Labeling (AAL) atlas template consisting of 90 cortical and subcortical brain regions, excluding the cerebellum, was used for brain segmentation. (B) Whole brain tractography was performed using ExploreDTI (see Materials and methods). (C) The numbers of streamlines connecting each pair of AAL regions were aggregated into a 90x90 weighted connectivity matrix. (D) The connectivity matrix was then visualized as a graph, composed of nodes representing brain regions and edges representing white matter connections. From the individual weighted brain networks, several network metrics were computed at both the global and regional levels.*

We quantified measures of network integration (characteristic path length) and segregation (clustering) for each network.[48] The characteristic path length L of a network is the average shortest path (distance) between all pairs of nodes in the network. It is defined as:

$$L = \frac{1}{n}\sum_{i \in N} \frac{\sum_{j \in N,\, j \neq i} d_{ij}}{n-1}$$

where d_{ij} is the shortest path length (distance) between nodes *i* and *j*. The global efficiency is the average inverse shortest path length in the network, and is inversely related to the characteristic path length.[53] In other words, networks with a small average characteristic path length are generally more efficient than those with large average characteristic path length. We also calculated local efficiency as a nodal graph metric. The regional efficiency is the global efficiency computed on node neighborhoods, and is related to the clustering coefficient.[54]

The clustering coefficient of a node is a measure of the number of edges that exist between its nearest neighbors and is quantified by counting the numbers of triangles formed around a node.[55,56] The clustering coefficient C of het network is the average clustering across all nodes and is quantified as:

$$C = \frac{1}{n}\sum_{i \in N} \frac{2t_i}{k_i(k_i - 1)}$$

where k_i is the number of connections (degree) for node i and *ti* is the number of triangles around a node *i*. The modularity is a graph metric that quantifies the degree to which the network may be subdivided into clearly delineated nonoverlapping groups of nodes in a way that maximizes the number of within-group edges, and minimizes the number of between- group edges. To evaluate the topology of the constructed networks, the obtained characteristic path length and clustering coefficient of each network were normalized to the corresponding mean values of null networks with the same degree-, weight- and strength-distributions as the network of interest,[57,58] using the null model algorithm implemented in BCT.[48]

We also computed the small-world index as the ratio of normalized clustering and normalized path length.[59,60] Thus, the small-worldness index of each network was obtained as $[C/C_{rand}]/[L/L_{rand}]$, where C_{rand} and L_{rand} are the mean clustering coefficient and the characteristic path length of random networks.[61] In a small-world network, the clustering coefficient is significantly higher than that of random networks (C/Crand ratio greater than 1), while the characteristic path length is comparable to random networks (L/Lrand ratio close to 1).

Finally, we have calculated node betweenness centrality, which is the fraction of all shortest paths in the network that contain a given node.[62] The betweenness centrality b_i of a node *i* is defined as:

$$b_i = \frac{1}{(N-1)(N-2)} \sum_{\substack{h,j \in G \\ h \neq j, h \neq i, j \neq i}} \frac{\rho_{hj\,(i)}}{\rho_{hj}}$$

in which *Phj* is the number of shortest paths between nodes h and j and *Phj(i)* is the number of shortest paths between nodes h and j that pass through node i. The nodes with the largest betweenness centrality can be considered to be pivotal nodes (i.e., hubs) in the network.

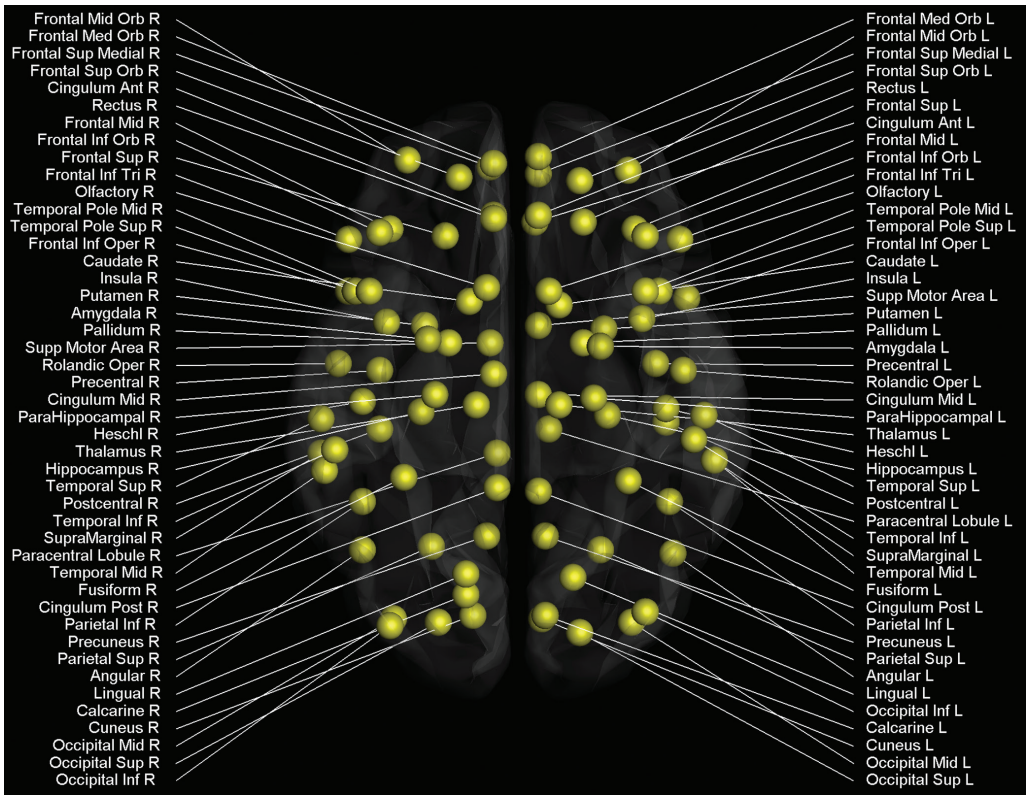

Figure 2. *Cortical and subcortical regions (45 in each hemisphere; 90 in total) as anatomically defined by the Automated Anatomical Labeling atlas template image in standard stereotaxic space.*

Statistical analysis

Interaction effects between group and time for the graph metrics were analysed using the Longitudinal plugin of the Graph Analysis Toolbox.[51,63] Specifically, networks were first normalized by the mean network strength and graph measures were quantified for the normalized networks. A non-parametric permutation test with 1000 repetitions was then used to test the statistical significance of the effects of time course for graph measures.[28,49] In each permutation, the calculated regional streamlines of each participant were randomly assigned to one of the two groups so that each randomized group had the same number of subjects as in the original groups. Finally, the actual difference in the slope between the original groups was compared to the obtained permutation distribution of difference in slope between randomized groups to obtain the p-value.

The same permutation procedure was used to test the significance of the differences in regional network measures. In this step, we compared regional network measures for the networks thresholded at minimum density. We obtained false discovery rate (FDR) corrected p-values as

measures of significance for the regional measures comparisons. In the present study, the p-values reported for regional differences between groups are FDR corrected for multiple comparisons (90 comparisons).

Baseline (i.e., visit 1) data of behavioural metrics (i.e., neurocognitive functioning scores) as well as graph metrics were used for cross-sectional analyses. A multivariate analysis of covariance (MANCOVA) was used, whereby statistical differences were assessed on multiple continuous dependent variables (graph metrics, cognitive and clinical variables) by an independent grouping variable (controls, preHD, early manifest HD), while controlling for a third variable (covariate). In the present study, age was added as covariate so that it could reduce error terms and so that the analysis eliminated the covariates' effect on the relationship between the independent grouping variable and the continuous dependent variables. We further subdivided the preHD group into two subgroups: preHD far from expected disease onset (preHD-A) and preHD close to expected disease onset (preHD-B).

To investigate the neuronal correlates of the behavioural tests, baseline data were analysed. Each participant's score on tests of clinical scales and neurocognitive functioning was correlated with that participant's graph metric (clustering coefficient, global efficiency, betweenness centrality) using partial correlations (age as confounding variable).

Our final aim was to investigate the relationship between changes in graph metrics with changes in behavioural performance. Difference scores for both behavioural performance and graph metrics were calculated as a measure of change by subtracting the visit 1 from the visit 2 scores.

Results

Baseline group comparison of demographic variables and performance in behavioural tests
Participants of the three groups (controls, preHD, early manifest HD) did not differ in terms of gender distribution ($p = 0.93$), handedness ($p = 0.95$), body mass index ($p = 0.64$) or intelligence quotient scores ($p = 0.38$). One-way ANOVAs revealed only a trend towards a difference in age between the groups ($p = 0.06$). Therefore, we included age as covariate in subsequent analyses. See Table I for group demographics and clinical and behavioural scores. The groups differed at baseline in their executive function performance (SWR and the switch cost of the TMT, all $ps < 0.05$). Post hoc Tukey testing showed significant differences between controls and (pre) HD groups.

Regional graph analyses
Graph metrics were evaluated at the nodal level to identify the nodes in the network that show a significant group by time interaction effect. Multiple testing correction was performed via False Discovery Rate (FDR),[64] where an FDR adjusted p-value < 0.05 was considered significant. The permutation test of the nodal betweenness centrality showed a significant group by time interaction for the left orbitofrontal cortex and left paracentral lobule (adjusted $ps < 0.05$). The

post-hoc two-sided Tukey t-test demonstrated a decrease of the betweenness centrality of the left orbitofrontal cortex in the early manifest HD group as compared to the control group ($p < 0.001$), from the first to the second visit. Moreover, preHD-B patients versus controls demonstrated a reduction of betweenness centrality of the left paracentral lobule from visit 1 to visit 2 ($p < 0.001$). Finally, the permutation test of the clustering coefficient revealed a significant group by time interaction for the left medial prefrontal cortex (adjusted $p < 0.05$). The post-hoc two-sided Tukey t-test showed that preHD showed a decrease of the clustering coefficient of the left medial prefrontal cortex compared to the healthy controls from visit 1 to visit 2 ($p = 0.02$) .

Important network regions as defined by hub-status in visits 1 and 2

Betweenness centrality was also used to identify the hub regions. In visit 1, the left precuneus was shared by all groups. Generally, a lower number of areas functioned as network hubs in visit 2 and a remarkable change in hub-status was apparent for regions in visit 2 in each group (as shown in Figure 3). Specifically in the early manifest HD group, the left thalamus and right medial part of the superior frontal gyrus achieved hub-status in visit 2. Also, many regions lost their hub-status in visit 2 within the early manifest HD group. Such areas included the left superior temporal pole, right lingual gyrus, right calcarine gyrus, and left middle occipital gyrus. The preHD group also showed hub-changes from visit 1 to visit 2, whereby the right medial part of the superior frontal gyrus lost hub-status. One brain region, the right superior parietal gyrus, achieved hub-status in visit 2. Network nodes in the precuneus, superior temporal pole, and putamen were consistently important as hubs throughout visits 1 and 2 in the preHD group.

Table II. *Graph metrics. Data is shown as mean and standard error of the groups for each visit*

			Healthy controls		Premanifest HD (A and B)		preHD-A		preHD-B		Early manifest HD	
			Mean	SE	Mean	SE	Mean	SE	Mean	SE	Mean	SE
Global network metrics	Global efficiency	V1	0.034	0.0004	0.034	0.0004	0.034	0.0007	0.034	0.0005	0.033	0.0009
		V2	0.035	0.0004	0.034	0.0005	0.034	0.0008	0.034	0.0005	0.033	0.0009
	Characteristic path length	V1	0.110	0.0025	0.111	0.0029	0.112	0.0047	0.109	0.0035	0.107	0.0056
		V2	0.115	0.0027	0.112	0.0033	0.111	0.0056	0.112	0.0036	0.108	0.0057
Small world metrics	Gamma	V1	1.620	0.0309	1.616	0.0307	1.652	0.0413	1.581	0.0448	1.535	0.0578
		V2	1.648	0.0300	1.594	0.0361	1.605	0.0591	1.583	0.0442	1.524	0.0530
	Lambda	V1	1.058	0.0022	1.059	0.0025	1.063	0.0034	1.056	0.0036	1.055	0.0056
		V2	1.057	0.0021	1.056	0.0024	1.055	0.0034	1.057	0.0036	1.053	0.0055
	Sigma	V1	1.530	0.0280	1.525	0.0261	1.553	0.0349	1.496	0.0383	1.453	0.0491
		V2	1.558	0.0266	1.508	0.0316	1.520	0.0517	1.496	0.0387	1.446	0.0433
Local network metrics	Local efficiency	V1	0.051	0.0008	0.051	0.0007	0.051	0.0011	0.050	0.0008	0.049	0.0014
		V2	0.052	0.0007	0.051	0.0008	0.051	0.0014	0.051	0.0010	0.049	0.0015
	Clustering coefficient	V1	0.027	0.0004	0.027	0.0004	0.028	0.0006	0.027	0.0003	0.026	0.0005
		V2	0.027	0.0003	0.027	0.0003	0.027	0.0005	0.027	0.0005	0.026	0.0006
	Modularity	V1	0.319	0.0072	0.315	0.0077	0.326	0.0122	0.304	0.0086	0.291	0.0147
		V2	0.327	0.0063	0.310	0.0091	0.315	0.0141	0.304	0.0120	0.294	0.0129
	Betweenness centrality	V1	90.836	1.0122	91.799	1.1947	92.321	1.8961	91.277	1.5313	89.942	2.5538
		V2	91.835	1.0970	91.100	1.2774	90.806	2.2531	91.394	1.3265	89.436	2.5774

HD = Huntington's disease, V1 = visit 1, V2 = visit 2.

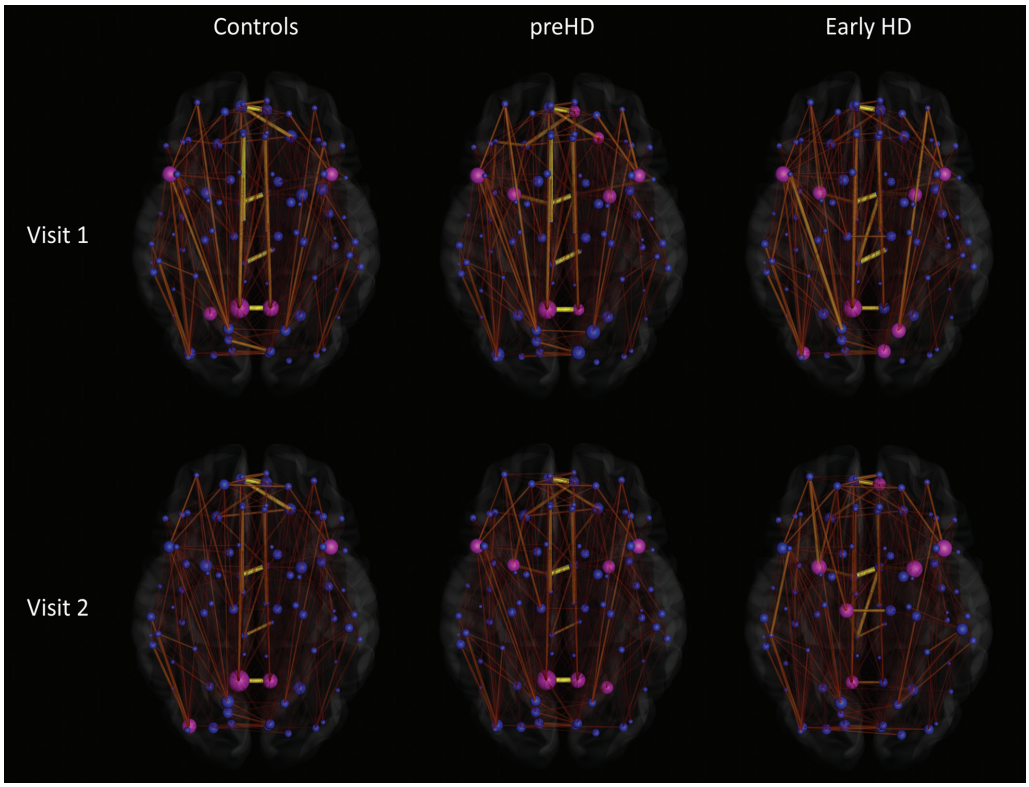

Figure 3. Group differences in betweenness centrality. Upper panel: visit 1, lower panel: visit 2. Size of the nodes (spheres) represents the betweenness centrality. Size of the edges (connections) represents streamline count. Magenta as colour of the nodes refers to hub regions.

Overall dynamics of the structural brain network

Both (pre-) HD and healthy controls showed a small-world organization of the structural brain networks (as shown in Table II) expressed by a normalized clustering coefficient gamma >1 (mean|SD; preHD: 1.62|0.14, early manifest HD: 1.54|0.18, healthy participants: 1.62|0.15) and lambda ~1 (mean|SD; preHD: 1.06|0.01, early manifest HD: 1.06|0.02, healthy participants: 1.06|0.01). The small-worldness (sigma) calculated from these indices was also larger than 1 (mean|SD; preHD: 1.52|0.12, early manifest HD: 1.45|0.16, healthy participants: 1.53|0.14). Furthermore, looking at the overall organization characteristics of the brain networks of patients, the normalized clustering coefficient gamma did not differ between preHD, early manifest HD, and healthy controls ($p = 0.31$), nor did the overall normalized path length lambda ($p = 0.69$). In summary, preHD and early manifest HD patients displayed gamma and lambda values close to the values of the brain networks of the healthy controls, suggesting an intact overall organization of the structural brain network in these disease stages.

Between-group differences in baseline graph metrics

Premanifest and early manifest HD patients did not show strong alterations (all *ps* > 0.05) in whole-brain graph metrics (Table II). The absence of these group effects suggests that global connectivity is relatively intact in early HD.

Baseline relationships between graph metrics and performance in behavioural benchmark tests

There was a significant negative correlation within the preHD group between baseline individual differences in the switch cost of the TMT on the one hand, and clustering coefficient (r = -0.44, p = 0.05) and local efficiency (r = -0.45, p = 0.04), on the other hand (see Figures 4A and B). Hence, better performance on the TMT (i.e., lower switch cost) was associated with an increase in efficiency and clustering coefficient within the preHD group. Using the subdivision, we found that the switch cost of the TMT was significantly negatively correlated with clustering coefficient (r = -0.78, p = 0.008, survived Bonferroni correction) and the local efficiency (r = -0.69, p = 0.03) within the preHD-B group. Moreover, within the preHD-B group, we also observed a positive correlation between the performance on the SWR and global efficiency (r = 0.62, p = 0.05, Figure 4C), with higher global efficiency being related to better performance on SWR.

Baseline relationships between graph metrics and burden

No significant correlations were found between burden and the graph organizational characteristics in the preHD or early manifest HD groups using a Bonferonni correction or even an exploratory uncorrected threshold of $p \leq 0.05$. From this, we cautiously conclude that burden did not explain our findings.

Longitudinal changes in benchmark behavioural tasks and graph metrics

For the investigation of longitudinal changes on the dependent variables of the behavioural tasks and graph metrics, we subjected each behavioural parameter and graph measure separately to a 2 x 3 permutation test with the between-subject factor group (controls, preHD, early manifest HD) and the within-subject factor time (visit 1, visit 2), while statistically controlling for the effects of age.

We observed a significant group by time interaction effect for the motor score ($F_{(2, 52)}$ = 17.62, p < 0.001). Post-hoc Tukey t-tests revealed that the early manifest HD group had an increased motor score (i.e., more motor abnormalities) compared to the preHD and healthy control groups. These group differences were even larger on the second visit (*ps* < 0.05). Also, main effects of the factor group were observed for TFC, SWR, and TMT. The subsequent post-hoc Tukey t-tests indicated generally higher performance for the controls compared to the early manifest HD group across both assessment times (*ps* < 0.001). Furthermore, post-hoc Tukey t-tests showed significantly superior performance on these behavioural tasks for the preHD group compared to the early manifest group (*ps* < 0.05).

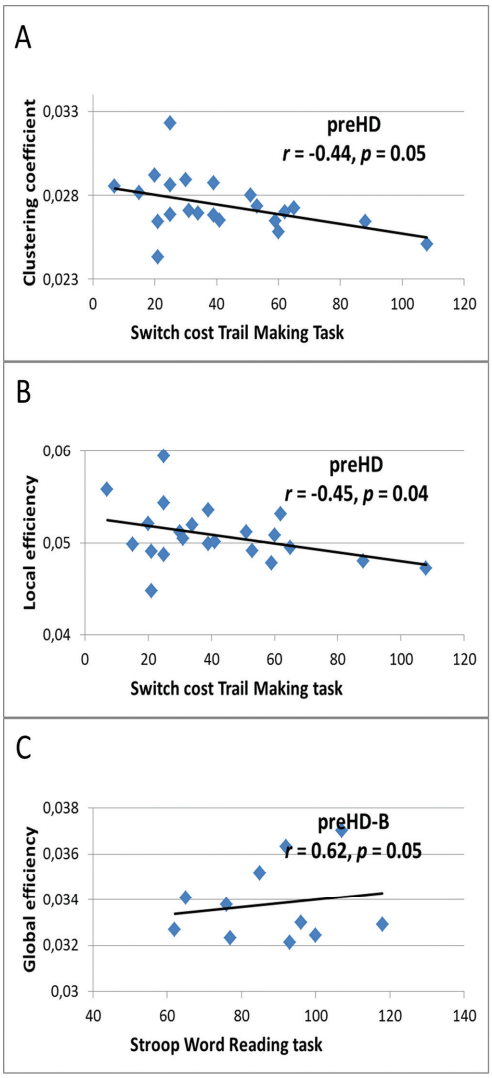

Figure 4. Baseline correlations between network measures and cognitive performance.

The permutation test on modularity showed a significant effect of group, ($F_{(2, 52)}$ = 3.58, p = 0.04, see Figure 5A). Across both assessment times, the control group had a larger modularity than the preHD-B and the early manifest HD group (*ps* < 0.05). Furthermore, a trend was observed for the effects of group by time on the normalized clustering coefficient (p = 0.08) and small-worldness (p = 0.06, Figure 5B), indicating a trend of increased 'wiring-efficiency' for the control group compared to the (pre) HD groups. Similar results were obtained with the statistical analyses with four groups.

Correlations between changes in graph metrics and changes in performance on tasks of executive functioning and clinical scales

Partial correlations (with age as confounding variable) between changes in graph metrics from visit 1 to visit 2 in the different groups and the concomitant alterations in the behavioural parameters showed moderate associations between changes in structural network connectivity and the changes in performance on tasks of executive functioning and clinical scales. For the early manifest HD group, there were correlations between the changes in motor score and changes in small-worldness (r = -0.67, p = 0.05, exploratory threshold, see Figure 6A). In other words, a decrease in 'wiring-efficiency' was associated with a higher motor score (i.e., more motor symptoms) in the early manifest HD group.

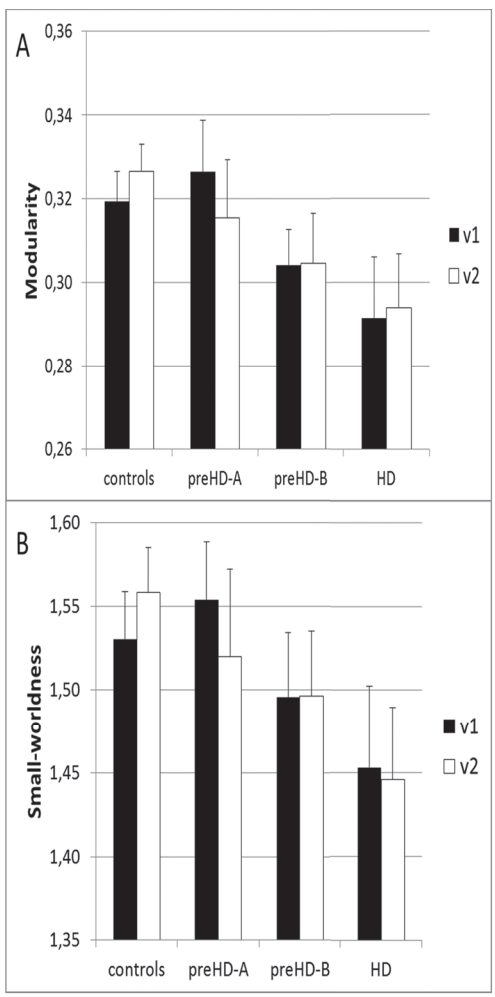

Figure 5. *Longitudinal changes of graph metrics. Visit 1, black bars; visit 2, white bars.*

For the combined preHD group, there was a significant negative correlation between normalized path length and scores on BDI-II, pairing more depression symptoms reported with decreased global integration (r = -0.58, p = 0.006, survived Bonferroni correction, Figure 6B). For the preHD-B group, correlations were present between changes in scores on the BDI-II and changes in betweenness centrality (r = -0.80, p = 0.006, survived Bonferroni correction), normalized path length (r = -0.84, p = 0.002, survived Bonferroni correction), global (r = -0.64, p = 0.05, exploratory threshold) and local efficiency (r = -0.66, p = 0.04, exploratory threshold), pairing more symptoms reported on BDI-II with reduced structural connectivity. Furthermore, the difference score of the switch cost of the TMT was significantly negatively correlated with changes in the clustering coefficient (r = -0.69, p = 0.03, exploratory threshold) within the preHD-B group (Figure 6C). In other words, an increase in clustering coefficient was associated with better switching performance (i.e., lower switch costs) in the preHD-B group. No correlations were present within the preHD-A group.

Discussion

We investigated *cross-sectional* and *longitudinal* differences in regional and global topological properties between subjects with premanifest and early manifest HD and healthy controls. In this first-of-its-kind analysis in HD, we revealed both baseline and longitudinal changes in the connectome of premanifest gene carriers and subjects with early manifest disease. We also demonstrated correlations between graph metrics on one hand, and clinical and behavioural measures, on the other hand. These results provide novel insights into the dynamics of brain neuropathology occurring in HD and the relationships with commonly used neurocognitive measures.

Longitudinal decreases in network measures

The principal finding from this study was a significant reduction over time of nodal betweenness centrality both in the early manifest HD and preHD-B groups within the two year study period as compared to the preHD-A and control groups. The locations of these nodes included the left orbitofrontal cortex and left paracentral lobule. The reduction of betweenness centrality in these regions indicates that the shortest paths passing through these areas were reduced. This in turn implies a decrease of importance of these nodes to overall network integrity.

The orbitofrontal cortex is involved in decision making and cognitive and emotional processing.[65] Atrophy in this structure has been associated with impaired recognition of negative emotions in HD.[66,67] The paracentral lobule, a component of the sensorimotor system,[68] has previously been implicated in HD where atrophy was also demonstrated.[69] The current results corroborate previous findings by demonstrating a longitudinal reduction in nodal betweenness centrality, suggesting a decreased capability of these nodes in facilitating communication between different brain regions in HD.

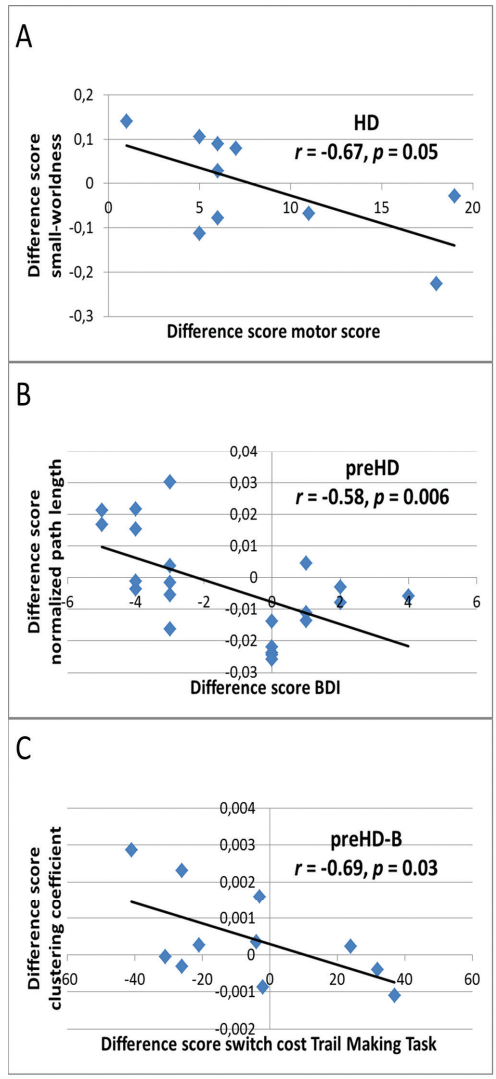

Figure 6. Correlations between changes in network parameters, and changes in clinical and neurocognitive functioning.

In the combined preHD group, a significant reduction over time of the clustering coefficient was also shown in the left medial prefrontal cortex when compared to healthy controls. This finding implies a decrease of functional segregation in this node. In other words, the left medial prefrontal cortex seems to become less densely interconnected with surrounding nodes over time, suggesting a local reduction of internodal processing of information. The medial prefrontal cortex is a region involved in planning and problem solving,[70] where in a previous study in preHD a lower functional connectivity has been demonstrated.[71] Moreover, a functional MRI

study in preHD and manifest HD revealed reduced connectivity of the medial prefrontal cortex, representing a functional correlate of impaired executive function.[72] Therefore, in our opinion, this is an important finding potentially providing a structural explanation for the dynamics of observed reductions in higher cognitive abilities occurring in gene carriers prior to manifestation of motor signs.

Preserved small-world organization in early HD

Another important finding is the preserved small-world organization within preHD and early manifest HD compared to healthy controls. With this finding in mind, we suggest that also in the early manifest stage of the disease, intervention could be aimed at preserving this brain organization associated with health, especially because of the presumed degradation of this network quality in advanced stages of the disease. Such a disruption in later stages of HD is yet to be established, though studies into different disorders affecting the brain have revealed disruptions in the small-world topological organization.[19,29] The results presented here imply that, at least at the preHD and early manifest stages of HD, there is no evidence for a 'disconnection syndrome' from a network perspective. Studies in other neurological disorders, such as multiple sclerosis,[24,25] Alzheimer's disease (reviewed by Xie and He),[73] schizophrenia[29] and traumatic brain injury[27] have found support for such a pathological model. The lack of this finding in this study is encouraging, as preservation of normal brain network architecture through intervention might be used as a secondary outcome for maintaining efficient brain function. It should be clear, though, that such a secondary outcome should be coupled with cognitive assessments given the intricate relationship between brain structure and function.

Making 'real-world' sense of network measures

Providing a translation from network measures to cognitive function and clinical state not only validates these measures, but also indicates possible usability in biomarker research. Interesting baseline correlations between graph metrics and neurocognitive measures were present in the preHD group. Specifically an inverse relationship between the switch cost of the TMT, regarded as a measure of cognitive flexibility, and clustering coefficient and local efficiency was found. These findings suggest that higher switching costs are associated with a loss in capability of processing information from a local network perspective. In the preHD-B group only, a positive correlation was observed between performance on SWR and global efficiency. This suggests that, in line with expectations, increases in the efficiency with which information can be transmitted globally are linked to higher processing speed.

Longitudinally, an increase in the UHDRS-TMS was negatively associated with small- worldness in the early manifest HD group, indicating that a decrease in 'wiring-efficiency' was related to an increase in motor score. The association found between increases on the reported symptoms on BDI-II and decreases in normalized path length in the preHD group provides evidence for coupled decreases in global integration with increases in depression scores. In the preHD-B group, we found that longitudinal increases in the switch cost of the TMT were correlated with longitudinal decreases in the clustering coefficient, again pointing to an association between this cognitive measure and local network properties.

Changing landscapes of hubs

Hubs are considered essential regions for coordinating brain functions, playing a central role in network resilience to brain injury.[48,74] The dynamic nature of hub-status found in this study could prove informative in understanding the nature of disease progression and compensatory mechanisms at play in (pre) HD as reflected by the temporal relation between hub-status loss and gain. A highlight from our findings in this context was the hub-status gain found in preHD in the right superior parietal gyrus in the second visit. Using functional MRI, this region has been shown to play a compensatory role in maintaining normal motor function in preHD.[75,76] Although admittedly speculative at this stage, this finding could be attributed to an increased need for compensation with progression of neurodegeneration in time, making a reorganisation of coordinating brain regions necessary for maintaining normal motor function. Another interesting finding was the contrast of hub-status gain for the right medial part of the superior frontal gyrus in early manifest HD compared to the loss of this status in the preHD group in the second visit. This type of information could further our understanding of compensatory mechanisms at play maintaining seemingly normal brain function in the premanifest stage of the disease, despite clear evidence of neurodegeneration provided by independent imaging studies even more than a decade prior to expected disease onset.[5,77]

Strengths and limitations

Strengths of this study include a standardized scan protocol with high-quality diffusion MRI data on two time points with assessments of multiple neurocognitive domains in a well described population from the TRACK-HD study. Moreover, in this study we have reconstructed the anatomical networks with constrained spherical deconvolution tractography, which in contrast to diffusion tensor imaging based tractography has the advantage of taking fibre crossings into account.[9,43,78]

There are several limitations in the methods being applied in the present study, such as the used parcellation scheme for defining the network nodes for the graph theoretical analysis. Multimodal integration of in- and ex-vivo data into a probabilistic atlas[79] may offer a better biologically principled approach as a parcellation scheme than the AAL atlas used in this study. Furthermore, while reproducibility studies have often demonstrated good or excellent intraclass correlation coefficient (ICC) measurements variance (for a recent review, see Welton et al.),[80] more studies measuring the test-retest reliability of graph metrics of structural networks are needed.

Moreover, the number of reconstructed fibres was used to weight the edges in the calculation of the connection matrix and consequently the network measures. Although other indices of white matter organization, such as fractional anisotropy, mean diffusivity, and level of myelination, have previously been applied to define the connectivity matrices,[81,82] there is currently no consensus on the optimal weighting method in terms of sensitivity and specificity to pathological effects.

Conclusions

This is the first study providing insights into longitudinal structural correlates with clinical state and cognitive function from a network perspective in HD. Strengthened by significant correlations with clinical and cognitive deficits, dynamics of the connectome, in the form of decreases of global and/or local efficiencies, were present in both the premanifest and early manifest stages of the disease. Furthermore, a changing hub landscape was demonstrated, contributing to our increased understanding of potential compensatory mechanisms at play, especially in preHD. The study further demonstrates preserved efficient dynamics of brain networks in the premanifest and early manifest stages of the disease. We conclude that assessing the connectome provides not only a novel approach with a biomarker potential in HD, but also potential new insights into compensatory strategies of the brain in neurodegenerative disorders.

Acknowledgments

TRACK-HD is supported by CHDI/High Q Foundation Inc., a not for profit organization dedicated to finding treatments for Huntington's disease. The research of A.L. is supported by VIDI Grant 639.072.411 from the Netherlands Organisation for Scientific Research (NWO). The authors wish to thank Sarah Tabrizi, University College London, who is the global PI for TRACK-HD and clinical site PI for London. The authors also wish to extend their gratitude to the TRACK-HD investigators responsible for collecting the data and to the study participants and their families.

References

1 The Huntington's Disease Collaborative Research Group. A novel gene containing a trinucleotide repeat that is expanded and unstable on Huntington's disease chromosomes. Cell 1993;72:971-983.
2 Aylward EH, Liu D, Nopoulos PC, et al. Striatal volume contributes to the prediction of onset of Huntington disease in incident cases. Biol Psychiatry 2012;71:822-828.
3 Hadzi TC, Hendricks AE, Latourelle JC, et al. Assessment of cortical and striatal involvement in 523 Huntington disease brains. Neurology 2012;79:1708-1715.
4 Sanchez-Castaneda C, Squitieri F, Di PM, et al. The role of iron in gray matter degeneration in Huntington's disease: a magnetic resonance imaging study. Hum Brain Mapp. 2015;36:50-66.
5 Tabrizi SJ, Langbehn DR, Leavitt BR, et al. Biological and clinical manifestations of Huntington's disease in the longitudinal TRACK-HD study: cross-sectional analysis of baseline data. Lancet Neurol. 2009;8:791-801.
6 Basser PJ, Mattiello J, LeBihan D. MR diffusion tensor spectroscopy and imaging. Biophys J. 1994;66:259-267.
7 Jones DK, Leemans A. Diffusion tensor imaging. Methods Mol Biol. 2011;711:127-144.
8 Pierpaoli C, Jezzard P, Basser PJ, et al. Diffusion tensor MR imaging of the human brain. Radiology1996;201:637-648.
9 Tournier JD, Mori S, Leemans A. Diffusion tensor imaging and beyond. Magn Reson Med. 2011;65:1532-1556.
10 Bohanna I, Georgiou-Karistianis N, Sritharan A, et al. Diffusion tensor imaging in Huntington's disease reveals distinct patterns of white matter degeneration associated with motor and cognitive deficits. Brain Imaging Behav. 2011;5:171-180.
11 Della NR, Ginestroni A, Tessa C, et al. Regional distribution and clinical correlates of white matter structural damage in Huntington disease: a tract-based spatial statistics study. AJNR Am J Neuroradiol. 2010;31:1675-1681.
12 Dumas EM, van den Bogaard SJ, Ruber ME, et al. Early changes in white matter pathways of the sensorimotor cortex in premanifest Huntington's disease. Hum Brain Mapp. 2012;33:203-212.
13 Hobbs NZ, Cole JH, Farmer RE, et al. Evaluation of multi-modal, multi-site neuroimaging measures in Huntington's disease: Baseline results from the PADDINGTON study. Neuroimage Clin. 2012;2:204-211.
14 Phillips O, Squitieri F, Sanchez-Castaneda C, et al. Deep white matter in Huntington's disease. PLoS One 2014;9:e109676.
15 Sritharan A, Egan GF, Johnston L, et al. A longitudinal diffusion tensor imaging study in symptomatic Huntington's disease. J Neurol Neurosurg Psychiatry 2010;81:257-262.
16 Vandenberghe W, Demaerel P, Dom R, et al. Diffusion-weighted versus volumetric imaging of the striatum in early symptomatic Huntington disease. J Neurol. 2009;256:109- 114.
17 Weaver KE, Richards TL, Liang O, et al. Longitudinal diffusion tensor imaging in Huntington's Disease. Exp Neurol. 2009;216:525-529.
18 Bach M, Laun FB, Leemans A, et al. Methodological considerations on tract-based spatial statistics (TBSS). Neuroimage 2014;100:358-369.
19 He Y, Chen Z, Evans A. Structural insights into aberrant topological patterns of large- scale cortical networks in Alzheimer's disease. J Neurosci. 2008;28:4756-4766.
20 Heringa SM, Reijmer YD, Leemans A, et al. Multiple microbleeds are related to cerebral network disruptions in patients with early Alzheimer's disease. J Alzheimers Dis. 2014;38:211-221.
21 Lo CY, Wang PN, Chou KH, et al. Diffusion tensor tractography reveals abnormal topological organization in structural cortical networks in Alzheimer's disease. J Neurosci. 2010;30:16876-16885.
22 Reijmer YD, Leemans A, Caeyenberghs K, et al. Disruption of cerebral networks and cognitive impairment in Alzheimer disease. Neurology 2013;80:1370-1377.

23 Supekar K, Menon V, Rubin D, et al. Network analysis of intrinsic functional brain connectivity in Alzheimer's disease. PLoS Comput Biol. 2008;4:e1000100.

24 He Y, Dagher A, Chen Z, et al. Impaired small-world efficiency in structural cortical networks in multiple sclerosis associated with white matter lesion load. Brain 2009;132:3366- 3379.

25 Shu N, Liu Y, Li K, et al. Diffusion tensor tractography reveals disrupted topological efficiency in white matter structural networks in multiple sclerosis. Cereb Cortex 2011;21:2565-2577.

26 Caeyenberghs K, Leemans A, Heitger MH, et al. Graph analysis of functional brain networks for cognitive control of action in traumatic brain injury. Brain 2012;135:1293-1307.

27 Caeyenberghs K, Leemans A, Leunissen I, et al. Altered structural networks and executive deficits in traumatic brain injury patients. Brain Struct Funct. 2014;219:193-209.

28 Bassett DS, Bullmore E, Verchinski BA, et al. Hierarchical organization of human cortical networks in health and schizophrenia. J Neurosci. 2008;28:9239-9248.

29 Liu Y, Liang M, Zhou Y, et al. Disrupted small-world networks in schizophrenia. Brain 2008;131:945-961.

30 Poudel G, Stout JC, Dominguez DJ, et al. White matter connectivity reflects clinical and cognitive status in Huntington's disease. Neurobiol Dis. 2014;65:180-187.

31 Tabrizi SJ, Scahill RI, Durr A, et al. Biological and clinical changes in premanifest and early stage Huntington's disease in the TRACK-HD study: the 12-month longitudinal analysis. Lancet Neurol. 2011;10:31-42.

32 Langbehn DR, Brinkman RR, Falush D, et al. A new model for prediction of the age of onset and penetrance for Huntington's disease based on CAG length. Clin Genet. 2004;65:267-277.

33 Penney JB, Jr., Vonsattel JP, MacDonald ME, et al. CAG repeat number governs the development rate of pathology in Huntington's disease. Ann Neurol. 1997;41:689-692.

34 Delmaire C, Dumas EM, Sharman MA, et al. The structural correlates of functional deficits in early huntington's disease. Hum Brain Mapp. 2013;34:2141-2153.

35 O'Rourke JJ, Beglinger LJ, Smith MM, et al. The Trail Making Test in prodromal Huntington disease: contributions of disease progression to test performance. J Clin Exp Neuropsychol. 2011;33:567-579.

36 Schmand B, Bakker D, Saan R, et al. The Dutch Reading Test for Adults: a measure of premorbid intelligence level. Tijdschr Gerontol Geriatr. 1991;22:15-19.

37 Leemans A, Jeurissen B, Sijbers J, et al. Explore DTI: a graphical toolbox for processing, analyzing, and visualizing diffusion MR data. 17th Annual Meeting of Intl Soc Mag Reson Med., Hawaii, USA 2009;p. 3537.

38 Irfanoglu MO, Walker L, Sarlls J, et al. Effects of image distortions originating from susceptibility variations and concomitant fields on diffusion MRI tractography results. Neuroimage 2012;61:275-288.

39 Tax CM, Otte WM, Viergever MA, et al. REKINDLE: Robust extraction of kurtosis INDices with linear estimation. Magn Reson Med. 2015;73:794-808.

40 Veraart J, Sijbers J, Sunaert S, et al. Weighted linear least squares estimation of diffusion MRI parameters: strengths, limitations, and pitfalls. Neuroimage 2013;81:335-346.

41 Jeurissen B, Leemans A, Jones DK, et al. Probabilistic fiber tracking using the residual bootstrap with constrained spherical deconvolution. Hum Brain Mapp. 2011;32:461-479.

42 Tax CM, Jeurissen B, Vos SB, et al. Recursive calibration of the fiber response function for spherical deconvolution of diffusion MRI data. Neuroimage 2014;86:67-80.

43 Tournier JD, Calamante F, Connelly A. Robust determination of the fibre orientation distribution in diffusion MRI: non-negativity constrained super-resolved spherical deconvolution. Neuroimage 2007;35:1459-1472.

44 Tzourio-Mazoyer N, Landeau B, Papathanassiou D, et al. Automated anatomical labeling of activations in SPM using a macroscopic anatomical parcellation of the MNI MRI single- subject brain. Neuroimage 2002;15:273-289.

45 Klein S, Staring M, Murphy K, et al. Elastix: a toolbox for intensity-based medical image registration. IEEE Trans Med Imaging 2010;29:196-205.
46 De Groot M, Vernooij MW, Klein S, et al. Improving alignment in Tract-based spatial statistics: evaluation and optimization of image registration. Neuroimage 2013;76:400-411.
47 Li Y, Liu Y, Li J, et al. Brain Anatomical Network and Intelligence. PLoS Comput Biol. 2009;5:e1000395.
48 Rubinov M, Sporns O. Complex network measures of brain connectivity: uses and interpretations. Neuroimage 2010;52:1059-1069.
49 Hosseini SM, Hoeft F, Kesler SR. GAT: a graph-theoretical analysis toolbox for analyzing between-group differences in large-scale structural and functional brain networks. PLoS One 2012;7:e40709.
50 Hosseini SM, Koovakkattu D, Kesler SR. Altered small-world properties of gray matter networks in breast cancer. BMC Neurol. 2012;12:28.
51 Hosseini SM, Black JM, Soriano T, et al. Topological properties of large-scale structural brain networks in children with familial risk for reading difficulties. Neuroimage 2013;71:260-274.
52 Van Wijk BC, Stam CJ, Daffertshofer A. Comparing brain networks of different size and connectivity density using graph theory. PLoS One 2010;5:e13701.
53 Latora V, Marchiori M. Efficient behavior of small-world networks. Phys Rev Lett. 2001;87:198701.
54 Sporns O, Zwi J. The small world of the cerebral cortex. Neuroinform. 2004;2:145-162.
55 Onnela JP, Saramaki J, Kertesz J, et al. Intensity and coherence of motifs in weighted complex networks. Phys Rev E Stat Nonlin Soft Matter Phys. 2005;71:065103.
56 Opsahl T, Panzarasa P. Clustering in weighted networks. Social Networks 2009;31:155-163.
57 Hosseini SM, Kesler SR. Influence of choice of null network on small-world parameters of structural correlation networks. PLoS One 2013;8:e67354.
58 Maslov S, Sneppen K. Specificity and Stability in Topology of Protein Networks. Science 2002;296:910-913.
59 Humphries MD, Gurney K. Network 'small-world-ness': a quantitative method for determining canonical network equivalence. PLoS One 2008;3:e0002051.
60 Watts DJ, Strogatz SH. Collective dynamics of 'small-world' networks. Nature 1998;393:440-442.
61 Bassett DS, Bullmore E. Small-World Brain Networks. The Neuroscientist 2006;12:512-523.
62 Freeman LC. Centrality in Social Networks Conceptual Clarification. Social Networks 1979;1:215-239.
63 Kesler SR, Wefel JS, Hosseini SMH, et al. Default mode network connectivity distinguishes chemotherapy-treated breast cancer survivors from controls. Proceedings of the National Academy of Sciences 2013;110:11600-11605.
64 Genovese CR, Lazar NA, Nichols T. Thresholding of statistical maps in functional neuroimaging using the false discovery rate. Neuroimage 2002;15:870-878.
65 Kringelbach ML, Rolls ET. The functional neuroanatomy of the human orbitofrontal cortex: evidence from neuroimaging and neuropsychology. Prog Neurobiol. 2004;72:341-372.
66 Henley SM, Wild EJ, Hobbs NZ, et al. Defective emotion recognition in early HD is neuropsychologically and anatomically generic. Neuropsychologia 2008;46:2152-2160.
67 Ille R, Schafer A, Scharmuller W, et al. Emotion recognition and experience in Huntington disease: a voxel-based morphometry study. J Psychiatry Neurosci. 2011;36:383-390.
68 White LE, Andrews TJ, Hulette C, et al. Structure of the human sensorimotor system. I: Morphology and cytoarchitecture of the central sulcus. Cereb Cortex 1997;7:18-30.
69 Kassubek J, Juengling FD, Kioschies T, et al. Topography of cerebral atrophy in early Huntington's disease: a voxel based morphometric MRI study. J Neurol Neurosurg Psychiatry 2004;75:213-220.
70 Alvarez JA, Emory E. Executive function and the frontal lobes: a meta-analytic review. Neuropsychol Rev. 2006;16:17-42.

71 Wolf RC, Sambataro F, Vasic N, et al. Default-mode network changes in preclinical Huntington's disease. Exp Neurol. 2012;237:191-198.
72 Unschuld PG, Liu X, Shanahan M, et al. Prefrontal executive function associated coupling relates to Huntington's disease stage. Cortex 2013;49:2661-2673.
73 Xie T, He Y. Mapping the Alzheimer's brain with connectomics. Front Psychiatry 2011;2:77.
74 Cole MW, Pathak S, Schneider W. Identifying the brain's most globally connected regions. Neuroimage 2010;49:3132-3148.
75 Kloppel S, Draganski B, Siebner HR, et al. Functional compensation of motor function in pre-symptomatic Huntington's disease. Brain 2009;132:1624-1632.
76 Scheller E, Abdulkadir A, Peter J, et al. Interregional compensatory mechanisms of motor functioning in progressing preclinical neurodegeneration. Neuroimage 2013;75:146-154.
77 Paulsen JS, Nopoulos PC, Aylward E, et al. Striatal and white matter predictors of estimated diagnosis for Huntington disease. Brain Res Bull. 2010;82:201-207.
78 Jeurissen B, Leemans A, Tournier JD, et al. Investigating the prevalence of complex fiber configurations in white matter tissue with diffusion magnetic resonance imaging. Hum Brain Mapp. 2013;34:2747-2766.
79 Eickhoff SB, Stephan KE, Mohlberg H, et al. A new SPM toolbox for combining probabilistic cytoarchitectonic maps and functional imaging data. Neuroimage 2005;25:1325-1335.
80 Welton T, Kent DA, Auer DP, et al. Reproducibility of Graph-Theoretic Brain Network Metrics: A Systematic Review. Brain Connectivity 2014;5:193-202.
81 Gong G, He Y, Concha L, et al. Mapping anatomical connectivity patterns of human cerebral cortex using in vivo diffusion tensor imaging tractography. Cereb Cortex 2009;19:524-536.
82 Van den Heuvel MP, Mandl RC, Stam CJ, et al. Aberrant frontal and temporal complex network structure in schizophrenia: a graph theoretical analysis. J Neurosci. 2010;30:15915-15926.

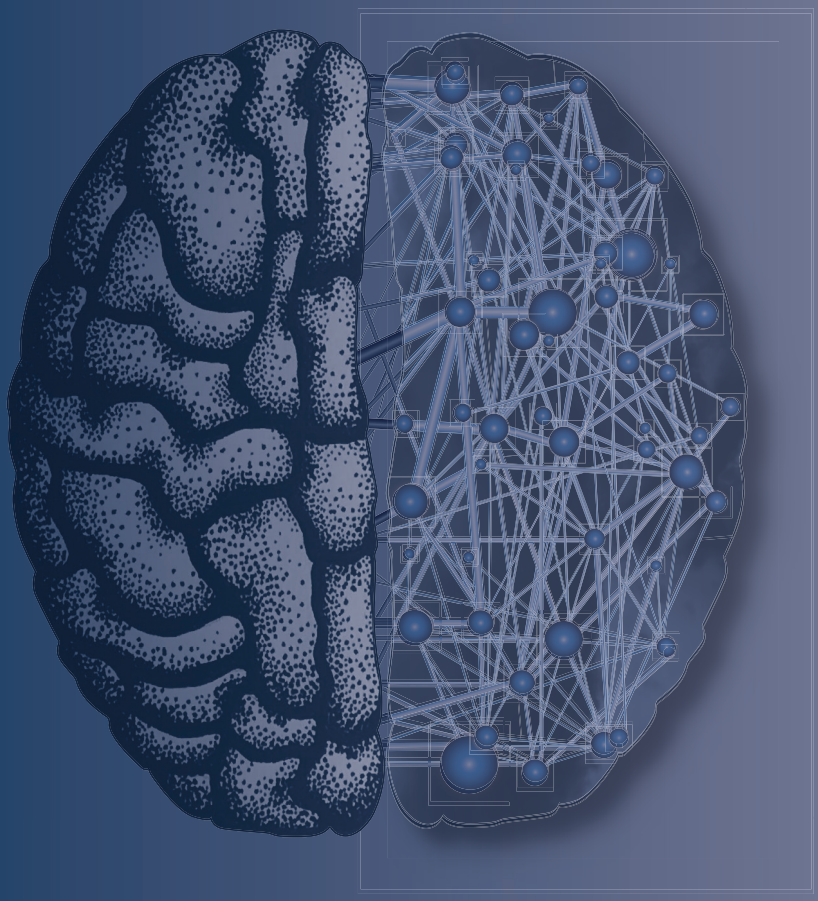

Progressive microstructural changes of the occipital cortex in Huntington's disease

CHAPTER 5

5

Omar F.F. Odish[1], Robert H.A.M. Reijntjes[1], Simon J.A. van den Bogaard[1], Raymund A.C. Roos[1], Alexander Leemans[2]

[1] Department of Neurology, Leiden University Medical Center, Leiden, The Netherlands
[2] Image Sciences Institute, University Medical Center Utrecht, Utrecht, The Netherlands

Brain Imaging and Behavior 2018;12:1786-1794

Abstract

Background

Objective and sensitive biomarkers quantifying disease progression in Huntington's disease (HD) are needed. In this study we longitudinally investigated the rate of microstructural alterations in the occipital cortex in different stages of HD by applying an automated atlas-based approach to diffusion MRI data. The choice for this region was driven by the mounting evidence that the occipital cortex is involved early on in HD neuropathology.

Methods

Twenty-two premanifest (preHD), 10 early manifest HD (early HD) and 24 healthy control subjects completed baseline and two-year follow-up scans. We stratified the preHD group based on their predicted years to disease onset into a far (preHD-A) and near (preHD-B) to disease onset group. We collected clinical and behavioural measures per assessment time point. We used an automated atlas-based DTI analysis approach to obtain the mean, axial and radial diffusivities of the occipital cortex.

Results

We found that the longitudinal rate of diffusivity change in the superior occipital gyrus (SOG), middle occipital gyrus (MOG), and inferior occipital gyrus (IOG) was significantly higher in early HD compared to both preHD and controls (all ps ≤ 0.005), which can be interpreted as an increased rate of microstructural degeneration. Furthermore, the change rate in the diffusivity of the MOG could significantly discriminate between preHD-B compared to preHD-A and the other groups (all ps ≤ 0.04). Finally, we found an inverse correlation between the Stroop Word Reading task and diffusivities in the SOG and MOG (all ps ≤ 0.01).

Conclusions

These findings suggest that diffusion measures obtained from the occipital cortex can serve as sensitive longitudinal biomarkers for disease progression in preHD-B and early HD. These could in turn be used to assess potential effects of proposed disease modifying therapies.

Introduction

Huntington's disease (HD) is a rare autosomal dominant neurodegenerative disorder caused by an expanded cytosine-adenine-guanine (CAG) repeat on chromosome 4. The hallmark feature in HD neuropathology is degeneration of the striatum. However, a growing amount of evidence from neuroimaging studies suggests that occipital regions are affected early on in the disease course.[1-14] Furthermore, metabolic abnormalities have also been reported in the occipital regions in HD.[15-17] Histologically, a study in HD found that atrophy of the occipital lobe was most pronounced compared to other cortical areas[18] and a more recent post-mortem study confirmed reductions in the absolute nerve cell number of the occipital lobe in HD.[19] The *in vivo* microstructural properties of the occipital cortex have, however, not been a primary focus in HD research to date.[1-22]

As carriers of a CAG repeat ≥ 40 within the mutant gene are certain to develop Huntington's disease if they live long enough, carriers in the phase before disease presentation could be examined to explore inevitable changes occurring while progressing towards disease manifestation. Viable markers representing disease progression in HD and its premanifest stage (preHD) are still needed in order to investigate potential intervention effects. To this end, various imaging techniques are being used in biomarker research settings. One such technique is diffusion MRI, where measures can be obtained based on the diffusion characteristics of water molecules in tissues. This, in turn, provides indirect information regarding the microstructure of these tissues.[23,24] Potential associations between disease state on the one hand and divergent longitudinal differences in diffusivities on the other hand, could give a tool for quantifying disease progression.

We previously explored whole-brain and striatal diffusivities in (pre) HD and healthy controls, where we found no evidence for significant longitudinal differences between the groups.[25] Other research groups have more recently demonstrated significant longitudinal differences in various white matter tracts between the groups,[11,22] where interestingly Harrington et al.[11] found differences only in the superior fronto-occipital fasciculus. Furthermore, recent cross-sectional studies have shown abnormalities related to the occipital regions, such as in white matter projections to the occipital lobe,[12] in superficial white matter[13] and in deep white matter tracts of the occipital lobe.[14]

Given the mounting evidence pointing to an early and preferential involvement of the occipital regions in HD,[1-19] this study aimed to investigate diffusion measures of the occipital cortex in premanifest and early manifest HD and matched healthy controls and explore potential differences in longitudinal changes between the groups and associations of changes herein with clinical and behavioural measures.

Materials and methods

Procedures regarding participant recruitment, inclusion criteria and clinical measures administered have been previously described in detail.[1,25] In summary, 56 subjects at the Leiden site of the prospective international TRACK-HD study completed a brain MRI scan at baseline and a second

scan two years later. The between-scan interval in months is shown in Table I, without significant between-group differences. The group consisted of 24 healthy controls (49.0 ± 8.2 years), 22 preHD (43.6 ± 8.7 years) and ten early manifest HD (50.2 ± 9.3 years) (Table I). As previously applied by Tabrizi et al.,[1] to assess the effect of expected proximity to disease onset on diffusion parameters, the preHD group was divided at baseline according to the median (10.9 years) for the predicted years to disease onset into preHD-A (≥ 10.9 years. Mean ± SD: 14.9 ± 4.7) and preHD-B (< 10.9 years. Mean ± SD: 8.6 ± 1.8). The predicted years to disease onset were calculated using the Langbehn method.[26] This resulted in two groups each consisting of eleven subjects (Table I). The Symbol Digit Modalities Test (SDMT) and the Stroop Word Reading (SWR) task, where visual processing is required, were administered to evaluate potential associations between these commonly used and sensitive longitudinal neurocognitive measures in HD[2] and occipital diffusivities. To monitor disease state, the following clinical measures were further evaluated longitudinally for all groups: Unified Huntington's Disease Rating Scale (UHDRS-TMS), Total Functional Capacity (TFC) and Beck Depression Inventory-II (BDI-II) scores. The study was approved by the Medical Ethics Committee of the Leiden University Medical Center and written informed consent was obtained from all participants.

Magnetic resonance imaging acquisition

MRI acquisition was performed with a 3-Tesla whole-body scanner (Philips Achieva, Healthcare, Best, The Netherlands) with an eight channel SENSE head coil. T1-weighted image volumes were acquired using a 3D MPRAGE acquisition sequence with the following imaging parameters: TR = 7.7 ms, TE = 3.5 ms, FOV = 24 x 24 cm^2, matrix size 224 x 224, number of slices = 164, slice thickness = 1.00 mm, and no slice gap. A single-shot echo-planar diffusion tensor imaging sequence was applied with 32 measurement directions and the following scan parameters:[24] TR = 10,004 ms, TE = 56 ms, FOV = 220 x 220 mm^2 with an acquisition matrix of 112 x 110, 2.00 mm slice thickness, transversal slice orientation, no slice gap, flip angle = 90°, reconstruction voxel dimensions of 1.96 x 1.96 x 2.00 mm^3, number of slices = 64, b-value = 1,000 s/mm^2, halfscan factor = 0.61. Parallel imaging (SENSE) was used with a reduction factor of two, NSA = 1, and fat suppression was applied. DTI acquisition time was 6.55 min.

Image processing

DTI data were analysed using the diffusion MR toolbox 'ExploreDTI',[27] as previously described.[25] Automated atlas based analysis[28] using the LPBA40 parcellation map from the SRI24 atlas[29] (available at http://www.nitrc.org/projects/sri24/) was performed using affine and elastic registration based on 'Elastix'.[30] All DTI data were visually checked in terms of quality of tensor estimation and quality of registration. As no significant differences were found between hemispheres, left and right hemisphere values of mean diffusivity (MD), axial diffusivity (AD) and radial diffusivity (RD) were calculated and averaged per occipital region as provided by SRI24/LPBA40.[29] To correct for multiple comparisons (three occipital regions), a Bonferroni corrected p-value ≤ 0.017 (0.05/3) was considered significant for omnibus F-tests. As fractional anisotropy is not an informative measure in cortical grey matter regions,[31,32] MD, AD and RD are reported.

Table I. *Group demographics with clinical and behavioural scores*

		Healthy controls	Premanifest HD (A and B)	preHD-A	preHD-B	Early manifest HD
N		24	22‡	11	11	10
Gender M/F		11/13	9/13	4/7	5/6	4/6
Age in years (at V1), mean (SD)		49.0 (8.2)	43.6 (8.7)	44.2 (5.7)	43.0 (11.2)	50.2 (9.3)
Handedness R/L		20/4	18/4	9/2	9/2	9/1
Level of education (ISCED), median (range)		4 (3)	4 (3)	4 (3)	4 (3)	4 (3)
DART-IQ, mean (SD)		105.0 (9.4)	100.5 (11.2)	101.3 (9.7)	99.6 (13.0)	101.8 (13.5)
CAG repeat length, mean (SD)		n/a	42.6 (2.7)	41.3 (1.4)	43.9 (3.1)^	42.5 (1.2)
Estimated years to onset, mean (SD)		n/a	11.8 (4.7)	14.9 (4.7)	8.6 (1.8)^	n/a
Total functional capacity, mean (SD)						
	V1	13.0 (0.2)	12.8 (0.5)	12.7 (0.7)	12.8 (0.4)	11.0 (1.5)Φ
	V2	12.9 (0.5)	12.6 (0.9)	12.7 (0.6)	12.5 (1.0)	10.3 (2.2)Φ
UHDRS-TMS, mean (SD)						
	V1	2.6 (2.5)	2.6 (1.5)	2.0 (1.5)	3.1 (1.2)	14.6 (7.7)Φ
	V2	2.1 (1.6)	5.7 (5.1) ¥	3.5 (2.2)	8.3 (6.1)*^	23.0 (12.1)Φ
SDMT, mean (SD)						
	V1	49.4 (8.9)	50.1 (11.0)	53.5 (9.3)	46.7 (11.9)	41.2 (9.2)Φ
	V2	50.9 (9.3)	50.6 (10.0)	54.7 (10.0)	46.6 (8.5)^	39.2 (10.6)Φ
SWR, mean (SD)						
	V1	100.1 (13.2)	91.9 (14.2)*	95.6 (9.6)	88.3 (17.3)*	87.7 (14.7)*
	V2	102.0 (15.6)	87.9 (15.7)*	91.4 (9.4)	84.4 (20.0)*	86.4 (18.6)*
BDI-II, mean (SD)						
	V1	4.1 (4.4)	6.4 (6.4)	4.9 (6.0)	7.9 (6.8)	10.2 (8.2)*
	V2	3.9 (4.1)	5.1 (5.6)	3.2 (4.9)	6.9 (5.9)	8.2 (8.4)
Between-scan interval in months, mean (SD)		23.0 (0.8)	23.0 (0.7)	23.2 (0.6)	22.7 (0.7)	23.5 (0.7)

N = number of participants, SD = Standard deviation, n/a = not applicable, ISCED = International Standard Classification of Education, DART-IQ = Dutch Adult Reading Test Intelligence Quotient, CAG = Cytosine-Adenine-Guanine, UHDRS-TMS = Unified Huntington's Disease Rating Scale-Total Motor Score, SDMT = Symbol Digit Modalities Test, SWR = Stroop Word Reading task, BDI-II = Beck Depression Inventory-II, V1 = visit 1, V2 = visit 2.
*Significance at p ≤ 0.05 level: * significantly different from controls, Φ significantly different from controls and preHD, ¥ significantly different from controls and HD, ^ significantly different from preHD-A.*
‡ Including five subjects progressing to the early manifest stage during the two year follow-up period.

Statistical analysis

We used linear mixed models (in R version 3.0.0, R Foundation for Statistical Computing, Vienna, Austria) to model the outcome variables with patient as a random factor to accommodate the within-person repeated nature of the data and to assess the effect of group, corrected for age at time of scanning. Correlations between neurocognitive measures and diffusion metrics were tested in the model. Statistical analyses of group demographics were performed with SPSS (version 20, IBM, USA). Distributions and assumptions were checked. Either Analysis of Variance (ANOVA) or Chi-squared tests were applied where this was appropriate. Potential longitudinal change in clinical measures between the groups was also investigated. Difference values were computed and an ANOVA was performed on these delta-scores to evaluate potential group

differences. In case of a significant omnibus F-test, exploratory post-hoc analysis using Fisher's least significant difference was performed to assess which means were significantly different from each other. As absolute values of diffusivities do not convey meaningful information per se, we report percentage change as an informative longitudinal parameter. Supplementary Figure 1 shows the evolution of the absolute diffusivity levels between the groups and on individual study participant level from the first to the second visit. A statistical power analysis was performed for sample size estimation based on data from our study, with a Bonferroni corrected $\alpha = 0.01$ and power = 90%. Differences in group demographics between preHD-A and preHD-B were compared using either independent-samples t-tests or Chi-squared tests, where appropriate.

Results

There were no statistically significant differences in demographic characteristics between the groups. Only a trend towards a difference in age ($p = 0.06$) was observed. Hence, age was included as a covariate in subsequent analyses. See Table I for group demographics and clinical and behavioural scores. The *early HD* group differed significantly at baseline in their performance in SDMT and SWR when compared to both *controls* and *preHD* subjects. For the *preHD* group, a significantly lower baseline score compared to controls was found for SWR. Furthermore, at the second visit, the *preHD-B* group showed a significantly lower SDMT score compared to *preHD-A*. All results presented hereafter are based on the dynamics during the two-year duration of the study.

Superior Occipital Gyrus diffusivities

Longitudinal changes in MD were significantly larger in *early HD* compared to both *preHD* and *controls* (+12.3%, +7.9% and +6.1%, respectively; $p = 0.001$). Similar patterns were found for AD (+12.7%, +8.0% and +5.6%, respectively; $p < 0.001$) and RD (+12.0%, +7.8% and 6.4%, respectively; $p = 0.005$) for the three groups. No further longitudinal diffusivity differences in this structure were found upon stratifying the *preHD* group based on expected time to disease onset into *preHD-A* and *preHD-B*. See Table II and Figure 1 for a summary of the results.

Middle Occipital Gyrus diffusivities

Longitudinal changes in MD were significantly larger in *early HD* compared to both *preHD* and *controls* (+9.0%, +5.4% and +3.8%, respectively; $p < 0.0001$). Similar patterns were found for AD (+8.3%, +4.5% and +2.7%, respectively; $p < 0.0001$) and RD (+9.4%, +5.9% and +4.5%, respectively; $p < 0.001$) for the three groups. Upon stratification of the *preHD* group based on expected time to disease onset, significantly larger longitudinal changes in *preHD-B* compared to *preHD-A* were found in MD (+6.2 % vs. +4.4%, respectively; $p = 0.03$), AD (+5.1% vs. +3.7%, respectively; $p = 0.04$) and RD (+6.8% vs. +4.8%, respectively; $p = 0.02$). See Table II and Figure 1 for a summary of the results (data for preHD-B vs. preHD-A are not shown in figure).

Inferior Occipital Gyrus diffusivities

Longitudinal changes in MD were significantly larger in *early HD* compared to both *preHD* and *controls* (+4.6%, +1.0% and -1.1%, respectively; p = 0.001). Similar patterns were found for AD (+3.4%, +0.3% and -1.8%, respectively; p = 0.002) and RD (+5.3%, +1.4% and -0.6%, respectively; p = 0.001). No further longitudinal diffusivity differences were found upon stratifying the *preHD* group based on expected time to disease onset into *preHD-A* and *preHD-B*. See Table II and Figure 1 for a summary of the results.

Table II. *Longitudinal percentage change in diffusion parameters from v1 to v2†*

	Controls			preHD (A and B)‡			preHD-A			preHD-B			Early HD		
N	24			22			11			11			10		
	SOG	MOG	IOG	SOG	MOG	IOG	SOG	MOG	IOG	SOG	MOG	IOG	SOG	MOG	IOG
MD	+ 6.1	+ 3.8	-1.1	+ 7.9	+ 5.4	+ 1.0	+ 8.4	+ 4.4	+ 0.5	+ 7.4	+ 6.2 ^	+ 1.4	+12.3Φ	+ 9.0Φ	+ 4.6Φ
AD	+ 5.6	+ 2.7	-1.8	+ 8.0	+ 4.5	+ 0.3	+ 8.8	+ 3.7	+ 0.1	+ 7.2	+ 5.1 ^	+ 0.5	+12.7Φ	+ 8.3Φ	+ 3.4Φ
RD	+ 6.4	+ 4.5	- 0.6	+ 7.8	+ 5.9	+ 1.4	+ 8.2	+ 4.8	+ 0.8	+ 7.4	+ 6.8 ^	+ 1.9	+12.0Φ	+ 9.4Φ	+ 5.3Φ

SOG = Superior Occipital Gyrus, MOG = Middle Occipital Gyrus, IOG = Inferior Occipital Gyrus, MD = mean diffusivity, AD = axial diffusivity, RD = radial diffusivity.

Significance at p ≤ 0.017 for the omnibus F-test following Bonferroni correction: Φ significantly different from controls and preHD, ^ significantly different from preHD-A, early HD and controls. The MOG is underlined as a prime region of interest based on these results.

† Calculated from mixed model-based estimates of the group means for diffusion measures, corrected for age.

‡ Including five subjects progressing to the early manifest stage during the two year follow-up period.

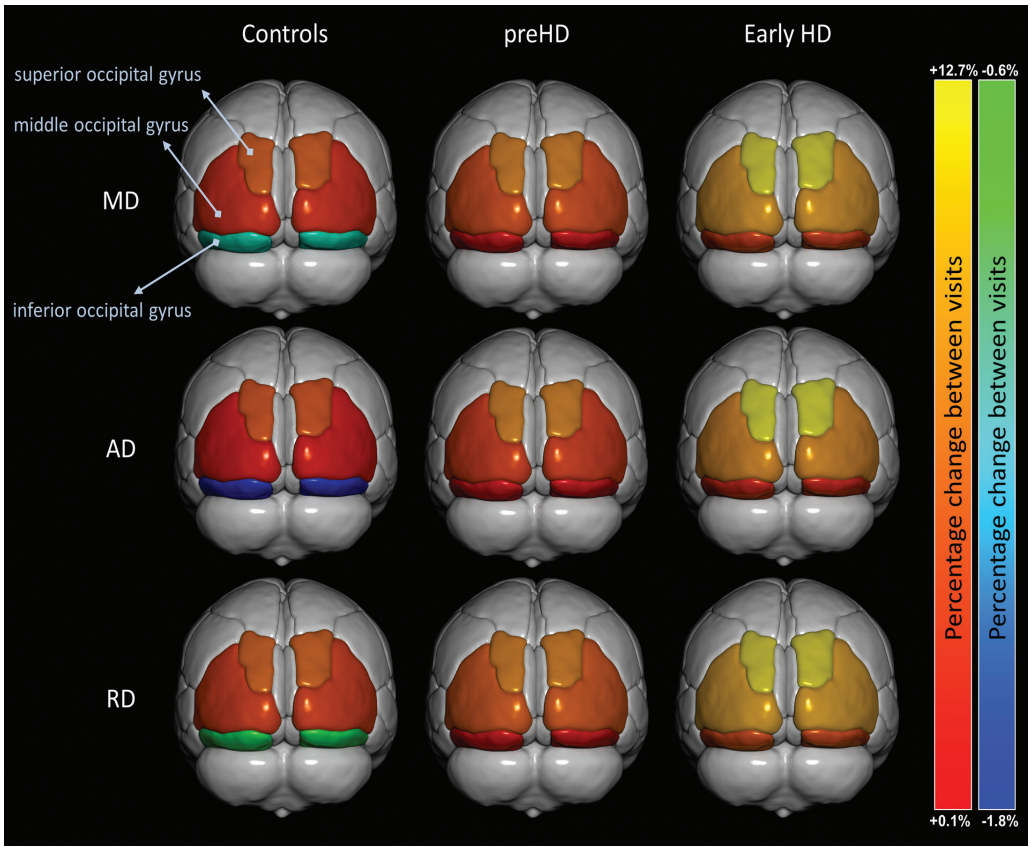

Figure 1. Two-year percentage change in mean diffusivity (MD), axial diffusivity (AD) and radial diffusivity (RD) of the three occipital regions of the groups. Significance levels are indicated in Table II.

Associations between occipital diffusivities and neurocognitive measures

The associations between occipital diffusivities and neurocognitive measures were not statistically different between the *preHD* and *early HD* groups. No significant associations were found between the diffusivities of any of the three occipital structures and SDMT (all *ps* > 0.05). The SWR showed strong associations with the AD of the Superior Occipital Gyrus (SOG) ($p = 0.005$), and the MD ($p = 0.01$), AD ($p = 0.009$) and RD ($p = 0.01$) of the Inferior Occipital Gyrus (IOG). No significant associations with any of the diffusivities of the MOG and neurocognitive measures were present. See Table III for a summary of the significant associations.

Table III. *Associations between occipital diffusivities and neurocognitive measures*

Diffusion parameter	SWR score	*P*
↓ 1.8%	↑ 10 points	0.005
↓ 1.2%	↑ 10 points	0.011
↓ 1.1%	↑ 10 points	0.009
↓ 1.3%	↑ 10 points	0.013

SOG = Superior Occipital Gyrus, IOG = Inferior Occipital Gyrus, MD = mean diffusivity, AD = axial diffusivity, RD = radial diffusivity.
This table is valid for all participants with a CAG repeat expansion included in the study, as no specific group effects were found on correlations between diffusion parameters and neurocognitive measures. Only significant correlations are shown. ↓ = decrease, ↑ = increase.

Power analysis

Power analysis using these results show that a minimum of 9 subjects per group would be needed to detect a significant longitudinal difference in diffusivity values in 2 years within the occipital cortex (90% power and $\alpha = 0.01$). There were no significant differences in power between the different diffusivity measures. However, the MOG was the region most prone to longitudinal alteration, thereby most sensitive to demonstrating change. The minimum number of subjects needed to find statistically significant longitudinal difference in the diffusivity of the three occipital regions was as follows: SOG 14, MOG 9 and IOG 12.

Discussion

We investigated longitudinal microstructural property changes of the occipital cortex in HD. Using a fully automated procedure, we revealed highly divergent longitudinal quantitative imaging measures between preHD, early HD and controls. Associations were found between diffusivity change rates and disease stage in the preHD and early HD groups, providing evidence for an accelerated rate of change correlated with disease progression. Significant correlations between behavioural measures and diffusivity changes in HD were found.

Differences observed in the rate and significance of longitudinal change of SOG, MOG and IOG diffusivities were similar for all measures tested (MD, AD and RD). As such, it does not seem of added value to assess these different diffusivity values individually. However, some of the associations found with cognitive functions were present only with specific measures, for example the inverse relationship found between the Stroop Word Reading task and the AD of SOG. Therefore, it would seem useful to further examine the behaviour of the separate diffusion measures in future investigations, as this may provide specific associations with cognitive tests. In preHD, only changes in diffusivities of the MOG could significantly differentiate between preHD-B

compared to preHD-A and the other groups. This structure might thus be preferentially affected in the premanifest phase of HD and, in light of these results, could be viewed as a prime region of interest for neuroimaging change within the occipital cortex in preHD. Our power analysis also demonstrated that the MOG is the most sensitive structure of the three examined in detecting longitudinal change between the groups.

The occipital cortex is deservingly gaining interest in HD research. Previous, often serendipitously found alterations in this region increasingly pointed to this structure as relevant in the neuropathology of HD.[33] This study provides strong evidence for a highly differential longitudinal change of diffusion measures in this structure between the studied groups. The relatively short time-frame of the study concomitant with a relatively high rate of change, makes it likely that these disease-related changes could also be reproduced in shorter study intervals, making these measures potentially suitable to use as outcome parameters in shorter clinical trials. These results also pave the way for further investigations into the underlying mechanisms with which the occipital cortex is affected in HD and what the clinical relevance is. Although no specific visual symptoms are known to exist in HD, performance on cognitive tasks examining visuospatial and visuomotor function is known to be reduced in the disorder.[34,35] A study investigating the cross-sectional relationship between visual area resting state functional MRI (RS-fMRI), volumetric changes, and cognitive function revealed differences between HD and controls with significant cognitive correlations to visual area RS-fMRI.[36] It is further known that impaired emotion recognition is a feature of preHD and early HD (see Henley et al.[37] for a systematic review), and results from a previous task-based functional MRI study in preHD revealed reduced neuronal activity in various regions during emotion processing, including the MOG studied in the present report.[38]

Previous longitudinal reports using diffusion MRI in HD provide heterogeneous findings.[11,22,25,39-42] Using a tract-based spatial statistics (TBSS) approach, Weaver et al.[40] compared scans from seven controls, four preHD and three manifest HD subjects obtained one year apart. Significant longitudinal decreases in white matter fractional anisotropy (FA) and AD in the seven mixed preHD and manifest HD group were found compared to the healthy controls. In the study by Sritharan et al.,[41] a region of interest approach was used to investigate several regions of the brain in 17 controls and 18 manifest HD subjects over a one-year period, where no significant longitudinal differences in MD were found. Vandenberghe et al.[39] also applied a region of interest approach in eight manifest HD subjects over a two-year period, where no longitudinal differences between the groups were found in MD. In our previous histogram-based study, both global and striatal differences in cross-sectional diffusivities between preHD, early HD and controls were observed, without evidence for any longitudinal differences.[25]

Using TBSS, a study by Poudel et al.[42] provided evidence for a significantly increased rate of longitudinal change in FA of the corpus callosum and cingulum of HD patients compared to preHD and controls. Also applying TBSS, Harrington et al.[11] demonstrated significant longitudinal differences in MD of the superior fronto-occipital fasciculus between preHD and controls using a cohort from the prospective international Predict-HD study.[43] It should be noted, however, that

the definition of the premanifest phase in the aforementioned study is different than in our study, making a direct comparison difficult. In the study of Harrington et al.[11] mutant gene-carriers scoring more than 5 points on the UHDRS-TMS were also included to the preHD group, as long as a diagnostic confidence level of 4 was not reached, a level in which an examiner had to have ≥ 99% confidence of seeing unequivocal signs of HD. In our clinical phenotypic characterization of preHD, mutant gene carriers had an UHDRS-TMS of ≤ 5, making the selection much more stringent and the results of the "preHD" group not comparable. Another study by Shaffer et al.[22] demonstrated longitudinal differences in cortico-striate tracts using a whole brain tractography approach in a larger cohort of preHD subjects from the same Predict-HD study. The inconsistencies in the literature might very well be attributed to inconsistencies in defining the regions/tracts of interest, not selecting the regions/tracts of interest most prone to change, variations in the definition of the premanifest phase, and/or other methodological limitations, such as for TBSS.[44]

This present study investigates cortical grey matter, where FA is generally not informative[31,32] and where MD, AD and RD were derived instead. Although the underlying structures studied by Poudel et al.[42] are different than in this study, one of the goals in HD biomarker research remains to identify the most sensitive longitudinal tools differentiating between preHD, early HD and healthy controls. The annualized rates of diffusivity measure changes in white matter microstructure found by Poudel et al.[42] were between 1.5%-3.5%, which given the period in the present study would roughly translate into a 3%-7% change rate. Also, no evidence was found for a longitudinal difference in diffusivity change for the preHD group in that report. The rates of change found in the present study are generally more prominent compared to those reported by Poudel et al.[42] Moreover, a distinct longitudinal diffusivity change was demonstrated in preHD-B, implying that investigating the occipital cortex as a region of interest may provide a more sensitive way to track disease advancement in preHD compared to the corpus callosum and/or cingulum. An important quality for a robust biomarker is reproducibility of results. This makes unbiased, fully automated approaches desirable in order to investigate the effect of an intervention within and between centres as easily and reliably as possible.

Inference of biological meaning based on the observed changes in diffusivity is challenging, especially in grey matter.[31,32] Therefore, caution should be taken when attempting to interpret these results in the light of a disease-specific microstructural effect on the occipital cortex. The findings of small changes in diffusivity values within the healthy control group in the two-year between-scan interval is most likely explained by natural, ongoing, age-related processes of the brain.[45,46] It is likely that the findings of increased changes in the diffusivities of both preHD and early HD subjects reflect progressive disruption of cell boundaries in this cortical region with disease advancement, causing an increase in tissue permeability and interaxonal spacing due to neural tissue loss.[20,47] Evidence for ongoing macrostructural neurodegeneration in HD is already known from previous MRI volumetric investigations.[1-7,9,10,39] The value of the current results lie in the high rate of observed microstructural changes that is disease stage-specific. Potential effects of a therapeutic agent could theoretically be examined by concomitant monitoring of the rate of change in microstructural integrity of the occipital cortex, thereby inferring potential protective effects.

Strengths of this study include a longitudinal design specifically focused on DTI measures obtained from the occipital cortex in HD. Also, an automated atlas based procedure was applied, which has already shown to provide objective and reproducible results in the clinical setting.[28] Furthermore, between-scan intervals were alike between all the groups and the same scanner and scan protocol were used at both time points, reducing test-retest variation in DTI data.[48] Potential limitations of this study include the relatively small sample size of early HD patients and potential imperfect atlas-based segmentations of the occipital cortex.[28] Notwithstanding these concerns, these results provide evidence for a robust effect on longitudinal diffusivity measures in HD.

Conclusions

Findings in this study reinforce previous research of disease-stage related occipital involvement in HD, adding evidence for a divergent longitudinal evolution of diffusion measures reflecting microstructural change compared to healthy controls. The results were complemented by significant associations between diffusion measures and SWR, a cognitive task frequently administered in HD research. Investigating the occipital cortex with DTI measures seems to be a promising and sensitive tool to assess the efficacy of future planned disease modifying clinical trials in premanifest and early manifest HD.

Acknowledgments

TRACK-HD is supported by CHDI/High Q Foundation Inc., a not for profit organization dedicated to finding treatments for Huntington's disease. The research of A.L. is supported by VIDI Grant 639.072.411 from the Netherlands Organisation for Scientific Research (NWO). The authors wish to thank Sarah Tabrizi, University College London, who is the global PI for TRACK-HD and clinical site PI for London. The authors also wish to extend their gratitude to the TRACK-HD investigators responsible for collecting the data and to the study participants and their families.

References

1 Tabrizi SJ, Langbehn DR, Leavitt BR, et al. Biological and clinical manifestations of Huntington's disease in the longitudinal TRACK-HD study: cross-sectional analysis of baseline data. Lancet Neurol. 2009;8:791-801.
2 Tabrizi SJ, Reilmann R, Roos RA, et al. Potential endpoints for clinical trials in premanifest and early Huntington's disease in the TRACK-HD study: analysis of 24 month observational data. Lancet Neurol. 2012;11:42-53.
3 Henley SM, Wild EJ, Hobbs NZ, et al. Relationship between CAG repeat length and brain volume in premanifest and early Huntington's disease. J Neurol. 2009;256:203-212.
4 Rosas HD, Salat DH, Lee SY, et al. Cerebral cortex and the clinical expression of Huntington's disease: complexity and heterogeneity. Brain 2008;131:1057-1068.
5 Hobbs NZ, Henley SM, Ridgway GR, et al. The progression of regional atrophy in premanifest and early Huntington's disease: a longitudinal voxel-based morphometry study. J Neurol Neurosurg Psychiatry 2010;81:756-763.
6 Muhlau M, Weindl A, Wohlschlager AM, et al. Voxel-based morphometry indicates relative preservation of the limbic prefrontal cortex in early Huntington disease. J Neural Transm. 2007;114:367-372.
7 Coppen EM, van der Grond J, Hafkemeijer A, et al. Early grey matter changes in structural covariance networks in Huntington's disease. Neuroimage Clin. 2016; 12:806-814.
8 Dogan I, Eickhoff CR, Fox PT, et al. Functional connectivity modeling of consistent cortico-striatal degeneration in Huntington's disease. Neuroimage Clin. 2015;7:640-652.
9 Ciarochi JA, Calhoun VD, Lourens S, et al. Patterns of Co-Occurring Gray Matter Concentration Loss across the Huntington Disease Prodrome. Front Neurol. 2016; 7:147.
10 Johnson EB, Rees EM, Labuschagne I, et al. The impact of occipital lobe cortical thickness on cognitive task performance: An investigation in Huntington's Disease. Neuropsychologia 2015;138-146.
11 Harrington DL, Long JD, Durgerian S, et al. Cross-sectional and longitudinal multimodal structural imaging in prodromal Huntington's disease. Mov Disord. 2016;31:1664-1675.
12 Matsui JT, Vaidya JG, Wassermann D, et al. Prefrontal cortex white matter tracts in prodromal Huntington disease. Hum Brain Mapp. 2015;36:3717-3732.
13 Phillips OR, Joshi SH, Squitieri F, et al. Major Superficial White Matter Abnormalities in Huntington's Disease. Front Neurosci. 2016;10:197.
14 Wu D, Faria AV, Younes L, et al. Mapping the order and pattern of brain structural MRI changes using change-point analysis in premanifest Huntington's disease. Hum Brain Mapp. 2017;38:5035-5050.
15 Martin WR, Wieler M, Hanstock CC. Is brain lactate increased in Huntington's disease? J Neurol Sci. 2007;263:70-74.
16 Feigin A, Leenders KL, Moeller JR, et al. Metabolic network abnormalities in early Huntington's disease: an [(18)F]FDG PET study. J Nucl Med. 2001;42:1591-1595.
17 Reetz K, Romanzetti S, Dogan I, et al. Increased brain tissue sodium concentration in Huntington's Disease - a sodium imaging study at 4 T. Neuroimage 2012;63:517-524.
18 Lange HW. Quantitative changes of telencephalon, diencephalon, and mesencephalon in Huntington's chorea, postencephalitic and idiopathic parkinsonism. Verhandlungen der Anatomischen Gesellschaft 1981;75:923-925.
19 Rub U, Seidel K, Vonsattel JP, et al. Huntington's Disease (HD): Neurodegeneration of Brodmann's Primary Visual Area 17 (BA17). Brain Pathol. 2015;25:701-711.
20 Sotak CH. Nuclear magnetic resonance (NMR) measurement of the apparent diffusion coefficient (ADC) of tissue water and its relationship to cell volume changes in pathological states. Neurochem Int. 2004;45:569-582.

21 Bourbon-Teles J, Bells S, Jones DK, et al. Myelin breakdown in human Huntington's disease: Multi-modal evidence from diffusion MRI and quantitative magnetization transfer. Neuroscience 2017;doi: 10.1016/j.neuroscience.2017.05.042.

22 Shaffer JJ, Ghayoor A, Long JD, et al. Longitudinal diffusion changes in prodromal and early HD: Evidence of white-matter tract deterioration. Hum Brain Mapp. 2017;38:1460-1477.

23 Basser PJ, Mattiello J, LeBihan D. MR diffusion tensor spectroscopy and imaging. Biophys J. 1994;66:259-267.

24 Jones DK, Leemans A. Diffusion tensor imaging. Methods Mol Biol. 2011;711:127-144.

25 Odish OF, Leemans A, Reijntjes RH, et al. Microstructural brain abnormalities in Huntington's disease: A two-year follow-up. Hum Brain Mapp. 2015; 36:2061-2074.

26 Langbehn DR, Brinkman RR, Falush D, et al. A new model for prediction of the age of onset and penetrance for Huntington's disease based on CAG length. Clin Genet. 2004;65:267-277.

27 Leemans A, Jeurissen B, Sijbers J, et al. Explore DTI: a graphical toolbox for processing, analyzing, and visualizing diffusion MR data. 17th Annual Meeting of Intl Soc Mag Reson Med. 2009, Hawaii, USA. p. 3537.

28 Kersbergen KJ, Leemans A, Groenendaal F, et al. Microstructural brain development between 30 and 40weeks corrected age in a longitudinal cohort of extremely preterm infants. Neuroimage 2014;103C:214-224.

29 Rohlfing T, Zahr NM, Sullivan EV, et al. The SRI24 multichannel atlas of normal adult human brain structure. Hum Brain Mapp. 2010;31:798-819.

30 Klein S, Staring M, Murphy K, et al. elastix: a toolbox for intensity-based medical image registration. IEEE Trans Med Imaging 2010;29:196-205.

31 Beaulieu C. The basis of anisotropic water diffusion in the nervous system - a technical review. NMR Biomed 2002;15:435-455.

32 Jones DK, Knosche TR, Turner R. White matter integrity, fiber count, and other fallacies: the do's and don'ts of diffusion MRI. Neuroimage 2013;73:239-254.

33 Dogan I, Eickhoff SB, Schulz JB, et al. Consistent neurodegeneration and its association with clinical progression in Huntington's disease: a coordinate-based meta-analysis. Neurodegener Dis. 2013;12:23-35.

34 Tabrizi SJ, Scahill RI, Owen G, et al. Predictors of phenotypic progression and disease onset in premanifest and early-stage Huntington's disease in the TRACK-HD study: analysis of 36-month observational data. Lancet Neurol. 2013;12:637-649.

35 Say MJ, Jones R, Scahill RI, et al. Visuomotor integration deficits precede clinical onset in Huntington's disease. Neuropsychologia 2011;49:264-270.

36 Wolf RC, Sambataro F, Vasic N, et al. Visual system integrity and cognition in early Huntington's disease. Eur J Neurosci. 2014;40:2417-2426.

37 Henley SM, Novak MJ, Frost C, et al. Emotion recognition in Huntington's disease: a systematic review. Neurosci Biobehav Rev. 2012;36:237-253.

38 Novak MJ, Warren JD, Henley SM, et al. Altered brain mechanisms of emotion processing in pre-manifest Huntington's disease. Brain 2012;135:1165-1179.

39 Vandenberghe W, Demaerel P, Dom R, et al. Diffusion-weighted versus volumetric imaging of the striatum in early symptomatic Huntington disease. J Neurol. 2009;256:109-114.

40 Weaver KE, Richards TL, Liang O, et al. Longitudinal diffusion tensor imaging in Huntington's Disease. Exp Neurol. 2009;216:525-529.

41 Sritharan A, Egan GF, Johnston L, et al. A longitudinal diffusion tensor imaging study in symptomatic Huntington's disease. J Neurol Neurosurg Psychiatry 2010;81:257-262.

42 Poudel GR, Stout JC, Dominguez DJ, et al. Longitudinal change in white matter microstructure in Huntington's disease: The IMAGE-HD study. Neurobiol Dis. 2014;74C:406-412.
43 Paulsen JS, Langbehn DR, Stout JC, et al. Detection of Huntington's disease decades before diagnosis: the Predict-HD study. J Neurol Neurosurg Psychiatry 2008;79:874-880.
44 Bach M, Laun FB, Leemans A, et al. Methodological considerations on tract-based spatial statistics (TBSS). Neuroimage 2014;100:358-369.
45 Hsu JL, Leemans A, Bai CH, et al. Gender differences and age-related white matter changes of the human brain: a diffusion tensor imaging study. Neuroimage 2008;39:566-577.
46 Hsu JL, Hecke W, Bai CH, et al. Microstructural white matter changes in normal aging: a diffusion tensor imaging study with higher-order polynomial regression models. Neuroimage 2010;49:32-43.
47 Tellez-Nagel I, Johnson AB, Terry RD. Studies on brain biopsies of patients with Huntington's chorea. J Neuropathol Exp Neurol. 1974;33:308-332.
48 Takao H, Hayashi N, Kabasawa H, et al. Effect of scanner in longitudinal diffusion tensor imaging studies. Hum Brain Mapp. 2012;33:466-477.

Supplementary material

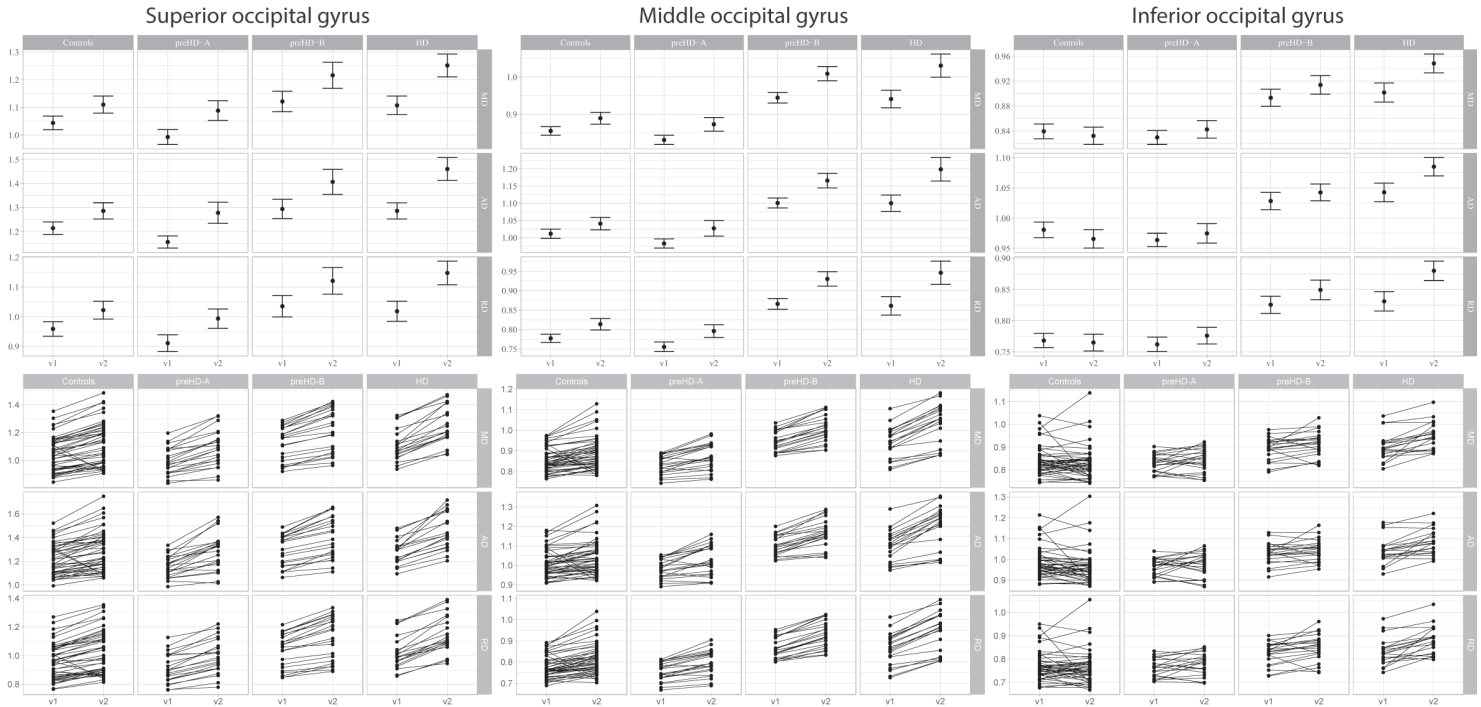

Supplementary Figure 1. *Two-year absolute change in mean diffusivity (MD), axial diffusivity (AD) and radial diffusivity (RD) of the three occipital regions of the groups. MD, AD and RD in mm^2/s (shown $x10^3$ for readability). Standard error bars are also shown. V1 = visit 1, v2 = visit 2.*

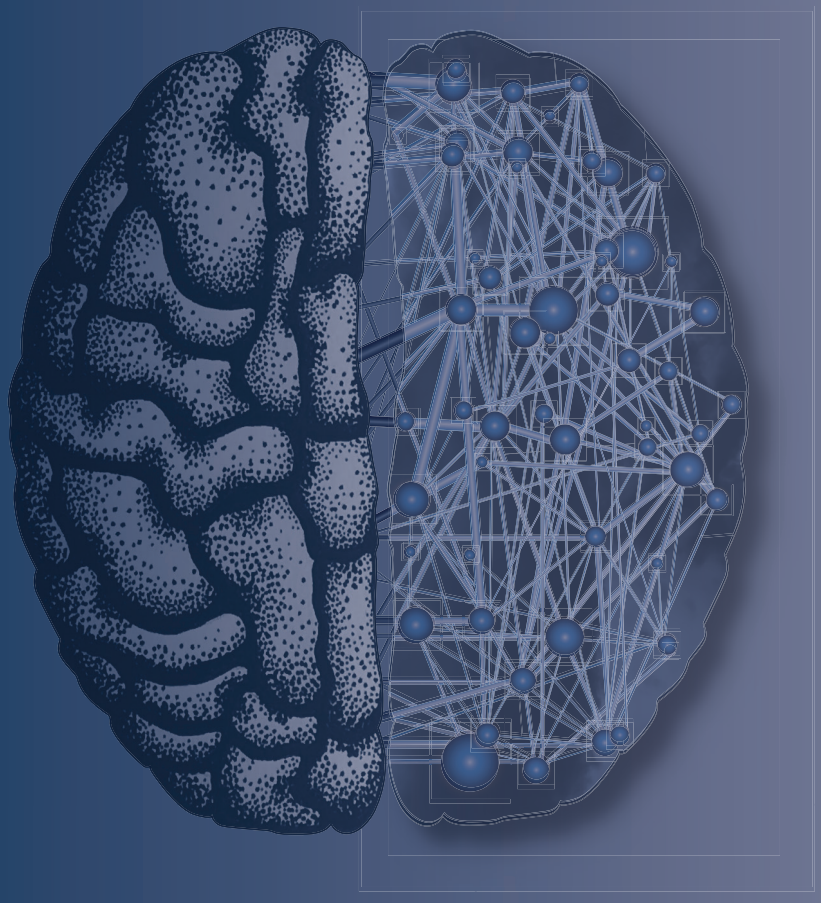

EEG may serve as a biomarker in Huntington's disease using machine learning automatic classification

CHAPTER 6

6

Omar F.F. Odish[1], Kristinn Johnsen[2], Paul van Someren[3], Raymund A.C. Roos[3], J. Gert van Dijk[3]

[1] Department of Neurology, University Medical Center Groningen, Groningen, The Netherlands
[2] MentisCura ehf., Reykjavík, Iceland
[3] Department of Neurology, Leiden University Medical Center, Leiden, The Netherlands

Scientific Reports 2018;8:16090

Abstract

Background

Reliable markers measuring disease progression in Huntington's disease (HD), before and after disease manifestation, may guide a therapy aimed at slowing or halting disease progression. Quantitative electroencephalography (qEEG) may provide a quantification method for possible (sub)cortical dysfunction occurring prior to or concomitant with motor or cognitive disturbances observed in HD. In this pilot study we construct an automatic classifier distinguishing healthy controls from HD gene carriers using quantitative qEEG and derive qEEG features that correlate with clinical markers known to change with disease progression in HD, with the aim of exploring biomarker potential.

Methods

We included twenty-six HD gene carriers (49.7 ± 8.5 years) and 25 healthy controls (52.7 ± 8.7 years). EEG was recorded for three minutes with subjects at rest. An EEG index was created by applying statistical pattern recognition to a large set of EEG features, which was subsequently tested using 10-fold cross-validation. The index resulted in a continuous variable ranging from 0 to 1: a low value indicating a state close to normal and a high value pointing to HD. qEEG features that correlate specifically with commonly used clinical markers in HD research were derived.

Results

The classification index had a specificity of 83%, a sensitivity of 83% and an accuracy of 83%. The area under the curve of the receiver operator characteristic curve was 0.9. qEEG analysis on subsets of electrophysiological features resulted in two highly significant correlations with clinical scores.

Conclusions

The results of this pilot study suggest that qEEG may serve as a biomarker in HD. The indices correlating with modalities changing with the progression of the disease may lead to tools based on qEEG that help monitor efficacy in intervention studies.

Introduction

Huntington's disease (HD) is an autosomal dominant neurodegenerative disorder characterized by motor, cognitive and psychiatric symptoms with a mean age at onset between 30-50 years.[1] It is caused by an expanded cytosine-adenine-guanine (CAG) trinucleotide repeat in the huntingtin gene on the short arm of chromosome 4. The disease causes widespread brain pathology. Magnetic resonance imaging (MRI) studies in HD have revealed extensive brain atrophy, most notably in the striatum.[2,3,4] With disease progression, neurodegenerative changes further extend to the cortical grey-matter areas.[5,6] Cortical atrophy is found in both premanifest (preHD) as well as manifest stages of HD, with an increasing cortical thinning detectable with progressing disease severity.[2,7]

A challenge in HD research is to establish reliable markers to measure disease progression, both before and after disease manifestation, in preparation for the advent of new therapy aiming to slow or halt disease progression. This will be of tantamount importance for carriers of CAG repeat lengths of 40 or higher as they will develop manifest HD with certainty.

Electroencephalography (EEG) is an easy, cheap and rapid technique to assess (sub)cortical pathology. Quantitative electroencephalography (qEEG) provides objective parameters to assess (sub)cortical dysfunction occurring prior to or concomitant with motor or cognitive disturbances in HD. Combining such measures with clinical tests in HD gene carriers may provide added insights into progression of pathology and increased sensitivity for detecting subtle changes. Previous studies have found EEG abnormalities in HD.[8] A study using a different automated method compared to the one used in this paper, called automated artificial neural networks (ANN), showed promising results in discriminating between EEGs of HD gene carriers and controls.[9]

In this pilot study, we hypothesized that machine learning automatic classification of EEG patterns may discern healthy controls from HD gene carriers. If so, this would be the first step to assess this technique as a longitudinal biomarker in HD. Secondly, we aimed to derive qEEG features that correlate with commonly used clinical and cognitive markers in HD research, known to change with disease progression. This is done to evaluate the usefulness of these qEEG features as biomarkers for tracking disease state and progression in HD.

Table I. *Group characteristics and clinical scores*

	Healthy controls	Combined(pre)HD	preHD	Early HD
N	25	26	6	20
Gender M/F	7/18	10/16	1/5	9/11
Age in years (at V1), mean (SD)	52.7 (8.7)	49.7 (8.5)	49.1 (4.9)	49.9 (9.4)
Handedness R/L	24/1	22/4	5/1	17/3
Level of education (ISCED), median (range)	4 (6)	5 (5)	4.5 (4)	5 (5)
CAG repeat length, mean (SD)	n/a	43.2 (2.3)	41.3 (1.2)	43.8 (2.2)¥
Estimated years to onset, mean (SD)	n/a	n/a	10.8 (2.6)	n/a
Total functional capacity, mean (SD)	13.0 (0.2)	12.3 (1.2)*	12.8 (0.4)	12.1 (1.3)Φ
UHDRS-TMS, mean (SD)	1.3 (1.7)	10.5 (6.9)*	2.8 (2.1)	12.8 (6.1)Φ
SDMT, mean (SD)	54.7 (11.5)	49.3 (10.0)^	56.7 (10.4)	47.1 (9.0)*
SWR, mean (SD)	108.0 (16.1)	95.0 (14.5)*	99.0 (7.2)	93.9 (16.0)*
BDI-II, mean (SD)	3.6 (3.9)	6.6 (7.3)^	3.3 (2.9)	7.6 (8.0)Φ

N = number of participants, SD = Standard deviation, n/a = not applicable, ISCED = International Standard Classification of Education, CAG = Cytosine-Adenine-Guanine, UHDRS-TMS = Unified Huntington's Disease Rating Scale-Total Motor Score, SDMT = Symbol Digit Modalities Test, SWR = Stroop Word Reading task, BDI-II = Beck Depression Inventory-II.

*Significance at p ≤ 0.05 level: * significantly different from controls, Φ significantly different from controls and preHD, ¥ significantly different from preHD. ^ p = 0.07.*

Materials and methods

Participants

Twenty-six HD gene carriers and 25 healthy controls were recruited from the Neurology outpatient clinic of the Leiden University Medical Center (LUMC), the Netherlands (Table I). The preHD group (6 subjects) had a CAG repeat ≥ 40 with a total motor score on the Unified Huntington's Disease Rating Scale (UHDRS-TMS) ≤ five. The early manifest HD group (20 subjects) had a CAG repeat ≥ 40 with a UHDRS-TMS ≥ five and a Total Functional Capacity score (TFC) ≥ 7. A burden of pathology score greater than 250 ((CAG repeat length - 35.5) x age) was required as a further inclusion criterion for the HD gene carrier group.[2,10] Healthy gene-negative partners (or family members in three instances) were recruited as controls (25 subjects). None of the participants suffered from a concomitant neurological or psychiatric disorder or had a history of severe head injury. The study was approved by the Medical Ethics Committee of the Leiden University Medical Center and written informed consent was obtained from all participants. All methods were performed in accordance with the relevant guidelines and regulations.

Clinical measures

The following clinical measures were evaluated in all participants: UHDRS-TMS, TFC, Symbol Digit Modalities Test (SDMT), Stroop Word Reading (SWR) and Beck Depression Inventory-II (BDI-II) scores.

The UHDRS-TMS is the current gold-standard which defines manifest disease state in HD. The SDMT and SWR have been shown to be sensitive neurocognitive measures in HD, independent of disease related motor effects.[11]

EEG recording

The International 10–20 system was used for electrode placement using 19 Ag/AgCl electrodes. The average potential was used as a reference in subsequent analyses. Two horizontal bipolar eye movement leads and one for the electrocardiogram were applied to monitor artefacts. The EEG was recorded for three minutes with subjects at rest with eyes closed. Subjects were instructed to sit comfortably in a chair and close their eyes, but to remain awake. Subjects were alerted if they became visibly drowsy or if there were indications of that on the EEG. EEGs were recorded using a Nihon Kohden Neurofax 1200 system. Matlab (MathWorks® Version 7.1) and the LIBSVM toolbox[33] were used for analyzing the data.

EEG and statistical analysis

The analysis started by calculating the power spectrum followed by the connectivity and synchronization between electrodes. This was done to extract features from the recordings that reflect the variations of the spatial and temporal information in the multivariate data. First the power spectrum was calculated in the average montage for the signal at each individual electrode using a Fast Fourier Transformation (FFT) algorithm[12] for consecutive 2 second segments with an overlap of 1 second. The EEG of each segment was subjected to a Bartlett window and a power spectrum using the FFT method was calculated, so for each electrode/lead N spectra were obtained, in which N was the number of segments. A final estimate for the power spectrum was then obtained by applying robust fits[13] for each point in the spectrum, over the ensemble of N spectra. The second step of the analysis involved the connectivity and synchronization between electrodes, through the power spectrum of the auto correlation function between all possible pairs of electrodes. This was done in the average montage. The same segments were used as described above. The choice of 2 second segments resulted in a spectral resolution of 0.5 Hz. We chose to work with a spectral cut-off of 45 Hz. This resulted in 91 spectral power values for each spectrum. The total number of spectral estimates entering the evaluation was 19 for the spectra for each electrode as well as 171 for all the possible autocorrelation spectra. Together, there were 17290 spectral features for each qEEG. The full spectrum was considered for investigation of the group level differences between the single electrode spectra. For the statistical pattern recognition (SPR) analysis the feature set was reduced. To do so, each spectrum was first reduced by dividing it into overlapping bands of 8 Hz width with an overlap of 4 Hz. Each band was modulated by a Bartlett window reducing the number of features from 91 spectral features to 11. This procedure reduced the total number of features to 2090.

As the cohort in this study was small, it was important to avoid instability and overfitting in the SPR analysis if all features were taken into account simultaneously. This can occur even though support vector machine are applied in the SPR, which depend on the number of support vectors but not the number of features.[14] A subset of only 20 features were used in the analysis. The

subset of features was chosen by applying a genetic algorithm that optimized the area under the curve (AUC) of the resulting receiver operator characteristic (ROC) curve.[15] The ROC statistics were estimated for each candidate feature subset using 10-fold cross-validation.[16] For comparison of bias, 3- and 5-fold cross-validations were also performed, where the resulting estimates of the ROC statistics did not differ significantly. The combined HD gene carrier group (26 subjects) was pooled in the EEG analysis due to low numbers of preHD participants when considered separately, where it was not feasible to create a separate classifier, and in order to increase overall power. Furthermore, combining data from the preHD group with the early HD group did not affect outcomes. A classifier was constructed that contrasted the control group and the HD gene carrier group. The classifier yielded an HD vs. control (HDvsCT) Index, ranging from 0 to 1, with low values for controls and high values indicating HD. The performance of the classifier was determined using repeated 10-fold cross-validation.

Correlations between the electrophysiology and clinical modalities were sought using a similar approach. In this case, however, principal component analysis (PCA) was applied on each feature subset. The linear Pearson correlation between the principal components and the clinical modalities was optimized. Statistical analysis of group demographics and clinical measures was performed using IBM SPSS Statistics (version 20, IBM, USA). Distributions and assumptions were checked and appropriate statistical tests were applied.

Results

Group characteristics and clinical scores

The groups did not differ significantly in terms of age, gender, handedness or level of education. TFC and SWR were significantly lower for the HD gene carrier group compared to the control group ($p = 0.007$ and $p = 0.004$, respectively; Mann–Whitney *U* test and independent-samples t-test, respectively). The HD gene carrier group had higher UHDRS-TMS than controls ($p = 0.00001$, independent-samples t-test). There was a trend for lower SDMT scores and higher BDI-II scores for the HD gene carrier group compared to controls (both $p = 0.07$; independent-samples t-tests). The early HD group had lower SDMT scores compared to controls only ($p = 0.02$; analysis of variance) and higher BDI-II scores compared to both preHD and controls ($p = 0.04$ and $p = 0.01$, respectively; analysis of variance). See Table I for a summary of these results.

The HD classifier

A classifier was constructed that optimized the contrast between the HD gene carrier and control groups with a specificity of 83%, a sensitivity of 83% and an accuracy of 83%. The AUC was 0.9 (Figure 1). The estimated group distributions are illustrated in Figure 2. There were no significant relationships between the HDvsCT Index and any of the clinical measures.

Correlating qEEG subsets with clinical modalities

The analysis of the correlations between electrophysiological features and clinical modalities resulted in two highly significant correlations in the HD gene carrier cohort. The first factor,

referred to as Index-A, correlated strongly with the SDMT score, see Figure 3. Pearson's correlation coefficient was 0.86 (p = 0.0001). The second factor, referred to as Index-B, correlated strongly with the UHDRS-TMS, see Figure 4 (r = 0.84, p = 0.0001). See Supplementary Figures 1 and 2 for an overview of the spatial and spectral dependence of the coherences entering indices A and B.

Full power spectrum analysis

The full power spectra for the 19 electrodes were evaluated and group averages were compared (Supplementary Figure 3). The average spectra were significantly different (p = 0.001). Most prominently, the overall power was less in the HD gene carrier group. An extra resonance appeared in the average spectra of the HD gene carrier group at about 22 Hz, not present in the control group in the right temporal region. The alpha peak was distinctly divided into two peaks in the occipital, temporal and parietal areas.

qEEG spectral differences

In the area of the anterior prefrontal cortex (Brodmann area 10; BA10), channels Fp1 and Fp2, the HD gene carrier group had a higher power than controls in the delta band. At all other locations significant difference in power was such that the power was higher in the control group except for the delta bands (higher in the HD gene carrier group): at the frontal eye fields (BA8), F3, F4 and Fz (theta); at the primary somatosensory cortex (BA2) and motor cortex (BA4), C3 (delta, theta and alpha), C4 (theta and alpha), Cz (theta); at the temporal regions influenced by the auditory somatosensory cortex (BA42), primary somatosensory cortex (BA2) and motor cortex (BA4), T3 (theta and alpha), T4 (delta, theta and alpha); and also influenced by the fusiform gyrus (BA37), T5 (theta and alpha), T6 (delta and theta); finally in the parietal area (BA7), Pz (theta and alpha). See Table II for a summary of these results, including p-values, t-statistics and Cohen's d for effect sizes.

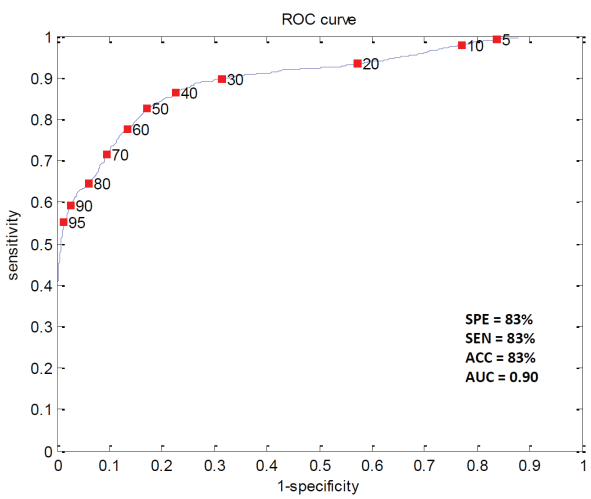

Figure 1. The ROC curve for the HD vs. control Index estimated with repeated 10-fold cross-validation along with the result. SPE = specificity; SEN = sensitivity; ACC = accuracy; AUC = area under the curve.

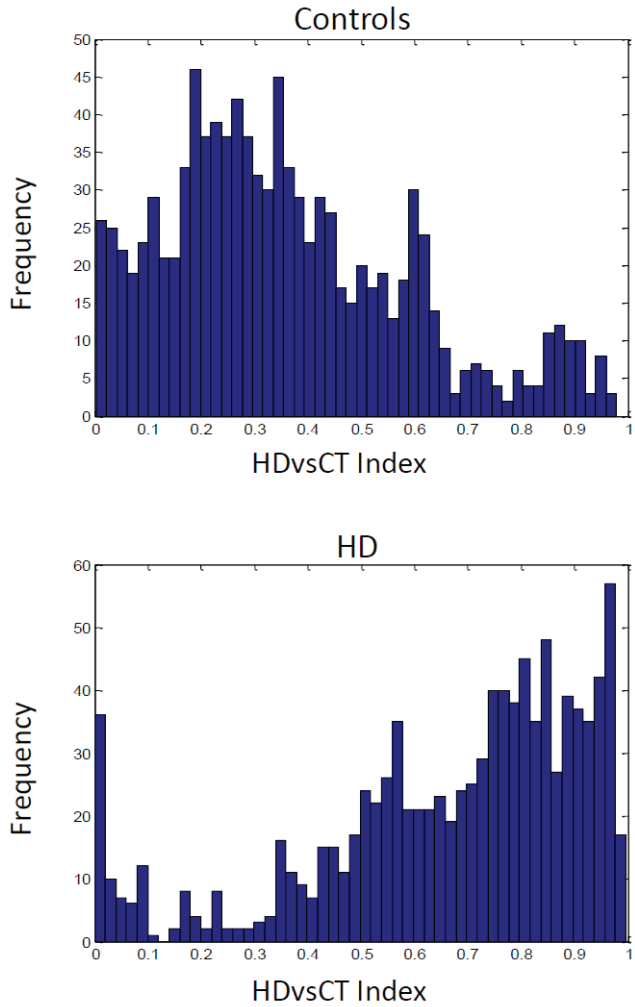

Figure 2. *Controls and Huntington's disease subjects in the HD vs. control (HDvsCT) Index as estimated with repeated 10-fold cross validation. The frequency is an estimate of the continuous likelihood distribution.*

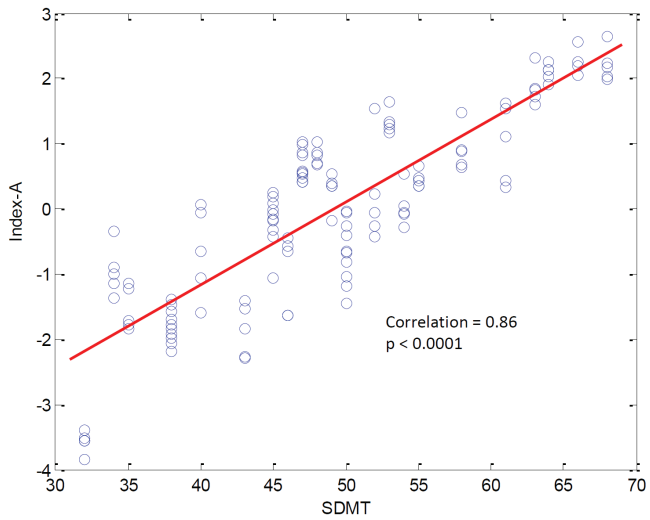

Figure 3. *Relationship between Index-A and the SDMT score. The contribution of Index-A was evaluated in 5 consecutive segments of the EEG recording for each subject. All results are shown, illustrating the inter-subject variability of Index-A.*

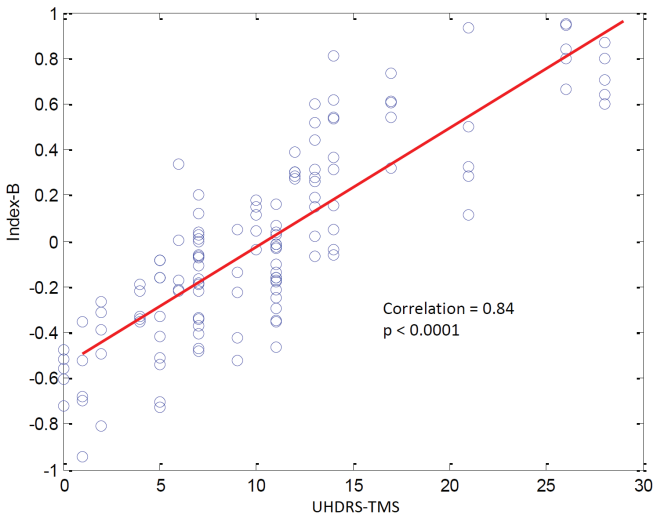

Figure 4. *Relationship between Index-B and the UHDRS-Total Motor Score. The contribution of Index-B was evaluated in 5 consecutive segments of the EEG recording for each subject. All results are shown, illustrating the inter-subject variability of Index-B.*

Discussion

In this exploratory study, the qEEG automatic classification index proved to separate HD gene carriers from healthy controls with good specificity and sensitivity. This method has therefore a potential to be further developed as a biomarker in HD. The study also revealed strong correlations between qEEG features and the UHDRS-TMS and SDMT, both relevant clinical markers in HD research. Finally, global EEG average power spectra were shown to be significantly lower in the HD gene carrier group compared to controls and qEEG spectral differences between the groups were demonstrated.

Table II. *Significant differences in qEEG spectral power*

Channel	Band	Power - Healthy controls (N = 25)	Power - Combined (pre)HD (N = 26)	*p*-value	t-statistic	Cohen's *d*
Fp1	delta	4.5	4.9	0.004	-3.0	0.85
Fp2	delta	4.5	4.9	0.005	-2.9	0.82
F3	theta	3.3	3.0	0.007	2.8	-0.78
F4	theta	3.3	3.1	0.016	2.5	-0.70
Fz	theta	3.4	3.1	0.003	3.1	-0.88
C3	delta	3.6	3.8	0.048	-2.0	0.57
C3	theta	3.1	2.9	0.011	2.7	-0.74
C3	alpha	3.2	2.9	0.025	2.3	-0.65
C4	theta	3.1	2.9	0.004	3.0	-0.85
C4	alpha	3.2	2.9	0.022	2.4	-0.66
Cz	theta	3.3	3.1	0.024	2.3	-0.65
T3	theta	3.3	3.1	0.025	2.3	-0.65
T3	alpha	3.4	3.1	0.049	2.0	-0.56
T4	delta	3.9	4.1	0.031	-2.2	0.62
T4	theta	3.3	3.1	0.024	2.3	-0.66
T4	alpha	3.4	3.1	0.047	2.0	-0.57
T5	theta	3.5	3.2	0.009	2.7	-0.77
T5	alpha	3.7	3.4	0.025	2.3	-0.65
T6	delta	3.9	4.1	0.042	-2.1	0.58
T6	theta	3.4	3.2	0.042	1.8	-0.51
Pz	theta	3.2	3.1	0.031	2.2	-0.62
Pz	alpha	3.5	3.1	0.042	2.1	-0.58

Power values are log10-transformed. N = number of participants. Two-tailed t-test p-values are reported. Degrees of freedom = 49.

Using the index created in this study, it is possible to separate EEGs of HD and control subjects with an accuracy of over 80%. Considering direct correlations between the index and commonly used clinical measures is interesting, though less likely to result in significant findings as the measure is derived globally from all recorded regions of the brain, therefore lacking specificity. The index did indeed not correlate with any of the commonly used clinical and neurocognitive measures in HD research. This finding is in line with a previous study using a classifier approach.[9] When specific EEG features were considered, highly significant correlations with the UHDRS and SDMT scores were found, disease measures that are known to be altered in a longitudinal fashion in the (pre-) manifest state compared to healthy controls. This highlights the importance of using different approaches in biomarker research based on structural and/or functional brain data. Analyses focusing on global versus local measures provide different insights on disease state and possible correlations with clinical measures. Previous machine learning studies using different MRI modalities to discriminate HD gene carriers and controls achieved accuracies up to 83% and 76%, respectively, when specific regions affected by the disease were preselected for analysis.[34,35]

On EEG average power spectra a global decrease in theta and alpha power in HD was found, while delta power was increased in a few brain areas in HD. As the earliest structural brain changes in HD start within the striatum, this conceivably leads to disrupted projections in the cortico-striato-thalamo-cortical loops, which in turn lead to disruptions in brain rhythms.[17] The striatum represents a crucial node in these loops.[18] Reductions in the theta band power in HD have been reported in previous studies,[19,20,21,22] while other studies found an increase in this band[9,23,24]. Reductions in the theta band power were correlated with increased cognitive and motor deficits.[20] There seems to be consensus in the literature regarding globalized reductions in the alpha band in (pre)HD.[9,20,21,24,25,26] Some studies reported that reductions in the alpha band correlated significantly with increases in cognitive and motor deficits in HD,[19,20] while others could not replicate this finding[9]. Both theta and alpha EEG rhythms appear to reflect important neuronal processes in human cognition.[27,28,29] Decreases,[20,24] as well as increases[19] in beta power in HD have been reported, something we could not replicate. Most studies point to an increase in delta power in HD,[9,19,20,22,24,26] which is corroborated by findings in our study. It has been observed that alterations in delta power might be disease stage dependent and increase in advanced stages of HD.[20] This might explain the localized differences in delta power between the groups observed in this particular study sample, which represents premanifest or early stage patients.

The GABAergic network is postulated to be a driving force in producing synchronized brain oscillations.[30] Combined with the knowledge that dysfunction and loss of GABAergic neurons occurs early on in the striatum of HD[31,32] we hypothesize that the difference found in this study, both in the classification index as well as in differences in power spectra, are primarily derived from a deregulation of brain network oscillations through GABAergic dysfunction in HD. Another potential explanation for these findings might be a neurodevelopmental difference of HD brains reflecting an endophenotype. To explore the latter point, it is necessary to conduct longitudinal trials evaluating the potential progressive nature of these differences with advancing disease.

In this study we have observed several statistically significant results in the performance of classifiers as well as indices designed to correlate with relevant modalities related to HD progression. As with EEG related physiological interpretation in general, it is very hard to assign physiological meaning to these indices as the knowledge of relationships between EEG activity and the underlying physiology are poorly known or understood. The field is still in its data driven empirical era, which the present work contributes to. We have also observed significant differences between classical qEEG features when comparing between HD gene carriers and controls. These are exploratory findings limited in scope when it comes to the number of subjects participating. It is therefore pertinent to confirm these findings in independent studies conducted with pre-defined end points. Also, there is an increased risk of overfitting the separation model when using a small sample size as the one in this study. Another potential limitation is the use of the same system to record all EEGs, possibly reducing the validity of the model on other EEG equipment. Also, as this is a cross-sectional study, we can only speculate about the expected changes to the findings occurring during clinical deterioration in HD. Therefore, longitudinal studies are needed to evaluate the true usefulness of these indices. However, the fact that we have found indices strongly correlating with clinical markers of decline support the notion of a measurable progressive change in HD brain function rather than a purely neurodevelopmental difference.

Conclusion

In this exploratory study we show promising results where qEEG related modalities may help to unravel how HD evolves and how different areas of the brain are influenced as the condition progresses. The indices correlating with modalities changing with the progression of the disease may lead to tools based on qEEG that can help monitor efficacy in intervention studies. These points will need further independent studies before such applications can be put into force.

Acknowledgements

We thank W.W.M. Huyser, M.J. Stijl-Pek, F.I. Kerkhof, G.H. van Beukering-Louwes and J.J.M. Witteman for their help with EEG registration. We also wish to extend our gratitude to the investigators responsible for collecting the clinical and neurocognitive data and to the study participants and their families.

Disclosure statement

K.J. is an employee of MentisCura ehf., which is a privately owned for-profit enterprise. The other authors declare that they have no competing interests.

References

1 Roos RA Huntington's disease: a clinical review. Orphanet J Rare Dis. 2010;5:40.
2 Tabrizi SJ, Langbehn DR, Leavitt BR, et al. Biological and clinical manifestations of Huntington's disease in the longitudinal TRACK-HD study: cross-sectional analysis of baseline data. Lancet Neurol. 2009;8:791-801.
3 Aylward EH, Liu D, Nopoulos PC, et al. Striatal volume contributes to the prediction of onset of Huntington disease in incident cases. Biol Psychiatry 2012;71:822-828.
4 Hadzi TC, Hendricks AE, Latourelle JC, et al. Assessment of cortical and striatal involvement in 523 Huntington disease brains. Neurology 2012;79:1708-1715.
5 Rosas HD, Liu AK, Hersch S, et al. Regional and progressive thinning of the cortical ribbon in Huntington's disease. Neurology 2002;58:695-701.
6 Kassubek J, Juengling FD, Kioschies T, et al. Topography of cerebral atrophy in early Huntington's disease: a voxel based morphometric MRI study. J Neurol Neurosurg Psychiatry 2004;75:213-220.
7 Rosas HD, Salat DH, Lee SY, et al. Cerebral cortex and the clinical expression of Huntington's disease: complexity and heterogeneity. Brain 2008;131:1057-1068.
8 Nguyen L, Bradshaw JL, Stout JC, et al. Electrophysiological measures as potential biomarkers in Huntington's disease: review and future directions. Brain Res Rev. 2010;64:177-194.
9 De Tommaso M, De Carlo F, Difruscolo O, et al. Detection of subclinical brain electrical activity changes in Huntington's disease using artificial neural networks. Clin Neurophysiol. 2003;114:1237-1245.
10 Penney JB, Jr., Vonsattel JP, MacDonald ME, et al. CAG repeat number governs the development rate of pathology in Huntington's disease. Ann Neurol. 1997;41:689-692.
11 Tabrizi SJ, Scahill RI, Durr A, et al. Biological and clinical changes in premanifest and early stage Huntington's disease in the TRACK-HD study: the 12-month longitudinal analysis. Lancet Neurol. 2011:10:31-42.
12 Cooley JW, John W. An algorithm for the machine calculation of complex Fourier series. Tukey Journal: Math Comp. 1965;19:297-301.
13 Wainer H, Thissen D. Three steps toward robust regression. Psychometrika 1976;41:9-34.
14 Cortes C, Vapnik V. Support-vector networks. Machine learning 1995;20:273-297.
15 Swets JA. Signal detection theory and ROC analysis in psychology and diagnostics: collected papers. Chapter 8, "Enhancing and Evaluating Diagnostic Accuracy". Page 185. Lawrence Erlbaum Associates, Mahwah, NJ 1996.
16 Kohavi R. A study of cross-validation and bootstrap for accuracy estimation and model selection. Proceedings of the Fourteenth International Joint Conference on Artificial Intelligence. San Mateo, CA: Morgan Kaufmann 1995;2:1137-1143.
17 Hughes SW, Crunelli V. Thalamic mechanisms of EEG alpha rhythms and their pathological implications. Neuroscientist 2005;11:357-372.
18 Draganski B, Kherif F, Klöppel S, et al. Evidence for segregated and integrative connectivity patterns in the human Basal Ganglia. J Neurosci. 2008;28:7143-7152.
19 Bylsma FW, Peyser CE, Folstein SE, et al. EEG power spectra in Huntington's disease: clinical and neuropsychological correlates. Neuropsychologia 1994;32:137-150.
20 Painold A, Anderer P, Holl AK, et al. EEG low-resolution brain electromagnetic tomography (LORETA) in Huntington's disease. J Neurol. 2011;258:840-854.
21 Ponomareva N, Klyushnikov S, Abramycheva N, et al. Alpha-theta border EEG abnormalities in preclinical Huntington's disease. J Neurol Sci. 2014;344:114-120.
22 Piano C, Mazzucchi E, Bentivoglio AR, et al. Wake and Sleep EEG in Patients With Huntington Disease: An eLORETA Study and Review of the Literature. Clin EEG Neurosci. 2017;48:60-71.

23 Streletz LJ, Reyes PF, Zalewska M, et al. Computer analysis of EEG activity in dementia of the Alzheimer's type and Huntington's disease. Neurobiol Aging 1990;11:15-20.
24 Painold A, Anderer P, Holl AK, et al. Comparative EEG mapping studies in Huntington's disease patients and controls. J Neural Transm. 2010;117:1307-1318.
25 van der Hiele K, Jurgens CK, Vein AA, et al. Memory activation reveals abnormal EEG in preclinical Huntington's disease. Mov Disord. 2007;22:690-695.
26 Hunter A, Bordelon Y, Cook I, et al. QEEG Measures in Huntington's Disease: A Pilot Study. PLoS Curr. 2010;2:RRN1192.
27 Schack B, Klimesch W, Sauseng P. Phase synchronization between theta and upper alpha oscillations in a working memory task. Int J Psychophysiol. 2005;57:105-114.
28 Jann K, Dierks T, Boesch C, et al. BOLD correlates of EEG alpha phase-locking and the fMRI default mode network. Neuroimage 2009;45:903-916.
29 Klimesch W. Alpha-band oscillations, attention, and controlled access to stored information. Trends Cogn Sci. 2012;16:606-617.
30 Gonzalez-Burgos G, Lewis DA. GABA neurons and the mechanisms of network oscillations: implications for understanding cortical dysfunction in schizophrenia. Schizophr Bull. 2008;34:944-961.
31 Vonsattel JP, Myers RH, Stevens TJ, et al. Neuropathological classification of Huntington's disease. J Neuropathol Exp Neurol. 1985;44:559-577.
32 Raymond LA, Andre VM, Cepeda C, et al. Pathophysiology of Huntington's disease: time-dependent alterations in synaptic and receptor function. Neuroscience 2011;198:252-273.
33 Chang CC, Lin CJ. LIBSVM: a library for support vector machines. ACM Trans Intell Syst Technol. 2011;2:27.
34 Klöppel S, Chu C, Tan GC, et al. Automatic detection of preclinical neurodegeneration: presymptomatic Huntington disease. Neurology 2009;72,426-431.
35 Rizk-Jackson A, Stoffers D, Sheldon S, et al. Evaluating imaging biomarkers for neurodegeneration in pre-symptomatic Huntington's disease using machine learning techniques. NeuroImage 2011;56:788-796.

Supplementary material

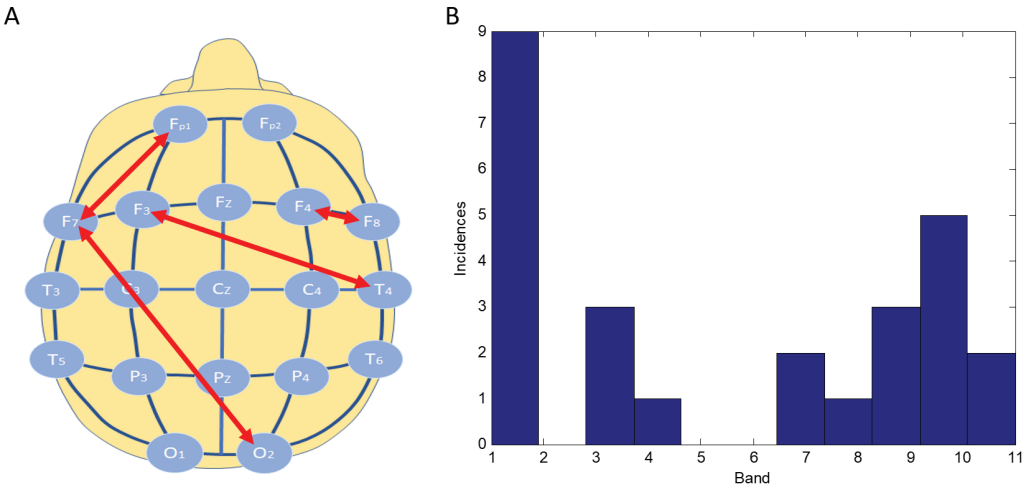

Supplementary Figure 1. *Spatial (A) and spectral (B) dependence of the coherences entering Index-A.*

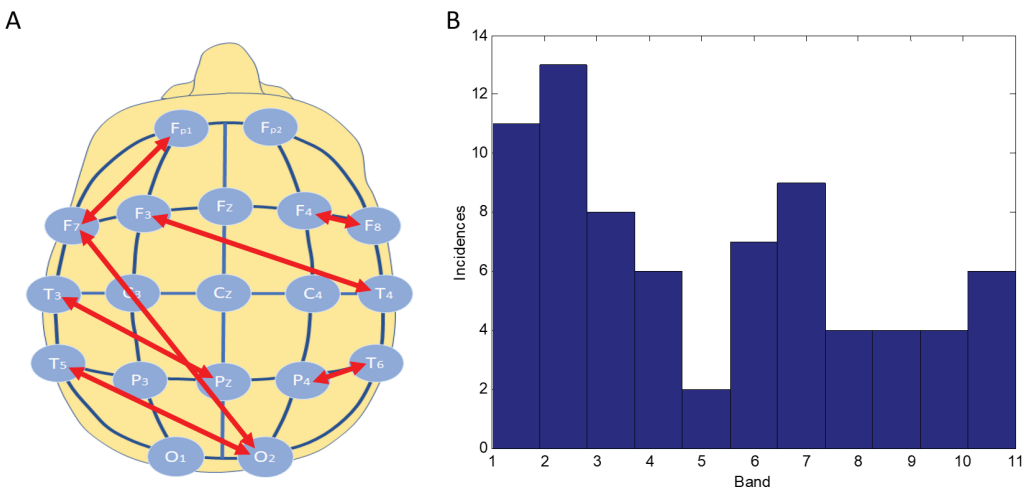

Supplementary Figure 2. *Spatial (A) and spectral (B) dependence of the coherences entering Index-B.*

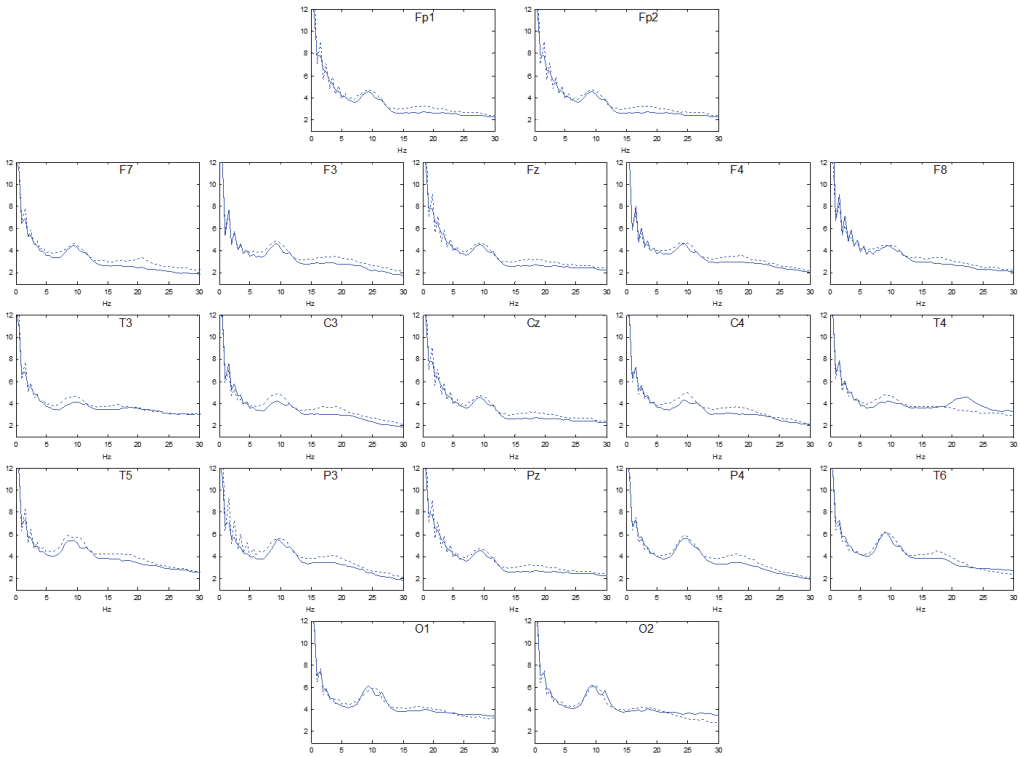

Supplementary Figure 3. *The average full power spectra on group level. The dotted curves are the average over the control group. The solid curves are the average over the HD gene carrier group.*

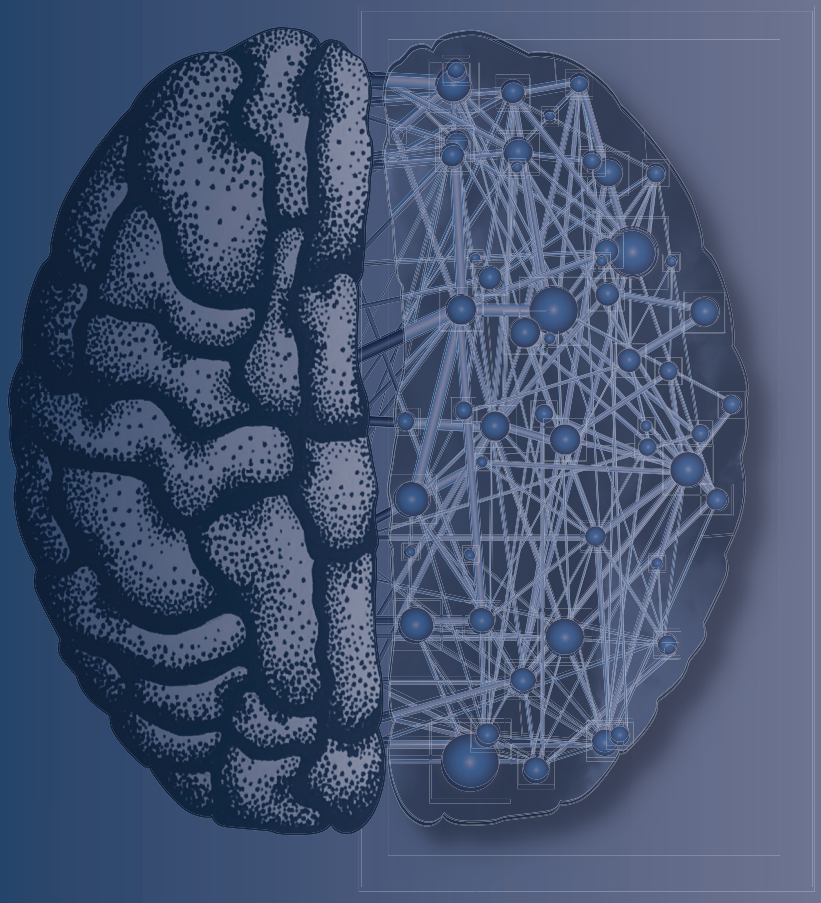

Multimodal characterization of the visual network in Huntington's disease gene carriers

CHAPTER 7

Sarah Gregory[1]*, Omar F.F. Odish[2]*, Isabella Mayer[3]*, James Mills[4], Eileanoir B. Johnson[1], Rachael I. Scahill[1], John Rothwell[5], Geraint Rees[6], Jeffrey D. Long[4,7], Sarah J. Tabrizi[1], Raymund A.C. Roos[8], Michael Orth[3]

[1] Huntington's Disease Centre, UCL Queen Square Institute of Neurology, London, UK
[2] Department of Neurology, University Medical Center Groningen, Groningen, The Netherlands
[3] Department of Neurology, Ulm University Hospital, Ulm, Germany
[4] Department of Psychiatry, University of Iowa, Iowa City, IA, USA
[5] Sobell Department of Motor Neuroscience and Movement Disorders, UCL Queen Square Institute of Neurology, London, UK
[6] Wellcome Trust Centre for Neuroimaging, University College London, London, UK
[7] Department of Biostatistics, University of Iowa, Iowa City, IA, USA
[8] Department of Neurology, Leiden University Medical Center, Leiden, The Netherlands
* Equal contribution

Clinical Neurophysiology 2019;doi:10.1016/j.clinph.2019.08.018

Abstract

Background
A sensorimotor network structural phenotype predicted motor task performance in a previous study in Huntington's disease (HD) gene carriers. We investigated in the visual network whether structure-function-behaviour relationship patterns, and the effects of the HD mutation, extended beyond the sensorimotor network.

Methods
We used multimodal visual network MRI structural measures (cortical thickness and white matter connectivity), plus visual evoked potentials and task performance (Map Search; Symbol Digit Modalities Test) in a cohort of healthy controls and HD gene carriers.

Results
Using principal component (PC) analysis, we identified a structure-function relationship common to both groups. PC scores differed between groups indicating decreased white matter organization (higher RD, lower FA) and slower, and more disperse, VEP signal transmission (higher VEP P100 latency and lower VEP P100 amplitude) in the HD group compared to the control group while task performance was similar.

Conclusions
These findings suggest that HD may be associated with reduced white matter organization and efficient visual network function, but normal behavioural performance. The lack of correlation with visual task performance indicates a possible dissociation between behaviour and the assessed properties of the visual network or alternatively, the possible effects of compensatory processes.

Introduction

Brain structure, function and behaviour are clearly linked, but the relationship between them is highly complex. In Huntington's disease (HD), for example, cerebral white and grey matter loss, particularly within the basal ganglia is detectable from 15-20 years prior to clinical diagnosis,[1-4] yet performance levels remain normal for a considerable time suggesting onset of compensatory processes.[5-7] On the other hand, structural imaging measures of brain volume, together with task performance can improve predictions of motor diagnosis based solely on the *HTT* mutation and age.[5] Together, this supports the notion that structural alterations contribute to functional brain changes underlying the manifestation of clinical signs of HD.

Examining the relationship between structure, function and task performance within *a priori* selected brain networks in HD gene carriers could help differentiate between a) network-wide changes that are specific to the presence of the *HTT* mutation and b) natural variations in network properties amongst healthy people that influence the effects of the *HTT* mutation. We previously examined this concept within the sensorimotor network in HD using multimodal structural and functional data.[8] We found a structural pattern of reduced volume and cortical thickness in sensorimotor regions coupled with increased diffusivity in white matter pathways that was closely linked to the HD mutation and predicted performance. However, we also identified an inverse relationship between axial diffusivity (AD; diffusivity in the main direction of the fibre) and radial diffusivity (RD; diffusivity perpendicular to the main fibre) that was common to both controls and HD gene carriers. This relationship pattern predicted HD disease status and motor performance independent of HD-associated factors such as CAG, age and brain volume. This relationship may, therefore, reflect a pattern of natural variability in white matter microstructure that itself does not cause disease. However, in the presence of the HD mutation it may modify the effects of HD pathogenesis on white matter microstructure.

Given our previous findings, here we asked to what extent these observations were specific to the sensorimotor network or whether they reflected patterns that are also present in other networks potentially impacted by HD pathology. This has important implications for disease modification in terms of network-wide versus network-specific patterns of structure, function and behaviour relationships. Although characteristically defined by motor, cognitive and neuropsychiatric symptoms, the visual cortex is one of the first areas affected in HD with evidence of neuronal loss,[3,9-13] white matter pathway degeneration[14] and deficits in visual-processing.[15-17]

Consistent with our earlier study, we used multimodal MRI and electrophysiological data to examine the relationship between structural integrity, functional processing and task performance in the visual network in a cohort of controls and HD gene carriers. We investigated both structure (V1 cortical thickness; visual pathway connectivity) and function (Visual Evoked Potentials (VEP)) in conjunction with task performance on Map Search and Symbol Digit Modalities Test (SDMT). We investigated correlations between individual measures and then used Principal Component

Analysis (PCA) to identify patterns across modalities. Finally, we examined to what extent these patterns identified group status. We predicted independent structure-function relationships a) characteristic of HD only and b) common to both controls and HD reflecting natural variability.

Methods

Participants

Participants were recruited from the Leiden site of the international multi-site Track-On HD study[8] and comprised 20 HD gene mutation carriers (mean age 49.2 years, 12 female) and 24 healthy controls (mean age 52.5 years, 16 female). All HD gene mutation carriers had a CAG repeat length ≥40; and a burden of pathology score (disease burden) greater than 250 ((CAG repeat length - 35.5) x age) (Table I).[9,18] Healthy family members without the HD mutation or partners were recruited as control participants. All participants were screened for major psychiatric, neurological or medical disorders or a history of severe head injury. Education was measured using the International Standard Classification of Education (ISCED) that distinguishes 10 different levels of education. The total motor score was obtained from the motor part of the Unified Huntington's Disease Rating Scale (UHDRS). Visual acuity was documented prior to VEP acquisition, and all participants had normal or corrected-to-normal vision. The study was approved by the Leiden University Institutional Review Board. All participants gave their written informed consent to the study, and all methods were used and experiments performed, in accordance with the ethical standards laid down in the 1964 Declaration of Helsinki and its later amendments.

Table I. *Demographics and clinical measures*

	Full sample			PCA sample		
Variable	Control (N=24)	HD (N=20)	Test statistic (p-value)	Control (N=20)	HD (N=16)	Test statistic (p-value)
Gender N (%F)	16. (66.7)	12 (60.0)	$X^2_1 = 0.21$ (0.65)	15 (75.0)	9 (56.3)	$X^2_1 = 1.41$ (0.24)
Age (SD; range)	52.5 (9.1; 33-68)	49.2 (9.6; 32-68)	t = -1.15 (0.26)	53.2 (8.9; 33-68)	49.4 (9.4; 32-68)	t = -1.26 (0.22)
Education (SD; range)	3.7 (1.2; 2-6)	4.3 (0.9; 2-5)	t = 1.97 (0.06)	3.6 (1.3; 2-6)	4.5 (0.7; 3-5)	t = 2.80 (0.01)
CAG repeat length (SD; range)	--	42.8 (3.0; 39-50)	--	--	42.5 (2.9; 39-50)	--
Disease burden (SD; range)	--	338 (79; 192-478)	--	--	326 (79; 192-469)	--
Motor score (SD; range)	1.3 (1.7; 0-5)	12.8 (11.4; 1-50)	t = 4.48 (0.0002)	1.2 (1.7; 0-5)	10.1 (7.6; 1-28)	t = 4.59 (0.0003)

Behavioural measures

The Map Search Task is a subtest from the Test of Everyday Attention and measures visuospatial selective attention.[19] Participants were presented with an A3 sized map, which displayed a portion of the city of Philadelphia in the United States. They were then timed for two minutes while they searched for and circled a target symbol that occurred in multiple places on the map among other distracter symbols. After one minute, the examiner exchanged the pen for a different colour to facilitate differentiation of those responses made in the first and second minutes of testing. Test

performance was measured as the number of correctly circled target symbols, scored separately at one minute and at two minutes with a maximum possible score of 80. For the current study, we used the percentage number of correct responses in two minutes as a behavioural measure.

The Symbol Digit Modalities Test (SDMT) is a test of visuomotor integration, measuring visual attention and motor speed. Participants were required to match symbols and digits as quickly as possible, following a key located at the top of the page during a 90 second period; the total number of correct responses were recorded and included as our second behavioural measure.

Electrophysiology measures

Four Ag/AgCl electrodes were attached to the scalp at position O1, O2 and Oz with Cz as a reference according to the international 10-20 system for electrode placement. Participants were seated at a distance of 1m in front of a 23 inch computer screen displaying a checkerboard pattern that filled the entire screen with squares of 1˚ visual angle flashing at a frequency of 2Hz. The brightness of the squares was 100lux with a black/white contrast. For each eye, 2 x 100 trials were recorded. The duration of each trial was dependent on the registered signals, approximately one minute in duration, or 30 seconds per trial. The stimulus was presented continuously and flashing, with no stop between trials. VEPs were obtained using Medelec Synergy version 11.0 (Oxford Instruments, Abingdon, United Kingdom). Data were filtered and visually checked for artefacts, noisy trials were deleted from the set. The trials were averaged and peak latencies and peak-to-peak amplitudes of N70, P100 and N135 were identified. The N70 was defined as the most prominent negative peak between 60 and 80ms post stimulus. For the P100 a time window of 90-115ms and for the N135 a time window of 115-150ms was applied.

MRI measures

Cortical thickness

3D T1 images were acquired as previously described.[5] Cortical thickness measures were generated for each participant using Freesurfer version 5.3.0 applying default parameters and optimized for 3T data.[20] Measures were extracted from Brodmann area in the left hemisphere: BA17 (Primary Visual Cortex) (https://surfer.nmr.mgh.harvard.edu/fswiki/BrodmannAreaMaps). All segmentations were visually inspected for accuracy, blind to participant status.

Diffusion tensor imaging

Diffusion-weighted images with 42 unique gradient directions ($b = 1000$ sec/mm^2) and one image with no diffusion weighting ($b = 0$ sec/mm^2) were acquired using a Phillips Achieva scanner. Acquisition parameters were as follows: TE = 56ms and TR = 11s, with voxel size 1.96 x 1.96 x 2; 75 slices were collected for each diffusion-weighted and non-diffusion weighted (B0) volume. The diffusion data were preprocessed using standard FSL pipelines.[21]

Data were initially quality checked for movement artefacts and then corrected for eddy current distortions. Diffusion tensors were fitted to the corrected data using dtifit; FA (fractional

anisotropy), AD and RD values were subsequently derived from the tensors. The B0 image and the T1-weighted structural image were both skull-stripped using the Brain Extraction Tool and then manually edited. The T1 image was then registered to the B0 image using FLIRT.[22] Crossing fibres were modelled using Bedpostx.[23] Probtrackx was used for fibre-tracking of the visual pathway using three regions of interest: the primary visual cortex (V1), extrastriate area V4 and the visual thalamus.[24] All seed regions were created in standard space using the Anatomy toolbox and then warped into native space (using the DARTEL inverse deformation parameters) for fibre-tracking. Masks were used to exclude streamlines that tracked into the right hemisphere and into grey matter, cerebrospinal fluid (CSF) or dura. The visual pathway images were then warped into diffusion space using FLIRT and FA, AD and RD values extracted for each participant.

Statistical analyses

Control and HD groups were compared for each individual modality using two sample t-tests with a false discovery rate (FDR) adjustment for multiple comparisons. The equality of variances assumption was tested and the Satterthwaite approximation of the standard errors and degrees of freedom were used when necessary. Pearson's correlations were performed between the structure-function and behavioural measures across a) HD gene carriers, and b) control participants. Structural integrity and functional processing measures were investigated through PCA, a method used to reduce the dimensionality of multivariate data by producing linear combinations of the original variables. These principal components (PC) are mutually independent and retain most of the variability present in the original measures.[25] The number of components was determined from the results of 2-fold split-sample validation.[26]

After obtaining the PCs, a series of ANCOVA models, adjusting for age and gender, were utilized to evaluate the relationships among the PCs, the behavioural measures, and group status. The first set of models was used to examine the relationship of the PCs and the behavioural measures with group status. The next set assessed the association of the PCs and the behavioural measures (1) without controlling for group status, (2) controlling for group status, and (3) with a group*component interaction. Corrections for multiple comparisons were made using an FDR threshold of $q = 0.05$ within all sets of analyses.[27]

Results

Individual modality analyses

Demographic and clinical data for the control and HD groups are presented in Table I. We focused on eight variables that captured the structure-function relationship within the visual system in the left hemisphere. These included 4 structural MRI measures (V1 cortical thickness, FA, RD, AD) and 2 electrophysiological measures (VEP P100 latency and amplitude recorded from O1) in addition to 2 behavioural measures (Map Search and SDMT). We first compared each individual modality in controls and the HD group (Table II). Group comparisions revealed evidence of significantly higher RD ($p = 0.014$, $q = 0.11$) in the visual pathway connecting the visual thalamic

region and V1 and non-significantly longer VEP P100 latencies (p = 0.082, q = 0.24) for those with HD versus controls. In contrast, V1 cortical thickness, FA, AD, VEP P100 amplitudes and both behavioural measures were similar in the HD group and the controls. Note that the Satterthwaite approximations for standard errors and degrees of freedom were used for FA, AD, and RD because of unequal variances between the groups for these measures.

Table II. *Individual modality results*

Modality		Controls		HD					
		Mean	SD	Mean	SD	t-test	df	p-value	q-value
CT	V1	3853	665	3713	513	0.77	42	0.45	0.45
DTI	FA	0.35	0.034	0.32	0.056	1.78	23.1	0.089	0.24
	AD	1.14	0.051	1.16	0.092	-0.85	22.0	0.44	0.45
	RD	**0.65**	**0.039**	**0.72**	**0.065**	**-2.86**	**23.0**	**0.014**	**0.11**
VEP P100	Latency	100.1	6.0	103.3	6.0	-1.78	42	0.082	0.24
	Amplitude	6.72	2.43	5.87	2.36	1.16	41	0.25	0.33
Behaviour	Map Search	65.63	8.09	62.40	9.12	1.24	42	0.22	0.33
	SDMT	55.42	11.87	50.16	10.53	1.52	41	0.14	0.27

Descriptive statistics and group comparison data for behavioural measure. Abbreviations: SD - standard deviation; df - degrees of freedom; q- value - false discovery rate adjusted p-value; CT - Cortical Thickness; DTI - Diffusion tensor Imaging; VEP - Visual Evoked Potentials; V1 - Primary Visual Cortex; FA - Fractional Anisotropy; RD - Radial Diffusivity; AD - Axial Diffusivity.

Multimodal structure-function-behaviour analyses

Correlations were performed between the structure-function and behavioural measures across a) HD gene carriers (Table III), and b) control participants (Table IV). Across HD participants, worse SDMT performance was associated with lower FA (r = 0.63, p = 0.0091, q = 0.055), higher RD (r = -0.55, p = 0.026, q = 0.11) and longer VEP P100 latency (r = -0.41, p = 0.079, q = 0.24); worse Map Search performance also correlated with longer VEP P100 latency (r = -0.60, p = 0.0056, q = 0.055) (Table III). Correlations for control participants, on the other hand, were not significantly different from zero (Table IV). We then used a regression model to further investigate the group factor. Before FDR adjustment, we found marginal significance between the groups in the association of SDMT with FA, RD, and VEP P100 amplitude (p = 0.063, 0.061, and 0.044 respectively) and in the association of Map Search with VEP P100 latency (p = 0.060). The FDR adjusted values are all non-significant (q > 0.15 for all).

Table III. *Correlations between two behaviour measures and six structure-function measures for HD participants*

	Map Search	SDMT
FA	r = -0.34 (p = 0.20; q = 0.47) 16	r = **0.63 (p = 0.0091; q = 0.055)** 16
AD	r = -0.16 (p = 0.56; q = 0.61) 16	r = 0.10 (p = 0.72; q = 0.72) 16
RD	r = 0.23 (p = 0.40; q = 0.60) 16	r = **-0.55 (p = 0.026; q = 0.11)** 16
V1 cortical thickness	r = 0.25 (p = 0.30; q = 0.59) 20	r = 0.16 (p = 0.50; q = 0.61) 19
VEP P100 latency	r = **-0.60 (p = 0.0056; q = 0.055)** 20	r = **-0.41 (p = 0.079; q = 0.24**) 19
VEP P100 amplitude	r = -0.15 (p = 0.52; q = 0.61) 20	r = 0.22 (p = 0.36; q = 0.60) 19

Pearson's correlations (p-value; q-value) and sample size for each MRI, electrophysiological and behavioural measure. Correlations greater than 0.40 or smaller than -0.4 are in bold. Abbreviations: V1 - Primary Visual Cortex; FA - Fractional Anisotropy; RD - Radial Diffusivity; AD - Axial Diffusivity.

Table IV. *Correlations between two behaviour measures and six structure-function measures for control participants*

	Map Search	SDMT
FA	r = -0.092 (p = 0.69; q = 0.86) 21	r = -0.079 (p = 0.73; q = 0.86) 21
AD	r = -0.077 (p = 0.74; q = 0.86) 21	r = 0.0080 (p = 0.97; q = 0.97) 21
RD	r = 0.15 (p = 0.53; q = 0.86) 21	r = 0.064 (p = 0.78; q = 0.86) 21
V1 cortical thickness	r = 0.13 (p = 0.53; q = 0.86) 24	r = -0.27 (p = 0.20; q = 0.86) 24
VEP P100 latency	r = -0.15 (p = 0.48; q = 0.86) 24	r = -0.13 (p = 0.53; q = 0.86) 24
VEP P100 amplitude	r = -0.27 (p = 0.21; q = 0.86) 23	r = -0.11 (p = 0.62; q = 0. 86) 23

Pearson's correlations (p-value; q-value) and sample size for each MRI, electrophysiological and behavioural measure. Abbreviations: V1 - Primary Visual Cortex; FA - Fractional Anisotropy; RD - Radial Diffusivity; AD - Axial Diffusivity.

Next, we employed PCA to describe the patterns of relationships within the dimensions of the structure-function measures (Figure 1; Table V). The PCA was run on a reduced number of 36 participants who had complete data (20 controls and 16 HD). The six structure-function measures and their relationships could be reduced to 3 principal components (Figure 1; Table V) as determined by 2-fold cross validation. The 3 components explained 74.5% of the variance.

The first PC (PC1) explained 34.0% of data variance and included correlations between increased FA, lower RD in the visual pathway connecting the visual thalamic region and V1, thicker V1, reduced VEP P100 latency and increased VEP P100 amplitude (Figure 1A). PC1 scores were associated with group status, differentiating between controls and HD participants ($t = -2.34$, $p = 0.026$, $q = 0.077$). The controls showed mean PC scores of 0.286 (4 of 20 had negative scores) compared to the HD group, in which the majority of participants (11 of 16) had negative scores with an average negative PC score of -0.474 (Figure 1B). This is indicative of higher RD, lower FA, higher VEP P100 latency and lower VEP P100 amplitude in the HD group compared to the control group.

Table V. *Correlations between three classic principal components and six structure-function measures*

	Comp1	Comp2	Comp3
FA	**0.63**	**- 0.76**	- 0.11
AD	- 0.38	**- 0.71**	**- 0.50**
RD	**- 0.89**	0.21	- 0.28
V1 cortical thickness	0.36	**0.41**	**- 0.72**
VEP P100 latency	**- 0.41**	- 0.089	- 0.23
VEP P100 amplitude	**0.64**	0.33	- 0.32

Pearson's correlations for each MRI and electrophysiological measure with the three principal components. Correlations greater than 0.40 or smaller than -0.4 are in bold. Abbreviations: V1 - Primary Visual Cortex; FA - Fractional Anisotropy; RD - Radial Diffusivity; AD - Axial Diffusivity.

The second PC (PC2; 23.6% of variance explained) showed a pattern of reduced FA and AD in the visual pathway connecting the visual thalamic region and V1, coupled with an increase in V1 cortical thickness (Figure 1A). The third PC (PC3; 16.9% of variance explained) captured a pattern of reduced AD in the visual pathway connecting the visual thalamic region and reduced V1 cortical thickness (Figure 1A). Neither PC2 ($t = -0.23$, $p = 0.82$, $q = 0.82$) nor PC3 ($t = -0.66$, $p = 0.51$, $q = 0.77$) were associated with group status (Figure 1C and D).

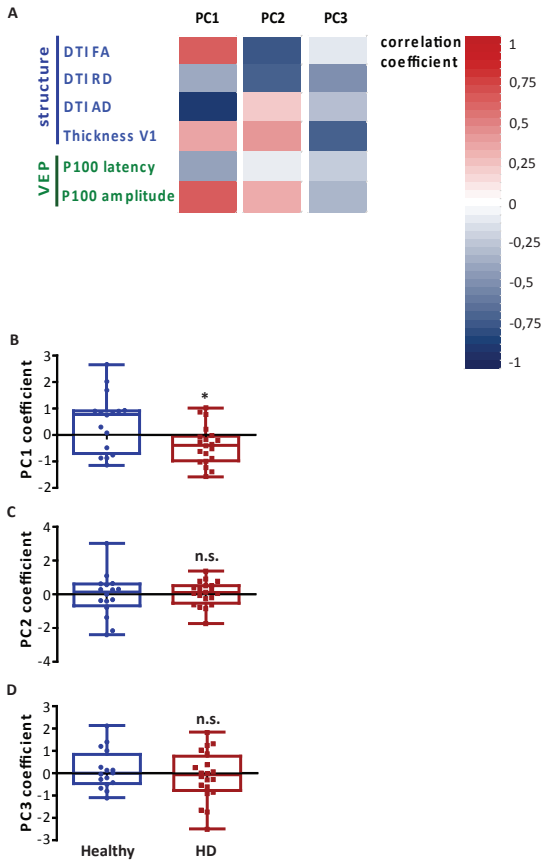

*Figure 1. Multimodal principal component (PC) analysis. A. Heat map of correlation coefficients for each modality with dimensions derived from principal component analysis for the combined group of healthy controls and HD participants. The first PC (PC1) showed the highest correlation with structural and functional measures including lower AD and RD in the visual pathway, and thicker V1. The second PC (PC2) showed a pattern of higher FA and lower RD in the visual pathway. The third PC (PC3) captured a pattern of higher RD in the visual pathway. B. Individual participants' PC1 scores differentiated significantly between the control and HD groups (*p=0.026) while PC2 (C) and PC3 scores (D) were similar in both groups.*
Abbreviations: VEP - visual evoked potentials; DTI - Diffusion Tensor Imaging; FA - Fractional Anisotropy; AD - Axial Diffusivity; RD - Radial Diffusivity; HD: Huntington's disease.

Discussion

In this study, we have identified structure-function relationships showing an association between structural integrity and efficient functional processing within the visual system in healthy controls and HD. Lower levels of white matter organization and VEP responsivity correlated with lower levels

of task performance in HD gene carriers, but not in control participants. We further examined these associations using Principal Component Analysis, identifying a structure-function relationship of white matter organization and VEP responsivity. Although this relationship was common to both HD and controls, the majority of HD gene carriers displayed negative scores, such that they were characterized by increased white matter disorganization in the visual pathway and a less effective visual processing system. However, despite this disrupted structure-function relationship, HD gene carriers performed visual tasks at a normal level. Given the correlations between structure-function measures and performance, this would indicate that despite an abnormal structure-function relationship, HD gene carriers may experience some degree of compensatory brain activity in the visual network.

We previously explored structure-function relationships within the sensorimotor network in HD and characterised a macro- and micro-structural phenotype associated with HD.[8] We showed that structural degeneration within the sensorimotor network was related to both motor performance and pathology, but we also identified an independent inverse relationship between axial and radial diffusivities that was common to both HD and control groups and which predicted motor performance and disease status. Here, we have similarly identified a white-matter structural pattern in the visual network common to both controls and HD gene carriers, but which were also associated with visual processing.

Using principal component analysis, we showed that controls and HD gene carriers shared a similar structure-function relationship of higher white matter organization (i.e., higher FA and lower RD) combined with higher VEP responsivity (i.e., higher amplitude and lower latency) and to a lesser extent higher cortical thickness in the V1. However, despite the fact that this relationship was common to both groups and, therefore, likely due to natural biological variation in these network properties in the population, it actually differentiated the control and HD gene carrier groups, i.e., the average PC scores for each group differed significantly. As such, the majority of the HD group displayed negative scores, exhibiting a converse pattern of reduced white matter organization (i.e., lower FA and higher RD) and VEP responsivity (i.e., lower amplitude and higher latency). This supports our previous findings whereby we identified a pattern of volume loss and increased diffusivity in the sensorimotor network, associated with HD pathology. In healthy people the structure-function relationship may be variable, something we found in the somatosensory and now in the visual network so that in some people white matter organization will be higher, and function better, than in others. The HD mutation may exert its effect on top of that normal variability, and it is conceivable that these effects may take longer in a person with, by nature, higher than in someone with lower white matter organization. Given that we find evidence to support this notion now in two networks it may be worth extending this to other networks, e.g. those involved in cognition.[28] While we have not examined clinical markers of HD in the current study, the effect of HD pathology on the efficiency of the visual network is evident and reflects a pattern not only of structural disturbance as was the case in the sensorimotor network, but also of functional impairment.

Despite this structural degeneration and functional deficit, there were no significant behavioural differences in visual task performance between controls and HD gene carriers at a group level. However, in the HD group the results of the correlation analyses between measures of structure-function (i.e., diffusivity and VEP responsivity) and behaviour, had shown that higher FA and reduced RD both correlated with improved SDMT performance, while shorter VEP latency tended to be associated with both better SDMT and Map Search performance.

PCA analyses further revealed relationships between structural and functional network properties that vary systematically between individuals including HD gene carriers. However, although HD pathology additionally affects network properties of efficient visual processing and associated structure, there was no evidence of abnormal task performance at the group level. The correlations between behaviour, which is unimpaired, and higher levels of white matter organization and VEP responsivity may, therefore, indicate some degree of compensatory brain activity.

The two remaining components from our PCA analysis display patterns that are common to both controls and HD, but are not related to pathology, i.e., they did not distinguish between groups. The second component shows a pattern of reduced FA, reduced AD and increased cortical thickness, while the third shows a pattern of reduced AD and reduced cortical thickness. Interestingly in both the second and third components, there is an inverse relationship between AD and (lower levels of) RD, similar to that within the sensorimotor network - this was also independent of group status. The underlying basis of reduced FA and AD in terms of white matter organization is unclear, but reduced FA may be associated with increased RD. This may also explain why FA reductions are substantially pronounced as part of component three, because here RD is considerably lower.

In summary, we have identified patterns of visual network white matter organization that were correlated with both visual processing and visual performance. Interestingly, the pattern of higher white matter organization and visual processing efficiency, while common to both control and HD gene carriers, distinguished the groups describing higher levels of white matter disorganization and impaired visual processing in HD. In common with our previous analysis of the sensorimotor network we also characterized inverse patterns of AD and RD in the visual network; however, in the sensorimotor network we had not seen a functional contribution as we did here in the visual network.[8] Our findings indicate that the structure–function relationships, and the susceptibility to the effects of the *HTT* mutation, may differ between brain networks in HD. This requires further investigation across a series of other networks, which may be particularly relevant and/or susceptible to the effects of HD pathology.

Acknowledgements

CHDI/High Q Foundation, a not-for-profit organization dedicated to finding treatments for HD, funded the study but had no role in the collection, analysis and interpretation of data and in the writing of the manuscript, or the decision to publish the findings. S.G., R.S., G.R., E.J. and S.T. receive support from a Wellcome Trust Collaborative Award (200181/Z/15/Z). The authors thank the Track-On investigators and extend their gratitude to the study participants and their families.

References

1 Thieben MJ, Duggins AJ, Good CD, et al. The distribution of structural neuropathology in pre-clinical Huntington's disease. Brain 2002;125:1815-28.
2 Aylward EH. Change in MRI striatal volumes as a biomarker in preclinical Huntington's disease. Brain Res Bull. 2007;72:152-8.
3 Rosas HD, Salat DH, Lee SY, et al. Cerebral cortex and the clinical expression of Huntington's disease: complexity and heterogeneity. Brain 2008;131:1057-68.
4 Georgiou-Karistianis N, Poudel GR, Dominguez DJ, et al. Functional and connectivity changes during working memory in Huntington's disease: 18 month longitudinal data from the IMAGE-HD study. Brain Cogn. 2013;83:80-91.
5 Tabrizi SJ, Scahill RI, Owen G, et al. Predictors of phenotypic progression and disease onset in premanifest and early-stage Huntington's disease in the TRACK-HD study: analysis of 36-month observational data. Lancet Neurol. 2013;12:637-49.
6 Klöppel S, Gregory S, Scheller E, et al. Compensation in Preclinical Huntington's Disease: Evidence From the Track-On HD Study. EBioMedicine 2015;2:1420-9.
7 Gregory S, Long JD, Klöppel S, et al. Testing a longitudinal compensation model in premanifest Huntington's disease. Brain 2018;141:2156-2166.
8 Orth M, Gregory S, Scahill RI, et al. Natural variation in sensory-motor white matter organization influences manifestations of Huntington's disease. Hum Brain Mapp. 2016;37:4615-4628.
9 Tabrizi SJ, Langbehn DR, Leavitt BR, et al. Biological and clinical manifestations of Huntington's disease in the longitudinal TRACK-HD study: cross-sectional analysis of baseline data. Lancet Neurol. 2009;8:791-801.
10 Tabrizi SJ, Reilmann R, Roos RA, et al. Potential endpoints for clinical trials in premanifest and early Huntington's disease in the TRACK-HD study: analysis of 24 month observational data. Lancet Neurol. 2012;11:42-53.
11 Wolf RC, Sambataro F, Vasic N, et al. Visual system integrity and cognition in early Huntington's disease. Eur J Neurosci. 2014;40:2417-26.
12 Rub U, Seidel K, Vonsattel JP, et al. Huntington's Disease (HD): Neurodegeneration of Brodmann's Primary Visual Area 17 (BA17). Brain Pathol. 2015;25:701-11.
13 Odish OFF, Reijntjes RHAM, van den Bogaard SJA, et al. Progressive microstructural changes of the occipital cortex in Huntington's disease. Brain Imaging Behav. 2018;12:1786-1794.
14 McColgan P, Gregory S, Seunarine KK, et al. Brain Regions Showing White Matter Loss in Huntington's Disease Are Enriched for Synaptic and Metabolic Genes. Biol Psychiatry 2018;83:456-465.
15 Scahill RI, Hobbs NZ, Say MJ, et al. Clinical impairment in premanifest and early Huntington's disease is associated with regionally specific atrophy. Hum Brain Mapp. 2013;34:519-29.
16 Paulsen JS, Long JD, Ross CA, et al. Prediction of manifest Huntington's disease with clinical and imaging measures: a prospective observational study. Lancet Neurol. 2014;13:1193-201.
17 Johnson EB, Rees EM, Labuschagne I, et al. The impact of occipital lobe cortical thickness on cognitive task performance: An investigation in Huntington's Disease. Neuropsychologia 2015;79:138-46.
18 Penney JB, Vonsattel JP, MacDonald ME, et al. CAG repeat number governs the development rate of pathology in huntington's disease. Ann Neurol. 1997;41:689-92.
19 Murray LL, Stout JC. Discourse Comprehension in Huntington's and Parkinson's Diseases. Am J Speech-Language Pathol. 2014; 8:137-148.
20 Fischl B, Dale AM. Measuring the thickness of the human cerebral cortex from magnetic resonance images. Proc Natl Acad Sci USA 2000;97:11050-5.

21 Smith SM, Jenkinson M, Woolrich MW, et al. Advances in functional and structural MR image analysis and implementation as FSL. Neuroimage 2004;23 Suppl 1:S208-19.
22 Jenkinson M, Smith S. A global optimisation method for robust affine registration of brain images. Med Image Anal. 2001;5:143-56.
23 Behrens TE, Berg HJ, Jbabdi S, et al. Probabilistic diffusion tractography with multiple fibre orientations: What can we gain? Neuroimage 2007;34:144-55.
24 Behrens TE, Woolrich MW, Jenkinson M, et al. Characterization and propagation of uncertainty in diffusion-weighted MR imaging. Magn Reson Med. 2003;50:1077-88.
25 Jolliffe IT. Principal component analysis. 2nd ed. Springer series in statistics. New York: Springer; 2002.
26 Eastment HT, Krzanowski WJ. Cross-validatory choice of the number of components from a principal component analysis. Technometrics 1982;24:73-7.
27 Benjamini Y, Hochberg Y. Controlling the False Discovery Rate - a Practical and Powerful Approach to Multiple Testing. J R Stat Soc Ser B-Methodological 1995;57:289-300.
28 Gregory S, Crawford H, Seunarine K, et al. Natural biological variation of white matter microstructure is accentuated in Huntington's disease. Hum Brain Mapp. 2018;39:3516-27.

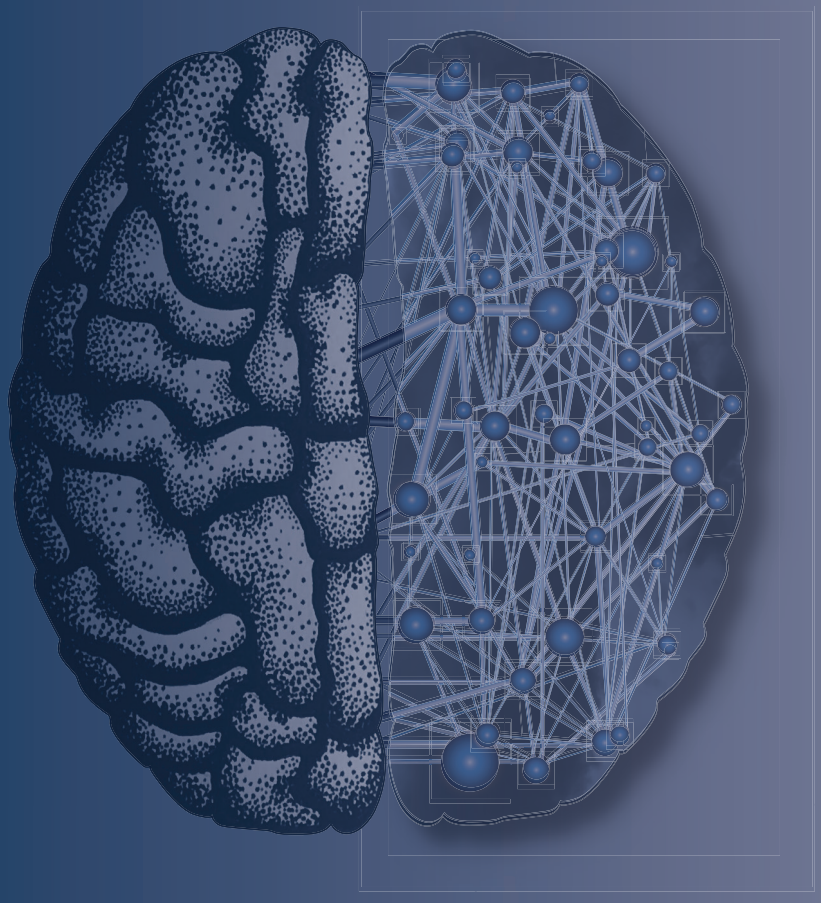

Summarizing remarks and future perspectives

CHAPTER 8

Summarizing remarks and future perspectives

The neuroimaging and neurophysiological findings presented in this thesis add several important insights into the potential usefulness of these parameters as biomarkers in Huntington's disease (HD). A wider understanding of structural and functional brain pathology at different stages of HD also enables us to formulate recommendations for future research. Using resting state functional magnetic resonance imaging (RS-fMRI), diffusion MRI, electroencephalography (EEG) and visual evoked potentials (VEP), we have provided a broad view into the interplay of structure and function in HD neuropathology and between disease state and progression. Using these methods, we laid out potential suitable objective surrogate clinical trial endpoints and enhanced our understanding of the (subclinical) change in the disease.

We could not demonstrate any longitudinal differences in functional connectivity changes between premanifest HD (preHD) subjects and healthy controls using RS-fMRI over a period of three years (**Chapter 2**). This was unexpected, as earlier cross-sectional results suggested that functional connectivity, at the group level, was a fairly sensitive measure to differentiate preHD subjects from controls.[1] Despite the fact that we used three different analysis methods, we could not demonstrate any longitudinal change in functional connectivity within our cohort in a time frame of three years with two measurement points. At the same time, striatal atrophy rates were significantly higher in preHD compared to healthy controls. Therefore, we concluded that these results indicate an inferior sensitivity of RS-fMRI in demonstrating longitudinal changes in the preHD population compared to volumetric striatal MRI measures. We speculate that the reason for the lower sensitivity is due to the low signal-to-noise ratio of RS-fMRI compared to volumetric measures. Alternatively, this might be due to compensatory mechanisms responsible for apparently normal brain function in preHD despite ongoing neurodegeneration. Either way, the conclusion is highly relevant in light of longitudinal biomarker research in preHD, suggesting that RS-fMRI may not be a feasible marker for assessing the efficacy of an intervention in this population during a realistic clinical trial time frame.

Using diffusion tensor imaging (DTI) we showed global as well as striatal microstructural brain abnormalities at different stages of HD as well as significant associations between neurocognitive and diffusivity measures (**Chapter 3**). Performance on the Symbol Digit Modalities Test (SDMT) was mostly associated with white matter diffusivity measures, whereas performance on the Stroop Word Reading task was only associated with grey matter diffusivities. These findings may guide the selection of the most suitable cognitive measures to assess, depending on the prime target of a treatment intervention. This study did not reveal any significant longitudinal differences in microstructural organization between manifest HD, preHD and healthy controls within the two-year study period. These results were also unexpected, as neurodegeneration in HD is a slow process and microstructural alterations are expected to be present before macrostructural abnormalities become apparent. However, this method was clearly less sensitive in detecting any longitudinal changes when compared to studies using longitudinal volumetric MRI measures (particularly of the striatum). This is most likely caused by the lower signal-to-noise ratio of

this method compared to volumetric MRI methods. Alternatively, this could be due to a true absence of observable significant alterations in the diffusion profile of the examined global and striatal structures using DTI in the two-year time frame. Nonetheless, this study did provide some interesting insights into the microstructural organization of the (pre)HD brain. In manifest HD we found a diffusivity pattern which could reflect an increase in tissue permeability, extracellular space fluid, and/or interaxonal spacing due to neural tissue loss. This pattern of diffusivity changes has been associated with chronic white matter degeneration.[2,3] In the preHD group we found that only the axial diffusivity of the white matter was significantly higher than that of healthy controls, a finding that may indicate axonal atrophy. These findings suggest that both axonal degeneration as well as myelin abnormalities play an important role in white matter pathophysiology of HD and are present throughout the entire brain. Given that the earliest detected abnormality is a higher axial diffusivity of the white matter in preHD subjects, this may point to axonal degeneration as preceding the pattern of chronic white matter degeneration found in later stages of the disease, reinforcing previous findings and further supporting this hypothesis.[4]

In a first-of-its-kind study in HD, we applied longitudinal graph theoretical analysis (GTA) to diffusion MRI (**Chapter 4**). Using this method, we described the dynamics of the connectome and characterized regional and global topological properties of brain networks in different stages of HD compared to healthy controls. By applying this method, we departed from the traditional neuroimaging approach of examining individual components of the brain, such as regions of interest, towards characterizing regional or global structure of networks. We showed both baseline and longitudinal differences between the different groups and correlations between graph metrics on the one hand, and clinical and behavioural measures on the other hand, providing us with novel insights into the dynamics of brain neuropathology occurring in HD. For instance, both the left orbitofrontal cortex and left paracentral lobule were affected longitudinally in early manifest HD as well in preHD-B (the group with the closest expected proximity to the occurrence of characteristic motor symptoms, which define the manifest stage). The orbitofrontal cortex is involved in decision making and cognitive and emotional processing, processes that are known to be progressively impacted in HD.[5] The paracentral lobule, a component of the sensorimotor system has previously been implicated in HD where atrophy was also demonstrated.[6] In the combined preHD group, the left medial prefrontal cortex was impacted when compared to healthy controls. This region is involved in planning and problem solving and a previous study linked reduced functional connectivity in the region to impaired executive function in HD.[7,8] These findings provide potential clues to the structural correlates of the reductions in higher cognitive capabilities occurring in gene carriers prior to manifestation of motor signs. We also showed that the small-world organization was preserved in preHD and early HD. We suggested that intervention could be aimed at preserving this brain organization quality associated with health, especially because of the presumed degradation of this network quality in advanced stages of the disease. Such a disruption in later stages of HD is yet to be established, but is suggested by the (non-significant) decreases we have observed in our cohort. Longitudinal increases in the Unified Huntington's Disease Rating Scale total motor score (UHDRS-TMS) were negatively associated with small-worldness in the early manifest HD group, indicating that a decrease in

'wiring-efficiency' was related to an increase in motor symptoms. A noteworthy finding in preHD was the hub-status gain of the right superior parietal gyrus in the second visit, as this structure has been previously implicated in a compensatory role for maintaining normal motor function in preHD.[9,10] We concluded that assessing the connectome not only provides a novel approach with a biomarker potential in HD, but also potential new insights into compensatory strategies of the brain in neurodegenerative disorders. Previous studies of the connectome in other neurodegenerative disorders such as Alzheimer's disease had already shown the usefulness of this approach.[11,12]

We investigated longitudinal microstructural changes occurring in the occipital cortex in different stages of HD (**Chapter 5**). This structure has not been the primary focus of HD research, even though mounting evidence has suggested early involvement of the occipital regions in HD neurodegeneration.[13-15] We found some distinctive disease stage-specific longitudinal differences in HD as well as correlations with behavioural measures. We concluded that these findings provide added evidence of a strong involvement of the occipital cortex in HD neuropathology. Moreover, as these findings were highly significant and obtained using a fully automated method, we concluded that this approach is an objective biomarker candidate in HD. The two-year duration of the study is also feasible for evaluating the potential effect of an intervention trial. In preHD-B patients, only the middle occipital gyrus showed a significant longitudinal difference in the diffusivity profile suggesting that this structure may be the earliest involved in the neurodegeneration cascade of the occipital regions in HD. We discussed that although no specific visual symptoms are known to exist in HD, performance in visuospatial, visuomotor, as well as emotion recognition is known to be impaired.[16-18] We suggested that investigating the occipital cortex as a region of interest may provide a more sensitive way to track disease advancement in preHD compared to the corpus callosum and/or cingulum.[19] Based on our findings, we hypothesized that disruption of cell boundaries due to neural tissue loss in the occipital cortical region during disease progression causes an increase in tissue permeability and interaxonal spacing. Although the reason for a preferential neurodegeneration of the occipital region in HD remains unknown, we speculate that this might be due to the high metabolic demand of this region making it more exposed to excitotoxicity.

Turning our attention to electrophysiology, we explored quantitative electroencephalography (qEEG) measures as potential biomarkers in HD (**Chapter 6**). In this cross-sectional study we created a high-quality classifier using a machine learning algorithm. In summary, we were able to separate EEGs of HD and healthy control subjects with an accuracy of over 80%. We concluded that this automatic classification method has a potential for further development as a biomarker in HD. Interestingly, we found strong correlations between qEEG measures, the UHDRS-TMS and SDMT, both clinical markers known to be altered in a longitudinal fashion in the (pre-) manifest state. We hypothesized that the differences found in this study are primarily derived from a deregulation of brain network oscillations through GABAergic dysfunction in HD. As this was a cross-sectional study, we need longitudinal studies to evaluate the potential usefulness of this method as a biomarker in HD. We do expect this potential to be present given the findings

of strong correlations with clinical markers of decline supporting the notion of a measurable progressive change in HD brain function. Correlations between qEEG and modalities changing with the progression of the disease may lead to tools based on qEEG that can help monitor efficacy in intervention studies.

Using a multimodal approach, we identified patterns that suggest a close relationship between structural organization of the visual system and efficient functional processing (**Chapter 7**). Our findings of higher diffusivity and less efficient processing within the visual system combined with reduced VEP responsivity point to a less effective visual processing system in HD. We could not, however, demonstrate correlations with the performance on two visual tasks. The latter might suggest different processing pathways for these tasks compared to the parameters of the visual system that we assessed in this study or compensatory brain activity at play. Although these results are not expected to be suitable as practical biomarkers in HD, these do provide added insights into the impact of neurodegeneration on the visual system in HD, relevant in light of findings described in Chapter 5. As the relationship between brain structure and function is highly complex, a multimodal approach such as the one we used here is most likely the best approach in attempting to elucidate such a relationship.

Future perspectives

We have presented potential HD biomarker options in the previous chapters. When viewing our findings together with these of the literature, we anticipate that a combination of different modalities and methodologies will reveal the most sensitive and accurate biomarker. In the case of (micro-)structural brain imaging, we predict that an imaging "polymarker" consisting of different imaging techniques would provide the best disease tracking measure. Longitudinal volumetric measures of the striatum combined with diffusion measures of the occipital cortex, for instance, may provide such a measure. Using machine learning algorithms to discern the best possible combination of discriminative imaging patterns is most likely a good approach to take.[20] On the brain function front, we do not expect (resting state) fMRI to play an important role as an effective longitudinal biomarker in HD. We do however think that EEGs analysed with advanced methods such as machine learning, may provide a biomarker of brain function in different stages of HD and as such be potentially useful in evaluating the effect of disease modifying therapies.

As stated in the introduction, HD should be viewed as a multisystem neurodegenerative disorder of the brain, which makes a multifaceted, multivariate biomarker approach a sensible one. Such a holistic approach would provide needed insights into the cascade of the different events leading to the final common pathway of neuronal dysfunction and death. We recommend using automated methods where possible to ensure the highest degrees of objectivity and to facilitate fast and standardized interpretation of data in large multi-centre studies. When using automated techniques for MRI segmentation, visual quality control remains essential.

Beyond the biomarkers investigated in this thesis, a combination with clinical and biofluid markers will be necessary to fully assess the effects of any interventional trial. These markers will provide complementary information, both on disease state and on the specific effects of a potential therapy. This is also important as the measurable effect of a therapy on the various markers may be different. Such an approach is central in elucidating the sequence in which different markers change, which in turn may help reduce the number of participants needed to demonstrate effects of an intervention by selecting disease stage-specific sensitive makers.[21] Also, these kinds of investigations could lead to improved predictions for the expected time to disease onset on the individual level. To conclude, the keyword we recommend for future biomarker research in HD is *combination*.

References

1 Dumas EM, van den Bogaard SJ, Hart EP, et al. Reduced functional brain connectivity prior to and after disease onset in Huntington's disease. Neuroimage Clin. 2013;2:377-384.
2 Burzynska AZ, Preuschhof C, Backman L, et al. Age-related differences in white matter microstructure: region-specific patterns of diffusivity. Neuroimage 2010; 49:2104-2112.
3 Concha L. A macroscopic view of microstructure: Using diffusion-weighted images to infer damage, repair, and plasticity of white matter. Neuroscience 2014;276:14-28.
4 Hobbs NZ, Cole JH, Farmer RE, et al. Evaluation of multimodal, multi-site neuroimaging measures in Huntington's disease: Baseline results from the PADDINGTON study. Neuroimage Clin. 2012;2:204-211.
5 Kringelbach ML, Rolls ET. The functional neuroanatomy of the human orbitofrontal cortex: evidence from neuroimaging and neuropsychology. Prog Neurobiol. 2004;72:341-372.
6 Kassubek J, Juengling FD, Kioschies T, et al. Topography of cerebral atrophy in early Huntington's disease: a voxel based morphometric MRI study. J Neurol Neurosurg Psychiatry 2004;75:213-220.
7 Alvarez JA, Emory E. Executive function and the frontal lobes: a meta-analytic review. Neuropsychol Rev. 2006;16:17-42.
8 Unschuld PG, Liu X, Shanahan M, et al. Prefrontal executive function associated coupling relates to Huntington's disease stage. Cortex 2013;49:2661-2673.
9 Klöppel S, Draganski B, Siebner HR, et al. Functional compensation of motor function in pre-symptomatic Huntington's disease. Brain 2009;132:1624-1632.
10 Scheller E, Abdulkadir A, Peter J, et al. Interregional compensatory mechanisms of motor functioning in progressing preclinical neurodegeneration. Neuroimage 2013;75:146-154.
11 He Y, Chen Z, Evans A. Structural insights into aberrant topological patterns of large-scale cortical networks in Alzheimer's disease. J Neurosci. 2008;28:4756-4766.
12 Reijmer YD, Leemans A, Caeyenberghs K, et al. Disruption of cerebral networks and cognitive impairment in Alzheimer disease. Neurology 2013;80:1370-1377.
13 Tabrizi SJ, Langbehn DR, Leavitt BR, et al. Biological and clinical manifestations of Huntington's disease in the longitudinal TRACK-HD study: cross-sectional analysis of baseline data. Lancet Neurol. 2009;8:791-801.
14 Henley SM, Wild EJ, Hobbs NZ, et al. Relationship between CAG repeat length and brain volume in premanifest and early Huntington's disease. J Neurol. 2009;256:203-212.
15 Hobbs NZ, Henley SM, Ridgway GR, et al. The progression of regional atrophy in premanifest and early Huntington's disease: a longitudinal voxel-based morphometry study. J Neurol Neurosurg Psychiatry 2010;81:756-763.
16 Tabrizi SJ, Scahill RI, Owen G, et al. Predictors of phenotypic progression and disease onset in premanifest and early stage Huntington's disease in the TRACK-HD study: analysis of 36-month observational data. Lancet Neurol. 2013;12:637-649.
17 Say MJ, Jones R, Scahill RI, et al. Visuomotor integration deficits precede clinical onset in Huntington's disease. Neuropsychologia 2011;49:264-270.
18 Henley SM, Novak MJ, Frost C, et al. Emotion recognition in Huntington's disease: a systematic review. Neuroscience and Biobehavioral Reviews 2012;36:237-253.
19 Poudel GR, Stout JC, Dominguez DJ, et al. Longitudinal change in white matter microstructure in Huntington's disease: The IMAGE-HD study. Neurobiology of Disease 2014;74:406-412.
20 Mason SL, Daws RE, Soreq E, et al. Predicting clinical diagnosis in Huntington's disease: An imaging polymarker. Ann Neurol. 2018;83:532-543.
21 Byrne LM, Rodrigues FB, Johnson EB, et al. Evaluation of mutant huntingtin and neurofilament proteins as potential markers in Huntington's disease. Sci Transl Med. 2018;10 (458).

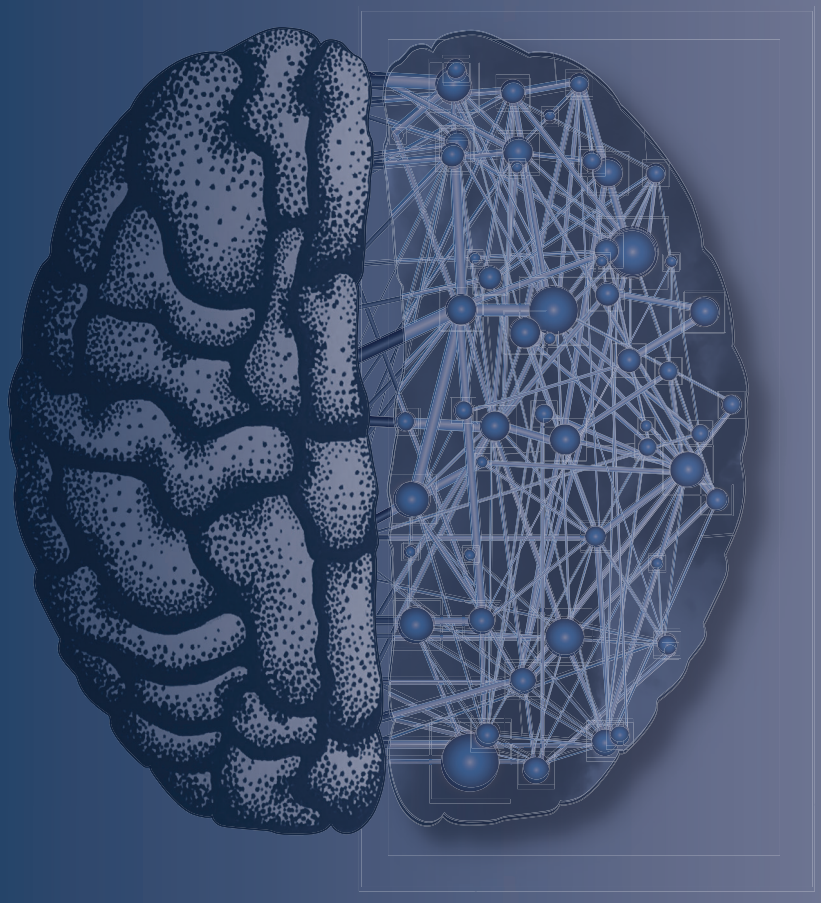

Nederlandse samenvatting
Dankwoord
List of publications
Curriculum vitae

Nederlandse samenvatting

De in dit proefschrift gepresenteerde neuroimaging en neurofysiologische bevindingen geven een aantal belangrijke inzichten in de potentiële waarde van deze parameters als biomarkers bij de ziekte van Huntington (HD). Een breder begrip van structurele en functionele hersenpathologie in verschillende stadia van HD helpt ons ook richting te geven aan toekomstig onderzoek. Door gebruik te maken van resting state functional magnetic resonance imaging (RS-fMRI), diffusie MRI, elektro-encefalografie (EEG) en visual evoked potentials (VEP), hebben wij gepoogd een brede benadering te hanteren om het samenspel tussen structuur en functie in de pathogenese van HD en tussen ziektestadia en progressie weer te geven. Door deze methodes toe te passen hebben wij potentiële objectieve surrogaatmarkers gepresenteerd die gebruikt kunnen worden als uitkomstmaten in klinisch onderzoek. Ook hebben wij ons begrip van de (subklinische) veranderingen van de ziekte vergroot.

In een vervolgonderzoek van drie jaar hebben wij ondanks het toepassen van drie verschillende analysemethodes geen verschillen in de mate van veranderingen in functionele connectiviteit kunnen vinden tussen premanifeste HD (preHD) en gezonde controles met RS-fMRI (**Hoofdstuk 2**). Dit was onverwacht gezien eerdere cross-sectionele resultaten die suggereerden dat functionele connectiviteit op groepsniveau een onderscheidende marker zou kunnen zijn tussen preHD en gezonde controles.[1] Tegelijkertijd was er wel significant meer striatale atrofie in preHD vergeleken met gezonde controles. Wij concludeerden dat deze resultaten wijzen op een lagere sensitiviteit van RS-fMRI om longitudinale verschillen in de preHD groep te laten zien vergeleken met volume MRI-maten van het striatum. Dit zou kunnen komen door de lagere signaal-ruisverhouding van RS-fMRI vergeleken met volumematen. Anderzijds zou dit mogelijk verklaard kunnen worden door compensatoire processen die zorgen voor een ogenschijnlijk normale hersenfunctie in preHD ondanks voortschrijdende neurodegeneratie dan wel volumeverlies. Wat de eigenlijke verklaring ook is, het is wel een zeer relevante bevinding in het kader van de zoektocht naar longitudinale biomarkers in preHD. Hierbij lijkt RS-fMRI geen reële kandidaat te zijn om de effectiviteit van interventies in deze populatie te beoordelen, zeker niet binnen een realistisch tijdskader voor een klinisch onderzoek.

Door gebruik te maken van diffusion tensor imaging (DTI) hebben wij laten zien dat zowel globale alsook striatale microstructurele hersenafwijkingen in verschillende stadia van HD voorkomen en dat er significante associaties zijn tussen neurocognitieve en diffusiematen (**Hoofdstuk 3**). Prestatie op de Symbol Digit Modalities Test (SDMT) was hoofdzakelijk geassocieerd met diffusiematen verkregen uit witte stof, terwijl prestatie op de Stroop Word Reading task alleen geassocieerd was met diffusiematen verkregen uit grijze stof. Dergelijke bevindingen kunnen de selectie van de meest geschikte cognitieve maten bevorderen, afhankelijk van het verwachte hoofdeffect van een interventiestudie. Deze studie heeft geen significante longitudinale verschillen in microstructurele organisatie tussen manifeste HD, preHD en gezonde controles laten zien over een tijdsperiode van twee jaar. Ook deze resultaten waren onverwacht, gezien het feit dat neurodegeneratie in HD een langzaam proces is en microstructurele veranderingen logischerwijs

vooraf moeten gaan aan de macrostructurele afwijkingen. Toch bleek ook deze methode minder sensitief te zijn in het aantonen van longitudinale verschillen vergeleken met volume MRI-maten (in het bijzonder van het striatum). Deze bevinding wordt waarschijnlijk veroorzaakt door de lagere signaal-ruisverhouding van deze methode vergeleken met volumematen. Anderzijds zou dit kunnen komen door een werkelijke afwezigheid van meetbare significante veranderingen in het diffusieprofiel van de bestudeerde globale en striatale structuren zoals gemeten met DTI binnen twee jaar. Niettemin gaf deze studie interessante inzichten in de microstructurele organisatie van (pre)HD hersenen. In manifeste HD vonden wij een diffusiepatroon wat kan wijzen op een toename van weefselpermeabiliteit, extracellulair vocht en/of interaxonale ruimte door neuronaal verval. Een dergelijk patroon van diffusieveranderingen is geassocieerd met chronische witte stof degeneratie.[2,3] In de preHD groep vonden wij dat alleen de axiale diffusiviteit in witte stof significant hoger was dan die van gezonde controles, een bevinding wat richting axonale atrofie kan wijzen. Deze bevindingen suggereren dat zowel axonale degeneratie als myeline veranderingen een belangrijke rol spelen in witte stof pathologie in HD en verspreid aanwezig zijn door de hersenen. Gezien het feit dat de eerste verandering die in preHD gezien wordt een hogere axiale diffusiviteit van witte stof is, kan dit betekenen dat axonale degeneratie optreedt voorafgaand aan het later gevonden patroon passend bij chronische witte stof degeneratie. Deze resultaten bevestigen eerdere bevindingen en geven meer steun aan deze hypothese.[4]

Voor het eerst in HD onderzoek hebben wij een longitudinale analyse uitgevoerd met behulp van grafentheorie (GTA) op diffusie MRI data (**Hoofdstuk 4**). Met behulp van deze methode hebben wij de dynamiek van het connectoom beschreven en regionale en globale topografische eigenschappen van hersennetwerken in kaart gebracht in verschillende stadia van HD vergeleken met gezonde controles. Door deze methode toe te passen hebben wij de traditionele neuroimaging aanpak van het bestuderen van losse hersencomponenten verruild voor een integraal netwerkaanpak. We lieten zowel cross-sectionele als longitudinale verschillen tussen de groepen zien en correlaties tussen graafeigenschappen enerzijds en klinische- en gedragsmaten anderzijds, wat ons nieuwe inzichten gaf in de dynamiek van hersenpathologie in HD. Zo waren zowel de linker orbitofrontale cortex als de linker lobulus paracentralis longitudinaal aangedaan in vroeg manifeste HD en in preHD-B (de groep die het dichtst zit bij het voorspelde optreden van de karakteristieke motore symptomen, waarna de manifeste fase volgens definitie begint). De orbitofrontale cortex is betrokken bij besluitvorming en cognitieve en emotionele verwerking, processen waarvan bekend is dat die progressief aangedaan raken in HD.[5] In de lobulus paracentralis, een component van het sensomotore systeem, is bij eerder onderzoek in HD atrofie aangetoond.[6] In de gecombineerde preHD groep was de linker mediale prefrontale cortex aangedaan vergeleken met gezonde controles. Deze regio is betrokken bij planning en probleemoplossing en eerder onderzoek heeft een verbinding gelegd tussen verminderde functionele connectiviteit aldaar met een aangetaste executive functie in HD.[7,8] Deze bevindingen geven potentiële aanwijzingen voor de structurele correlaten van de achteruitgang van hogere cognitieve functies in premanifeste gendragers. Daarnaast hebben wij laten zien dat de small-world organisatie nog gespaard is in preHD en in vroeg manifeste HD. We suggereerden dat interventie gericht kan zijn op het behoud van deze normale hersenorganisatie, zeker gezien de

verwachte achteruitgang hierin in latere stadia van de ziekte. Hoewel een dergelijke achteruitgang nog niet in studies aangetoond is, bestaat wel de suggestie hiervoor gezien de (niet significante) afname in deze maat die we binnen onze HD cohort vonden. Longitudinale toenames in de Unified Huntington's Disease Rating Scale total motor score (UHDRS-TMS) waren negatief gecorreleerd aan de small-world maat in de vroeg manifeste groep, wat suggereert dat een afname in de "bedradingsefficiëntie" gerelateerd was aan een toename in motorsymptomen. Een noemenswaardige bevinding in preHD was het verkrijgen van de hub-status van de rechter gyrus parietalis superior in het tweede meetmoment, aangezien deze structuur eerder aangewezen is als een gebied wat zorgt voor een compensatoir effect voor het behoud van normale motore functie in preHD.[9,10] We concludeerden dat het bestuderen van het connectoom niet alleen een nieuwe benadering biedt met een biomarker potentie in HD, maar ook nieuwe inzichten geeft in compensatoire strategieën van de hersenen in neurodegeneratieve aandoeningen. Voorgaande studies van het connectoom in andere neurodegeneratieve ziekten zoals de ziekte van Alzheimer hadden de waarde van deze benadering reeds laten zien.[11,12]

Wij hebben microstructurele veranderingen in de occipitale cortex in verschillende stadia van HD longitudinaal onderzocht (**Hoofdstuk 5**). Deze structuur heeft geen primaire aandacht genoten in HD onderzoek, terwijl er toenemend bewijs is voor een vroege betrokkenheid van de occipitale regio's in HD neurodegeneratie.[13-15] Wij vonden ziektestadium specifieke longitudinale verschillen in HD alsook correlaties met gedragsmaten. We concludeerden dat deze bevindingen het bewijs versterken van een belangrijke betrokkenheid van de occipitale cortex in HD neuropathologie. Omdat deze resultaten statistisch sterk significant waren en verkregen waren via een volledig automatische methode, hebben wij verder geconcludeerd dat deze benadering een objectieve biomarker kandidaat is in HD. De twee jaar tijdspanne van de studie is ook haalbaar voor het evalueren van potentiële effecten van een interventiestudie. In de preHD-B populatie liet alleen de gyrus occipitalis medius longitudinale veranderingen zien in diffusieprofiel, wat de suggestie wekt dat deze structuur als eerste betrokken raakt in de neurodegeneratieve cascade van de occipitale regio's in HD. We bespraken dat hoewel er geen specifieke visuele symptomen bekend zijn in HD, er wel afwijkingen zijn in visuomotore verwerking alsook problemen met emotieherkenning.[16-18] We suggereerden dat het bestuderen van de occipitale cortex mogelijk sensitiever is om ziekteprogressie in preHD te meten vergeleken met het corpus callosum en/of cingulum.[19] De gevonden afwijkingen in diffusieprofiel van de occipitale cortex in HD komen mogelijk door verstoring van celmembranen door neuronaal verval waarbij een toename van permeabiliteit en interaxonale ruimte ontstaat. Hoewel de oorzaak van een preferentiële neurodegeneratie van de occipitale regio in HD onbekend blijft, menen wij dat dit te maken kan hebben met de hoge metabole eisen aldaar. Hierdoor zouden de gevolgen van excitotoxiciteit in deze regio eerder merkbaar zijn.

We hebben vervolgens onze aandacht gevestigd op neurofysiologie, waarbij we kwantitatieve elektro-encefalografie (qEEG) maten als potentiële biomarkers in HD hebben onderzocht (**Hoofdstuk 6**). In deze cross-sectionele studie construeerden wij een calssifier van hoge kwaliteit door gebruik te maken van een machinaal leren algoritme. In het kort waren wij in staat om EEG's

van HD en gezonde controles van elkaar te onderscheiden met een nauwkeurigheid groter dan 80%. We concludeerde dat deze vorm van automatische classificatie potentie heeft om verder ontwikkeld te worden als een biomarker in HD. Interessant genoeg vonden wij sterke correlaties tussen qEEG maten en zowel de UHDRS-TMS als de SDMT, beide klinische maten waarvan bekend is dat die longitudinaal veranderen in de (pre-)manifeste fase. We veronderstelden dat de in deze studie gevonden afwijkingen primair worden gedreven door een deregulatie van hersennetwerk oscillaties door GABA-erge disfunctie in HD. Omdat het om een cross-sectionele studie ging, hebben wij longitudinale data nodig om de potentie van deze methode als biomarker in HD te kunnen evalueren. Wel verwachten we dat deze potentie aanwezig zal zijn gezien de sterke correlaties met klinische markers van achteruitgang, wat ondersteuning geeft aan het idee van een meetbare en progressieve verandering in hersenactiviteit bij HD. Correlaties tussen qEEG en modaliteiten die veranderen met ziekteprogressie kunnen tot qEEG gedreven tools leiden die helpen om het effect van interventiestudies te monitoren.

Door een multimodale benadering te hanteren, hebben wij patronen gevonden die een nauwe relatie suggereren tussen de structurele organisatie van het visuele systeem en de bijbehorende functionele verwerking (**Hoofdstuk 7**). Onze bevindingen van hogere diffusiviteit en minder efficiënte verwerking binnen het visuele systeem gecombineerd met een verlaagde VEP responsiviteit, wijzen op een minder effectief visueel verwerkingssysteem in HD. We konden echter geen correlaties vinden met twee visuele testen. Dat laatste zou kunnen komen door andere visuele netwerken die gebruikt worden voor het verwerken van deze testen of compensatoire hersenactiviteit. Hoewel niet verwacht wordt dat deze resultaten geschikt zullen zijn als praktische biomarkers in HD, bieden die wel additioneel inzicht in de gevolgen van neurodegeneratie op het visuele systeem in HD, wat relevant is in het kader van de bevindingen zoals beschreven in Hoofdstuk 5. Gezien de complexe relatie tussen hersenstructuur en -functie zal een multimodale benadering zoals we hier hebben gebruikt waarschijnlijk de meest geschikte manier zijn om dergelijke relaties te kunnen verhelderen.

Toekomstperspectieven

In de vorige hoofdstukken presenteerden wij potentiële biomarker opties voor HD. Wanneer we onze bevindingen samen met die in de literatuur beschouwen, verwachten we dat een combinatie van verschillende modaliteiten en methodologieën de meest sensitieve en accurate biomarker zal onthullen. In het geval van (micro-)structurele hersenbeeldvorming verwachten wij dat een "polymarker" van beeldvormingstechnieken de beste ziekteprogressie maat zal bieden. Longitudinale volumematen van het striatum gecombineerd met diffusiematen van de occipitale cortex, bijvoorbeeld, zouden een dergelijke maat kunnen bieden. Gebruikmaken van machinaal leren algoritmes om de best mogelijke combinatie van onderscheidende beeldvormingspatronen te vinden is waarschijnlijk een goede benadering.[20] Op het vlak van hersenfunctie verwachten wij niet dat (resting state) fMRI een belangrijke rol zal spelen als longitudinale biomarker in HD. Wel verwachten wij dat EEG's geanalyseerd met geavanceerde methodes zoals machinaal leren

mogelijk wel als biomarkers van hersenfunctie in HD zouden kunnen dienen, waarmee die mogelijk bruikbaar kunnen worden voor het beoordelen van het effect van ziekte-modificerende middelen.

Zoals in de introductie reeds benoemd, zou HD als een multisysteem neurodegeneratieve aandoening beschouwd moeten worden, wat maakt dat een veelzijdige, multivariate biomarker benadering doelmatig zal zijn. Een dergelijke holistische aanpak zou inzichten kunnen bieden in de achtereenvolgende veranderingen die uiteindelijk leiden tot de laatste gemeenschappelijke route van neuronale disfunctie en dood. We bevelen, waar mogelijk, het gebruik van geautomatiseerde methodes aan om de hoogste mate van objectiviteit te waarborgen en om snelle en gestandaardiseerde interpretatie van data te faciliteren in grote multicenter studies. Wel blijft visuele kwaliteitscontrole essentieel bij gebruik van automatische technieken voor MRI beeld segmentatie.

Als toevoeging aan de biomarkers onderzocht in dit proefschrift, zal een combinatie met klinische en biochemische markers nodig zijn om het effect van een interventiestudie volledig in kaart te brengen. Deze markers zullen complementaire informatie geven over zowel ziektestaat als specifieke effecten van een potentiële therapie. Het is verder van belang om verschillende markers te gebruiken, gezien het feit dat een therapie effect verschillend kan zijn op verschillende markers. Een dergelijke benadering is essentieel voor het verduidelijken van de sequentie waarin de verschillende markers tijdens het ziekteproces veranderen. Dit kan op zijn beurt helpen om het aantal deelnemers dat nodig is om een interventie effect aan te tonen te reduceren door selectie van ziektestadium specifieke markers.[21] Verder kunnen dergelijke onderzoeken leiden tot nauwkeurigere voorspellingen voor de verwachte tijd tot ziektepresentatie op individueel niveau. Resumerend raden wij als kernwoord voor toekomstig biomarker onderzoek in HD *combinatie* aan.

Referenties

1 Dumas EM, van den Bogaard SJ, Hart EP, et al. Reduced functional brain connectivity prior to and after disease onset in Huntington's disease. Neuroimage Clin. 2013;2:377-384.
2 Burzynska AZ, Preuschhof C, Backman L, et al. Age-related differences in white matter microstructure: region-specific patterns of diffusivity. Neuroimage 2010; 49:2104-2112.
3 Concha L. A macroscopic view of microstructure: Using diffusion-weighted images to infer damage, repair, and plasticity of white matter. Neuroscience 2014;276:14-28.
4 Hobbs NZ, Cole JH, Farmer RE, et al. Evaluation of multimodal, multi-site neuroimaging measures in Huntington's disease: Baseline results from the PADDINGTON study. Neuroimage Clin. 2012;2:204-211.
5 Kringelbach ML, Rolls ET. The functional neuroanatomy of the human orbitofrontal cortex: evidence from neuroimaging and neuropsychology. Prog Neurobiol. 2004;72: 341-372.
6 Kassubek J, Juengling FD, Kioschies T, et al. Topography of cerebral atrophy in early Huntington's disease: a voxel based morphometric MRI study. J Neurol Neurosurg Psychiatry 2004;75:213-220.
7 Alvarez JA, Emory E. Executive function and the frontal lobes: a meta-analytic review. Neuropsychol Rev. 2006;16:17-42.
8 Unschuld PG, Liu X, Shanahan M, et al. Prefrontal executive function associated coupling relates to Huntington's disease stage. Cortex 2013;49:2661-2673.
9 Klöppel S, Draganski B, Siebner HR, et al. Functional compensation of motor function in pre-symptomatic Huntington's disease. Brain 2009;132:1624-1632.
10 Scheller E, Abdulkadir A, Peter J, et al. Interregional compensatory mechanisms of motor functioning in progressing preclinical neurodegeneration. Neuroimage 2013;75: 146-154.
11 He Y, Chen Z, Evans A. Structural insights into aberrant topological patterns of large-scale cortical networks in Alzheimer's disease. J Neurosci. 2008;28:4756-4766.
12 Reijmer YD, Leemans A, Caeyenberghs K, et al. Disruption of cerebral networks and cognitive impairment in Alzheimer disease. Neurology 2013;80:1370-1377.
13 Tabrizi SJ, Langbehn DR, Leavitt BR, et al. Biological and clinical manifestations of Huntington's disease in the longitudinal TRACK-HD study: cross-sectional analysis of baseline data. Lancet Neurol. 2009;8:791-801.
14 Henley SM, Wild EJ, Hobbs NZ, et al. Relationship between CAG repeat length and brain volume in premanifest and early Huntington's disease. J Neurol. 2009;256:203-212.
15 Hobbs NZ, Henley SM, Ridgway GR, et al. The progression of regional atrophy in premanifest and early Huntington's disease: a longitudinal voxel-based morphometry study. J Neurol Neurosurg Psychiatry 2010;81:756-763.
16 Tabrizi SJ, Scahill RI, Owen G, et al. Predictors of phenotypic progression and disease onset in premanifest and early stage Huntington's disease in the TRACK-HD study: analysis of 36-month observational data. Lancet Neurol. 2013;12:637-649.
17 Say MJ, Jones R, Scahill RI, et al. Visuomotor integration deficits precede clinical onset in Huntington's disease. Neuropsychologia 2011;49:264-270.
18 Henley SM, Novak MJ, Frost C, et al. Emotion recognition in Huntington's disease: a systematic review. Neuroscience and Biobehavioral Reviews 2012;36:237-253.
19 Poudel GR, Stout JC, Dominguez DJ, et al. Longitudinal change in white matter microstructure in Huntington's disease: The IMAGE-HD study. Neurobiology of Disease 2014;74:406-412.
20 Mason SL, Daws RE, Soreq E, et al. Predicting clinical diagnosis in Huntington's disease: An imaging polymarker. Ann Neurol. 2018;83:532-543.
21 Byrne LM, Rodrigues FB, Johnson EB, et al. Evaluation of mutant huntingtin and neurofilament proteins as potential markers in Huntington's disease. Sci Transl Med. 2018;10 (458).

Dankwoord

Allereerst wil ik graag alle studiedeelnemers bedanken voor de langdurige en geduldige toewijding. Zonder hun inzet was het onmogelijk geweest om zulke nauwkeurige studies succesvol uit te voeren.

Mijn promotor prof. dr. Raymund Roos ben ik dankbaar voor het bieden van de mogelijkheid om aan dit onderzoek deel te nemen, voor het faciliteren van samenwerkingsverbanden en voor het helpen om mijn onderzoek in goede banen te leiden. Verder wil ik mijn dank uitspreken aan mijn copromotors, dr. Alexander Leemans en dr. Simon van den Bogaard, voor de inspirerende discussies en langdurige en enthousiaste support. Mijn paranimfen bedank ik voor hun ondersteuning en omdat ik ze ook mijn vrienden mag noemen. Ewoud, Ako, bedankt voor de ontelbare uren van gezelligheid, jullie steun en het feit dat jullie mij altijd weer hebben kunnen laten inzien waar het echt om gaat.

Bij naam wil ik verder niet specifiek iemand noemen, omdat ik dan geheid iemand onbedoeld vergeet. In zijn algemeenheid bedank ik graag mijn onderzoeksgroep, kamergenoten (J3-R-162), laboranten en studenten voor zowel de gezelligheid alsook voor het helpen met het verzamelen van de data en de uitvoering van het onderzoek. Verder ook mijn dank aan alle co-auteurs, zonder wie het werk voor u niet tot stand zou zijn gekomen. Mijn dank voor verschillende vrienden en collega AIOS die gedurende de onderzoeksperiode, al dan niet in combinatie met o.a. koffie, een luisterend oor hadden en mentale steun hebben geboden. Het positieve effect van dat laatste is niet te onderschatten. Mijn broertjes bedank ik voor het feit dat ze mij al sinds vele jaren ten onrechte "dr." noemen en mijn ouders voor hun liefdevolle support en onuitputtelijk vertrouwen.

Last but certainly not least, en jou noem ik bij uitzondering wel bij naam: dankjewel Marlous voor je steun, constante aanmoediging, de ruimte en de tijd die je mij hebt gegeven om dit werk goed te kunnen volbrengen. Op naar jouw proefschrift!

List of publications

Odish OF, Gotoh A, Liu YC, et al. Recurrent unbalanced whole-arm t(1;10)(q10;p10) in myelodysplastic syndrome: a case report and literature review. Cancer Genet Cytogenet. 2007;172:165-167.

Ly LV, **Odish OF**, Wolff-Rouendaal D, et al. Intravascular presence of tumor cells as prognostic parameter in uveal melanoma: a 35-year survey. Invest Ophthalmol Vis Sci. 2010;51:658-665.

Odish OF, van den Berg-Huysmans AA, van den Bogaard SJ, et al. Longitudinal resting state fMRI analysis in healthy controls and premanifest Huntington's disease gene carriers: a three year follow-up study. Hum Brain Mapp. 2015;36:110-119.

Odish OF, Leemans A, Reijntjes RH, et al. Microstructural Brain Abnormalities in Huntington's Disease: A Two-Year Follow-Up. Hum Brain Mapp. 2015;36:2061-2074.

Odish OF*, Caeyenberghs K*, Hosseini H, et al. Dynamics of the connectome in Huntington's disease: a longitudinal diffusion MRI study. NeuroImage: Clinical 2015;9:32-43.

Akkerman OW, **Odish OF**, Bolhuis MS, et al. Pharmacokinetics of Bedaquiline in Cerebrospinal Fluid and Serum in Multidrug-Resistant Tuberculous Meningitis. Clin Infect Dis. 2016;62:523-524.

Brown KE, …, **Odish O**, et al. The reliability of commonly used electrophysiology measures. Brain Stimul. 2017;10:1102-1111.

Odish OFF, Beudel M. Closed-Loop Medical Devices Might Reduce Iatrogenic Loss of Autonomous Action Selection. Camb Q Healthc Ethics 2017;26:688-690.

Odish OFF, Reijntjes RHAM, van den Bogaard SJA, et al. Progressive microstructural abnormalities of the occipital cortex in Huntington's disease. Brain Imaging Behav. 2018;12:1786-1794.

Odish OFF, Johnsen K, van Someren P, et al. EEG may serve as a biomarker in Huntington's disease using machine learning automatic classification. Sci Rep. 2018;8:16090.

Gregory S*, **Odish OFF***, Mayer I*, et al. Multimodal characterization of the visual network in Huntington's disease gene carriers. Clin Neurophysiol. 2019;doi:10.1016/j.clinph.2019.08.018

* Equal contribution

Curriculum vitae

Omar Odish werd geboren op 7 oktober 1984 in Bagdad, Irak. Het basis- en het begin van het voortgezet onderwijs heeft hij verspreid over Irak, Polen en Jordanië gevolgd en vanaf 1997 in Nederland voortgezet. Na het behalen van zijn VWO diploma in 2003 aan het Hofstad Lyceum te Den Haag, begon hij aan zijn studie geneeskunde aan de Universiteit Leiden. Delen van de studie heeft hij in Zweden, Japan en het Verenigd Koninkrijk gevolgd. Na het behalen van zijn artsexamen in 2010 heeft hij aansluitend als arts-assistent neurologie gewerkt in het Reinier de Graaf Gasthuis, het Sint Lucas Andreas Ziekenhuis en het Zaans Medisch Centrum.

Van 2012 tot 2015 was hij betrokken bij het internationale biomarker studie "Track-On HD", een studie ontworpen om ziektemarkers voor de ziekte van Huntington te vinden. In dat kader is hij gestart met zijn promotietraject onder leiding van prof. dr. R.A.C. Roos in het Leids Universitair Medisch Centrum bij de afdeling neurologie in samenwerking met dr. S.J.A. van den Bogaard van de afdeling neurologie en dr. A.L.G. Leemans van het Image Sciences Institute van het Universitair Medisch Centrum Utrecht. In april 2015 is hij gestart met de opleiding tot neuroloog in het Universitair Medisch Centrum Groningen (opleider prof. dr. H.P.H. Kremer).